Kinematical and Spatial Lopsidedness in Spiral Galaxies

Rabbi Akkiba Angiras

Thesis submitted to

The Mahatma Gandhi University

in partial fulfilment of the requirements

for the award of the degree of

Doctor of Philosophy in Physics

under the faculty of Science

School of Pure and Appplied Physics

Mahatma Gandhi University

Kottayam, Kerala

India

September 2008

Declaration

I hereby declare that this thesis entitled **Kinematical and Spatial Lopsidedness in Spiral Galaxies** is a record of the research work carried out by me under the joint supervision and guidance of **Dr. K. Indulekha**, Reader, School of Pure and Applied Physics, Mahatma Gandhi University, Kottayam, Kerala and **Dr. K. S. Dwarakanath**, Professor, Astronomy and Astrophysics Group, Raman Research Institute, Bangalore. No part of this thesis has been presented for any other Degree or Diploma earlier.

Kottayam,

20^{th} September 2008.

(Rabbi Akkiba Angiras)
School of Pure and Applied Physics
M.G. University

Dedicated to

my parents Prof. O. M. Mathew and Jolly Mathew

and

my wife Elizabeth and daughter Rabia

Acknowledgements

Over the last three years- the period of my doctoral work- I received support and help from many people. A major chunk of the support and help came from my guide K.Indulekha of the School of Pure and Applied Physics, Mahatma Gandhi University, Kottayam, Kerala and co-guide K.S.Dwarakanath, Astronomy and Astrophysics Group, Raman Research Institute, Bangalore, Karnataka. These two teachers guided me not only in my research but also in my life as a research scholar. Indulekha taught me an important component of research life: the way of proactive interaction with people and about dealing with the hurdles posed by administrative aspects of university research. Her stoic approach to life itself is something which I admire. Her sharp and probing questions about my research work have stood me in good stead. Dwaraka, calling him by that name is a skill I am yet to learn, is a person who was kind enough to give me a chance to pursue research. Without his active guidance, especially in matters related to planning radio observations and the support he gave me for trying out new things I would not have finished the thesis in the stipulated time. His ability to be logical and systematic in everything he does is one quality I would like to emulate in my life. He, his wife Chitra and daughter Mithali's way of treating me as part of their extended family was also a revelation for me.

In addition to my supervisors, there is one more person who taught me to cultivate a love for research and teaching. Prof. G. Srinivasan of RRI, motivated me to extend my research activities and took me by my hand to RRI to work with Dwaraka. This was a turning point in my life. He was also deeply interested and concerned about the progress I made in my research.

Prof. Chanda Jog of IISc was not only my teacher during the course

work period but also an active collaborator. Her enthusiasm about the work we carried out was really contagious. Her support and guidance were invaluable. Avinash Deshpande, Uday Shankar, Anish Roshi, Biman Nath, Biswajit, Shiv Sethi, Sridhar, Shukre, C. R. Subrahmanya, Ravi Subrahmanyan, Laxmi and Ramesh were the other persons at RRI who had to tolerate my crazy ideas and questions some time or the other and to suffer me calling them sir or ma'am. It is rather nice that none of them turned cold when they saw me; instead took time to teach me and clarify my doubts. Desh was one of the first people in RRI to invite me home. I still remember the fantastic food made by his wife Ranjana, the award winning chef. There were two other people at RRI, Dipankar and Sunita, who had to listen to my questions and arguments during lunch and tea breaks at RRI. Hope that was not the reason for their migration to IUCAA. Mousumi did not have to bear the burden of my questions and doubts too much. But her experience with galaxy bar strength calculations did me a lot of good. She was a good lunch companion too. Initially, I did not have much interaction with Nirvikar Prasad, partially due to the fact that our fields of research are separated by a factor of 10^{19} in size. However he proved to be a person with whom I could talk about subjects like Economics.

Now comes the *tear* part of any research scholar's life. Mostly it was tears of laughter. The brunt of my acerbic and some times childish wit, questions and ideas had to be borne by three people. Chandreyee, Atish and Harsha. Late comers to this scene are Ruta, Wasim and Yogesh. Without the presence of these people in the RRI students' room, I would have become a *geni-ass*. Chandreyee and Atish suffered me for two and a half years till they escaped to NCRA. The parties we used to regularly have for no reason and the fights Atish and *Comrade* Chandreyee used to have livened up the

place for me.

Harsha had to be provoked by me to join the gang. At least that is what I like to believe. Hope Harshaji will pass on the skill of making perfectly brewed cup of coffee to others. Thanks Harshaji for initiating me into the mystery of x-ray pulsars and quasi-periodic oscillations and for being the perfect target for my instant poems. You have been a great friend.

Peeyush and Shahram by virtue of being in the second students' room and RAL lab, escaped my clutches. The food they used to bring from home and the sweets from Iran are fondly remembered.

I had lots of fun with these friends but learned about other wavelength observations too. The only thing which never took off was a joint project. Hope I will get a chance to collaborate with these friends some time. I think this is the apt time to thank Shahram, Yogesh and Wasim for showing me how to carry out the tests of a radio antenna feed and Ruta for teaching me rudiments of bird watching and low frequency radio observations. Special thanks to Yogeshji for bombarding me with SMS jokes. Many hours of my dreary travel to the various parts of the country were enlivened due to them. In a nut shell, the freedom and friendship I experienced with these people is something I cherish.

The *close encounters* I had with Nishanth, Giri, Mamta during the Young Astronomers' Meet and the questions asked by Kanhaiya have shown me that a new set of students has become my friends. Their attempt at modernizing me in appearance and thought is greatly appreciated.

Interactions with *seniors* like Amitesh, Rekesh, Suparna and Rajesh were another aspect of my life at RRI. Amitesh introduced me to AIPS and GIPSY and was my collaborator. Before things could take off, he moved to ARIES and then to Netherlands. Rekesh was my computer guru. Rajesh

with his primordial magnetic fields and *cigs* kept me alive. Suparna was rather a mysterious entity for me. Not seen but heard. Unfortunately by the time I settled down in RRI she had gone over to IUCAA. Suparna's way is being followed by Raju Baddi. He occupies the same seat and position and is only heard and not seen.

The friends with whom I did my course work are another set of people with whom I enjoyed both studies and life. I still think about the classes I attended with Chaitra, Girish, Ambika, Kathiravan, Shanmugasundaram, Maheshwar and Amitesh. The one year of course work which I did with them was marvelous, especially the discussions we had about assignments.

Vidya's support in various office and administrative matters is gratefully acknowledged. Her help in keeping Atish and Chandreyee quiet is also acknowledged. I would have been in a soup without her support.

Thanks to Hanumanthappa and Laxmamma for looking after my fluid intake (coffee decoction).

It is now time to acknowledge the help I received from my *alma mater*, Mahatma Gandhi University. I would like to acknowledge all the help extended to me by the Director of School of Pure and Applied Physics, Prof. C. Venugopal. Without his support in managing the administrative hurdles, my research work would have come to a standstill. Prof. C. S. Menon gave me a lot of help and support in dealing with many administrative details during the early parts of my research work when I was learning my ropes. Prof. N. V. Unnikrishnan and Dr. G. V. Vijayagovindan of SPAP have helped me in various ways over a period of three years. In this context I deeply mourn the premature demise of Dr. G. V. Vijayagovindan. My respectful homage to him.

Inspite of the initial hurdles I had to face in Mahatma Gandhi University,

the administrative staff had been extremely nice to me. My sincere thanks to the S.O Bhanukuttan and the other office members as well as the library and technical staff of the department. Only during the Young Astronomers Meet (YAM) I had a chance to interact with them closely. It was a nice, unforgettable experience.

Among my fellow students at SPAP, Vinu, Toney and Noble stood by me through thick and thin. Without their support in getting things done at the University and their company, life in M. G. University would have been monotonous.

I would like to acknowledge the support given to me by the Honourable Vice-Chancellor, Dr. Jancy James. She is one of the vice-chancellors whom I found to be very approachable and amenable. Pro-Vice-Chancellor, Dr. K. K. Yunuskutty, Registrar, Prof. M. R. Unni and Joint Registrar, Shri. K. R. Sankaran Kutty have also been of immense help during various administrative processes.

My wife Elizabeth and daughter Rabia had to live in Bangalore without my presence for over three years. My wife used to be the un-official spell checker and grammar checker of my papers. My daughter's curiosity about my work helped me immensely as I had to simplify everything to make it understandable to a ten year old kid. My parents, Prof. O. M. Mathew and mother Jolly Mathew as well as my in-laws Prof. P. J. Chakko and Molly Chakko were sources of relief during hours of drudgery. Their support and prayers helped me a lot. My brothers Bhrigu and Kashyap, brothers in-law Chachu and Benu along with their family members also supported me by getting books and much running around to get things done. I acknowledge all their help in getting this thesis done.

I would also like to acknowledge the support by the University Grants

Commission (UGC) of India for granting me study leave under the Faculty Improvement Programme (FIP) of the X-plan. I shall be failing in my duty if I do not express my obligation to the management of St. Joseph's College, Bangalore and to Principal Rev. Fr. Dr. Ambrose Pinto S. J. in permitting me to avail myself of the FIP leave.

Rabbi Akkiba Angiras

20^{th} Sept. 2008

We thank the staff of the Giant Meterwave Radio Telescope (GMRT) who made these observations possible. GMRT is run by the National Centre for Radio Astrophysics of the Tata Institute of Fundamental Research

This study has made use of Digitized Sky Survey plates (POSS2).The Second Palomar Observatory Sky Survey (POSS-II) was made by the California Institute of Technology with funds from the National Science Foundation, the National Geographic Society, the Sloan Foundation, the Samuel Oschin Foundation, and the Eastman Kodak Corporation.

This research has made use of the NASA/IPAC Extragalactic Database (NED) which is operated by the Jet Propulsion Laboratory, California Institute of Technology under contract with the NASA

We acknowledge the use of NASA's Sky View facility located at the NASA Goddard Space Flight Center

Thanks to the creators of Astronomical Image Processing System (AIPS), Groningen Image Processing System (GIPSY), Image Reduction and Analysis Facility (IRAF), Karma visualization tool, LaTeX and GNU

Synopsis

Galaxies are the visible matter in the fabric of space-time. Traditionally, based on their appearance in the visible bands, they have been classified into elliptical and spiral galaxies. This classification scheme, introduced by Hubble, reveals not only the physical properties but also, to some extent, the evolution of galaxies. This is evident from the strong correlation that exists between the bulge to disk luminosity ratio, relative mass of atomic Hydrogen (HI) with luminosity, mass concentration, stellar population, nuclear properties, chemical abundance of interstellar medium, star formation history etc. seen right across the Hubble sequence.

In this thesis, another parameter called the lopsidedness that is seen in many of the galaxies has been estimated. Lopsidedness or the asymmetry seen in the matter distribution and its motion as a function of radius and azimuthal angle in the galactic disk is an important tool in studying the physical appearance and history of the galaxy. A large fraction of galaxies display this phenomenon. Some of the earlier works indicate that approximately 50 to 75% of galaxies show lopsidedness. These studies mainly used the HI spectral line observations or images obtained using near Infra-Red bands. In this study, the HI 21cm emission maps of galaxies are used to estimate the lopsidedness. Hence our study is restricted to spiral galaxies which are rich in HI.

The first step in the direction of estimating the lopsidedness is evolving a method for quantifying the lopsidedness. In this work, we have used the Fourier series technique to estimate the lopsidedness. This is the first time such a technique is being used to analyse the HI 21cm emission radio maps (surface density maps) of spiral galaxies. The next step in this progression was to compare the lopsidedness seen in HI maps with that seen in the stellar

disk of spiral galaxies. As a result of this analysis, it is demonstrated that for those galaxies where HI disk overlaps with the stellar disk, the lopsidedness of HI disk is comparable to that seen in the stellar disk. Although theoretical arguments exist to show that lopsidedness of gaseous disk is comparable to that of the stellar disk, it is the first time this has been observationally confirmed. Performing the lopsidedness analysis on HI maps also has an added advantage. In many galaxies, HI extends far beyond the stellar disk. Hence lopsidedness analysis on HI maps makes us capable of studying and understanding the cause of lopsidedness far beyond the stellar disk.

Although lopsidedness is seen in many galaxies, its physical origin is not clearly understood. The cause of disk lopsidedness has been attributed to a variety of physical processes such as the disk response to halo lopsidedness which could arise due to tidal interactions (Jog, 1997) or due to mergers with satellite galaxies (Zaritsky& Rix, 1997) or asymmetric gas accretion (Bournaud et al., 2005). The asymmetry can also be generated due to the stellar disk being offset in a spherical halo (Noordermeer et al., 2001). A study of HI asymmetry in the outer parts as done in this thesis using HI as a tracer can give a direct handle on the halo asymmetry.

Galaxies in groups were selected for lopsidedness analysis due to the following reasons. Galaxy groups generally have larger fraction of gas-rich spirals compared to clusters. This is because the velocity dispersion of galaxies and the Intra Group Medium (IGM) density in groups is low which makes ram-pressure stripping and the gas loss due to the effect of transport processes like the turbulent and viscous stripping inefficient. The above argument is further aided by the observation that IGM, if it exists, also has low X-ray luminosity and low temperature in a group environment. This implies that the only physical process to be concerned about is the tidal interaction.

On the basis of available data, studies on two loose groups namely Eridanus and Ursa Major have been carried out. In addition, six Hickson Compact Groups (HCGs) were also observed using Giant Meterwave Radio Telescope (GMRT), Pune, India for studying lopsidedness.

The Eridanus group of galaxies are at a mean distance of about 23 ± 2 Mpc. This group has about 180 galaxies that are confined to a volume of ~ 18 Mpc. The velocity dispersion of this group is ~ 240 km s^{-1}. This velocity dispersion which is lesser than the typical cluster velocity dispersion of ~ 1000 km s^{-1} and the number density of galaxies imply that Eridanus is dynamically a younger system compared to clusters. This group is expected to be in the process of evolving into a cluster. If we compare the fraction of S0 type galaxies in the Eridanus group, it lies in between a compact cluster like Fornax and a loose group like the Ursa Major. This factor aids the argument that galaxies in the Eridanus group are interacting with their neighbouring galaxies.

Using the GMRT, Omar & Dwarakanath (Omar & Dwarakanath, 2005a; Omar & Dwarakanath, 2005b) imaged about fifty of the galaxies belonging to the Eridanus group in HI 21cm emission. Out of these, 18 galaxies were selected for lopsidedness study based on their inclination and regular appearance. Four galaxies from this group were used to show the correlation between lopsidedness in their respective HI and stellar disks. As a result of the lopsidedness analysis, it was seen that the estimated lopsidedness in this group is about 3 times larger than that observed in the field galaxies. It was also seen that early type spirals show more lopsidedness compared to the late type galaxies. This trend is opposite to what is observed in the case of field galaxies. Based on the argument that ram-pressure stripping is ineffective in this group, the cause for observed lopsidedness is ascribed to

tidal interactions.

Ursa Major group of galaxies which is at a mean distance of about 15.5 Mpc has 79 galaxies associated with it. This group has a velocity dispersion of ~ 150 km s^{-1}. This implies that this group is dynamically younger and is more loosely bound than the Eridanus group. In this group no HI deficiency is seen. This might be partially due to the fact that tidal interactions between the galaxies may not be strong enough to cause the deficiency. Besides, X-ray emission from this group is also not seen. Hence the hot IGM and the associated ram pressure effects are assumed to be negligible.

The Ursa Major group was imaged in HI 21cm emission by Verheijen (Verheijen & Sancisi, 2001) using the Westerbork Synthesis Radio Telescope (WSRT), Netherlands. Eleven galaxies belonging to Ursa Major group were studied for lopsidedness. Here also, galaxies show significant lopsidedness; albeit to a lesser degree compared to the galaxies of the Eridanus group. This group is much more loosely bound than Eridanus. Hence tidal interactions are expected to be much weaker. This might explain the observed lopsidedness. Using the velocity maps available for galaxies belonging to the Ursa Major group, the kinematical lopsidedness was also estimated. For galaxies of this group, we also had estimated the ellipticity of dark matter halo potential from the surface density lopsidedness value. It is observed that the ellipticity of dark matter halo obtained from velocity maps is comparable to that derived from surface density maps.

HCGs are isolated compact groups that contain typically about five galaxies. From early x-ray observations of HCGs using ROSAT, it is known that most of the HCGs are gravitationally bound structures. They show a velocity dispersion of ~ 150 km s^{-1}. By virtue of the high number densities in HCGs which are comparable to a cluster environment, they provide us

with a laboratory where the effect of high galaxy density on lopsidedness could be studied. The six HCGs, observed using the GMRT, Pune, India, were selected mainly based on the suitability of their galaxies for lopsidedness analysis and the group size. Based on the earlier studies on Eridanus and Ursa Major group of galaxies, the lopsidedness of HCGs were expected to be much higher than what is seen in a typical group or field galaxies. However, due to the constraints imposed by the Fourier series analysis procedure, the lopsidedness could be estimated only for one galaxy. This galaxy shows a higher degree of lopsidedness compared to the group galaxies. The HI deficiency studies and Far Infra-Red (FIR) - Radio correlation studies on these HCG galaxies were also carried out.

Contents

List of Tables

List of Figures

List of Notations, Units and Constants

Notations & Definitions

Dark Matter	DM
Hubble constant	H_0
Intra Cluster Medium	ICM
Intra Group Medium	IGM
Navarro Frenk White	NFW
Noise (root mean square)	σ
Redshift	$z = \frac{\lambda_{observed} - \lambda_{emitted}}{\lambda_{emitted}}$
Speed of light	c
Systemic velocity	V_{sys}=cz
Wavelength	λ

Units & Constants

Hubble constant	75 km s^{-1} Mpc^{-1}
Solar mass	1 $M_\odot$ = 1.989×10^{30} kg
Solar luminosity	1 $L_\odot$ = 3.827×10^{26} J s^{-1}
Speed of light (c)	2.997925×10^8 m s^{-1}
Year	3.156×10^7 s
Parsec	1 pc = 3.086×10^{16} m
kpc, Mpc	10^3, 10^6 pc
Jansky	1 Jy =10^{-26} W m^{-2} Hz^{-1}
mJy	10^{-3} Jy
Mega Hertz (MHz)	10^6 Hz
Micron (μm)	10^{-6} m

There are two mistakes one can make along the road to truth– not going all the way, and not starting.

–Buddha (563-483 BC)

1 Introduction

1.1 Nature of Galaxies

Galaxies are the smallest tassels of luminous matter adorning the fabric of space-time which can be observed beyond the neighbourhood of Milky Way. Composed mainly of stars, gas, dust and the so far undetected entity called Dark Matter (DM), they have been a puzzle for the astronomers till the dawn of the 20^{th} century.

Based on galaxies' appearance in the visible bands, they have been classified into elliptical and spiral galaxies. Categorising the galaxies into these two broad groups was first proposed by Hubble (Hubble, 1936). A typical elliptical galaxy, as the name suggests, has a featureless elliptical shape in projection; while a spiral galaxy distinguishes itself with a nucleus (or bulge) and an associated, dominant, stellar disk on which a spiral pattern is superposed. The other major differences came to light when multi-wavelength and spectral observations of the galaxies began. The first and foremost among them was the systematic rotation seen in the disk of spiral galaxies. The flatness of the rotation curve (Rubin et al., 1980; Bosma, 1981)

indicated the presence of as yet un-identified form of matter termed dark matter surrounding the galaxy (Fig. 1.1).

At this juncture, it should be mentioned that the scenario described above will be tenable only by assuming the universal validity of the law of gravity at all scales. There are alternative theories which subscribe to a modification to the law of gravity (e.g. MOdified Newtonian Dynamics (MOND) (Milgrom, 1983)). As a result, such theories are able to explain many of the physical and kinematic features of galaxies without invoking the elusive *dark matter*. In this thesis, however, we presuppose the universal validity of the law of gravity and the standard model of particle physics.

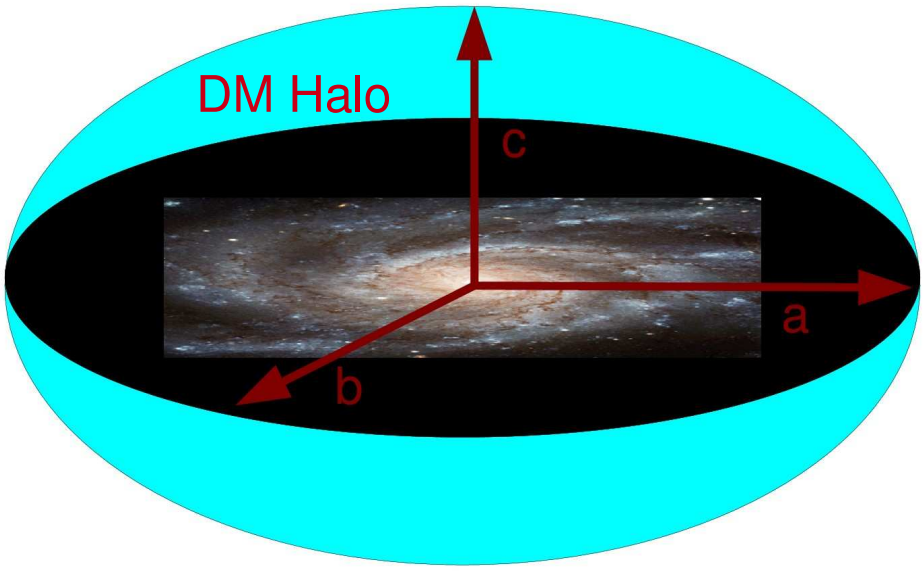

Figure 1.1: Representative picture of a spiral galaxy with Dark Matter halo. Quantities a, b, c represent the major, minor and orthogonal axes respectively.

Random motion of stars dominates over any systematic rotational motion in elliptical galaxies. Hence elliptical galaxies are assumed to be pressure supported systems unlike the spirals. Elliptical galaxies also seem to

be immersed in a sea of dark matter. In all these cases, from numerical simulations, dark matter is shown to have a universal density profile (Navarro et al., 1997).

Composition of stellar population is another major difference between the elliptical and spiral galaxies belonging to the local universe. Major constitution of the elliptical galaxies is the old stellar population (Population II stars). On the contrary, disks of the spiral galaxies are dominated by young stellar population (Population I). Significant amount of gas and dust are also observed in spiral galaxy disks. Interestingly, the bulge of a typical spiral galaxy has many similarities with the elliptical galaxies. Significant old stellar population, dearth of dust and gas, dominant random motion etc. are some of these similarities.

The Hubble classification scheme (Fig. 1.2), later modified to in-

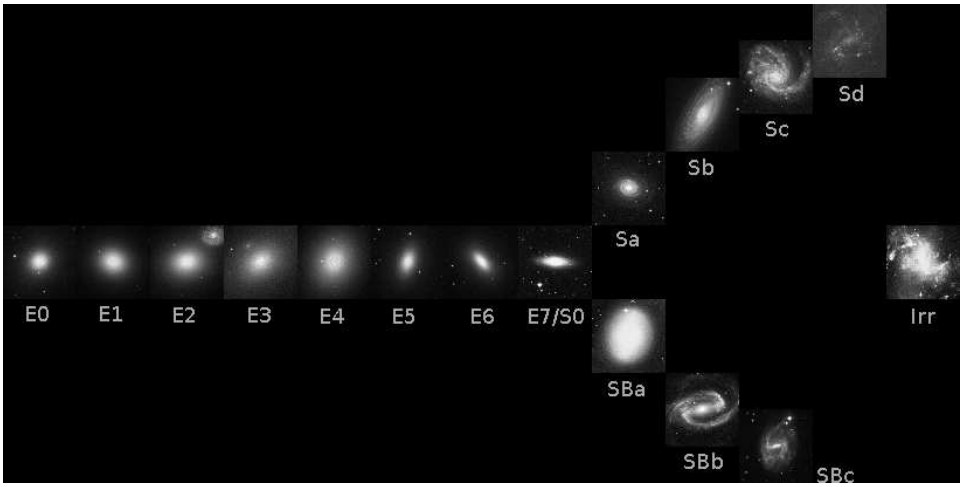

Figure 1.2: Hubble classification of galaxies. Images obtained from Digitized Sky Survey (DSS).

corporate finer nuances displayed by the galaxies, reveals not only the physical properties but also, to some extent reflect evolution of galaxies (Baugh, Cole, & Frenk, 1996). This is evident from the strong cor-

relation that exists between the bulge to disk luminosity ratio, relative mass of atomic Hydrogen (HI) with luminosity, mass concentration, stellar population, nuclear properties, chemical abundance of interstellar medium, star formation history etc. seen right across the Hubble sequence (Roberts & Haynes, 1994). It is not clear, however, whether the suggested evolution is triggered by the intrinsic properties of the galaxies or by the extrinsic effects on the galaxies.

1.2 Time and Space Effects on Galaxies

A large fraction of the galaxies in the local universe is seen to be associated with galaxy clusters or groups. Hence the effect of the environment on the galaxies is easier to study. The first indication of such an evolution that depends on environment came from the density-morphology relation of galaxies (Dressler, 1980) seen in galaxy clusters (Fig. 1.3).

Galaxy clusters are the largest gravitationally bound structures seen in the universe. Typically a cluster consists of $\sim$ 100–1000 galaxies which are gravitationally bound in a region of $\sim$ 2 Mpc. In addition to galaxies, this region consists of hot gas of $10^7 - 10^8$ K (Intra-cluster Medium or ICM) having typical number density of $\sim 10^{-3}$ cm^{-3}. From the velocity dispersion of galaxies in a cluster ($\sim$ 1000 km s^{-1}), it is seen that large amount of dark matter is also present in the cluster environment.

From the studies carried out on Virgo cluster (Crowl et al., 2006), it appears that the cluster core, i.e. region within one Abell radius (Abell radius $= 1.7'/z$, where z=redshift of the cluster) of the cluster centre, is dominated by the early type galaxies and S0 type galaxies. In many compact groups of galaxies containing smaller number of galaxies, the group environment is dominated by a giant elliptical galaxy. The observation that cluster envi-

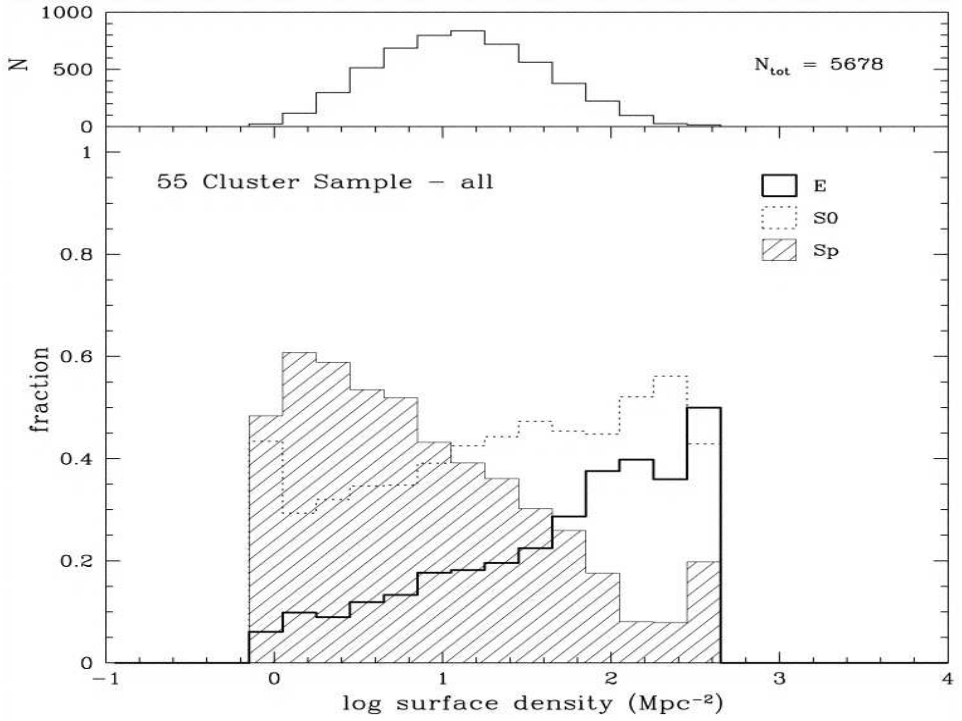

Figure 1.3: The density-morphology relation. Here the projected density is shown on the abscissa. High density clusters seems to be dominated by ellipticals and S0 galaxies (Dressler et al., 1997).

ronment stimulates galaxy evolution is also given added impetus by the observed morphological Butcher-Oemler effect (Butcher & Oemler, 1978; Tran et al., 2005) and the HI deficiency studies carried out on spiral galaxies by early observers (Solanes et al., 2001). As one moves away to the outer, less dense regions of the cluster the fraction of spiral galaxies appears to increase. The spiral galaxies often are dominated by the young, massive stars which are bluish in colour. Hence, the spiral galaxies in the outer edge of a cluster often appear bluish. This is called the morphological Butcher-Oemler effect (Butcher & Oemler, 1978; Tran et al., 2005). The heart of BO effect is the spiral to early type transformation.

The causes attributed to gas deficiency in cluster spiral galaxies com-

pared to field galaxies are many (Haynes et al., 1984). Ram-pressure stripping (Gunn & Gott, 1972), tidal interactions, repetitive encounters with other galaxies in the cluster and cluster potential (*galaxy harassment*) (Moore et al., 1999), and of late, by large amplitude density-wave perturbations (Zhang & Buta, 2007) etc. are some of the effects that can cause the morphological BO effect. For ram-pressure stripping to be an effective mechanism in removing HI from the outer regions of the galaxy, the galaxy has to move through a high density environment (high ICM density) with a high velocity relative to the medium. The inclination of the galaxy with respect to the direction of motion is also another important parameter. If the motion of the galaxy through the ICM is perpendicular to the disk then, significant HI deficiency can be generated. Tidal interactions on the other hand do not depend on the ICM density, but rather on the separation and mass of interacting galaxies. It has been shown by numerical studies that tidal interaction induced HI stripping will become important when the rotational speed of the galaxy is comparable to the relative speed with which another galaxy goes past it. As the ICM density and the velocity dispersion in cluster environment are high, explanations based on ram-pressure stripping appear to have gained currency for cluster galaxies.

In comparison to clusters, galaxy groups are much smaller entities. They typically contain fewer than 100 galaxies spread over 1-2 Mpc. Another major difference between clusters and groups is the velocity dispersion. Typically in a group the velocity dispersion of galaxies is $\sim$ 200 km s^{-1}. This velocity dispersion is comparable to the typical rotation velocities of spiral galaxies.

In the case of groups, the important ingredients for ram-pressure stripping to be effective, *viz.* high velocity dispersion and hot inter-group medium

are seldom seen. The fraction of spiral galaxies in a group environment is also higher compared to the cluster environment. Does it mean that we are looking at a different mechanism for the evolution of galaxies in a group environment? The answer to this question is not yet fully understood. As mentioned earlier, the velocity dispersion of galaxies belonging to groups is $\sim$ 200 km s^{-1}, while the density of Intra-Group Medium (IGM) is $\leq 10^{-4}$cm^{-3} (Sengupta & Balasubramanyam, 2006). The condition for ram-pressure to be an effective mechanism in stripping HI from a galaxy is that $\rho_{IGM} V_{gal}^2 \geq \Sigma_{gas} V_{rot}^2 R^{-1}$ where ρ_{IGM} is the density of Intra-Group Medium, V_{gal} is the speed of the galaxy through the IGM, Σ_{gas} is the surface density of HI and V_{rot} is the rotation velocity of the galaxy at a galactic centric radius R. Using the typical values for the velocity dispersion of galaxies in a group, IGM density and rotation velocity of a galaxy (150 km s^{-1} at R=10 kpc), the maximum ram-pressure a galaxy is subjected to is $\sim$ 10 cm^{-3} km^2 s^{-2}. This ram-pressure is $\sim 1-2$ order of magnitude lesser than that seen in galaxy clusters where ram-pressure stripping is found to be effective. In addition, the above mentioned IGM density and velocity dispersion can strip HI surface density less than 6×10^{19} cm^{-2} only. Most of the HI mass associated with the galaxies in groups is above this column density. Hence the HI deficiency is often attributed to tidal interactions (Omar & Dwarakanath, 2005b) which becomes the most efficient mechanism for removing HI when the velocity dispersion becomes comparable to the rotational velocities of galaxies.

Galaxy evolution stimulated by the internal effects are harder to study observationally. This is due to the fact that the evolution triggered by the internal effects of the galaxy will show up only after many years. The only way to address this issue is by numerical simulations of the galaxy. These

simulations, especially in the case of a spiral galaxy, are often limited by the numerical resolution and the procedure adopted by the simulator. The numerical resolution limitation is due to the number of particles (in the case of numerical simulations using particles) used and the spatial resolution used. The typical N-body simulation takes into account only 10^7 particles which makes each particle weigh about $10^3 M_\odot$. The procedure adopted in the numerical simulation has implications on the bulge formation and artificial angular momentum loss.

Due to the limitations of numerical simulations the question of galaxy evolution namely whether it results from their internal effects (nature) or due to the influence of the external agents (nurture) is not yet fully answered. In this work, we have been mainly concentrating on understanding the effect of environment on the galaxies. This is because the effect of environment is amenable to observations and is quantifiable. As these evidences are easily available in the case of spiral galaxies, we concentrate on them.

The observational evidence of the importance of environment comes mainly from three sources. The first and the most easily observable effect is the HI deficiency. Next is the star formation rate and associated enhancement of heavier elements in the ISM. The third and the most interesting effect is the observation of lopsidedness, which we estimate in this thesis for various group galaxies.

1.3 Lopsidedness in Spiral Galaxies

Lopsidedness or the asymmetry seen in the matter distribution and in the motion as a function of the galacto-centric radius and azimuthal angle in the galactic disk is an important tool in studying the physical appearance and the history of a galaxy. Another way of interpreting lopsidedness is by

observing the iso-surface density or iso-surface brightness contours in the disk of a galaxy. These contours are usually circular and are centred at the nucleus or about the dynamical centre (or the centre about which the matter moves) of the galaxy. In lopsided galaxies the centres of these contours are not concentric and tends to drift away from the nucleus or dynamical centre. Such behaviour is often seen not only in the case of surface density and surface brightness maps of galaxies but also in the iso-velocity contours of galaxies. A premier example for such a system is the spiral galaxy M101 or the *Pinwheel galaxy* (Fig. 1.4,Fig. 1.5, Fig. 1.6). Although elliptical galaxies also indicate lopsidedness to a smaller degree (Hernández-Toledo et al., 2006), we restrict ourselves to studying the asymmetries in spiral galaxies due to the ease of studying lopsidedness in them.

Figure 1.4: M101 Optical composite image. This is an example of an optically lopsided galaxy.

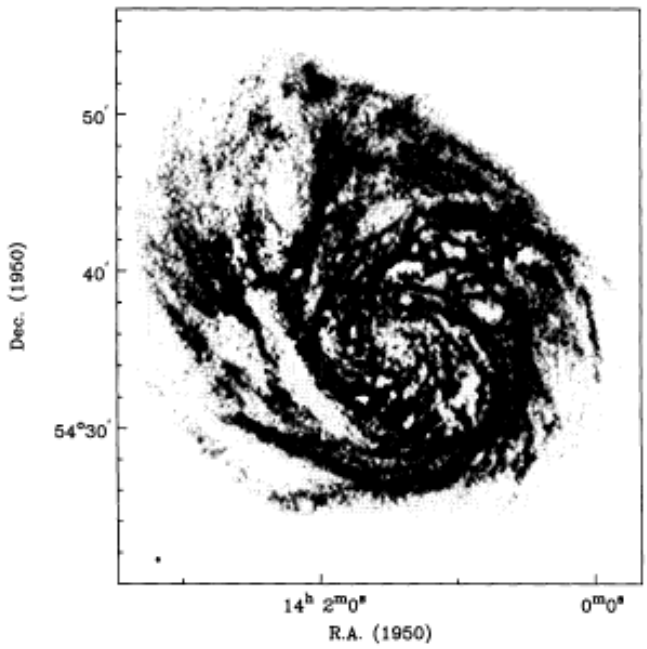

Figure 1.5: M101 galaxy. Radio surface density image obtained using Westerbork Synthesis Radio Telescope (Kamphuis, Sancisi, & van der Hulst, 1991).

A large fraction of spiral galaxies shows asymmetries. Some of the earlier works indicate that approximately 50 to 75% of spiral galaxies show lopsidedness (Richter & Sancisi, 1994; Haynes et al., 1998; Matthews et al., 1998). These studies mainly used the global HI spectral line observations (Fig. 1.5, Fig. 1.7) or images obtained using near Infra-Red bands (Rix&Zaritsky, 1995). The observation that a large fraction of spiral galaxies shows lopsidedness also indicates that lopsidedness in spiral galaxies is a long lived phenomenon which has persisted for at least a few rotation period of a galaxy and is not a transient phenomenon.

The lopsidedness studies based on global HI profile can give information of the combined effects of velocity and spatial asymmetries. To decouple

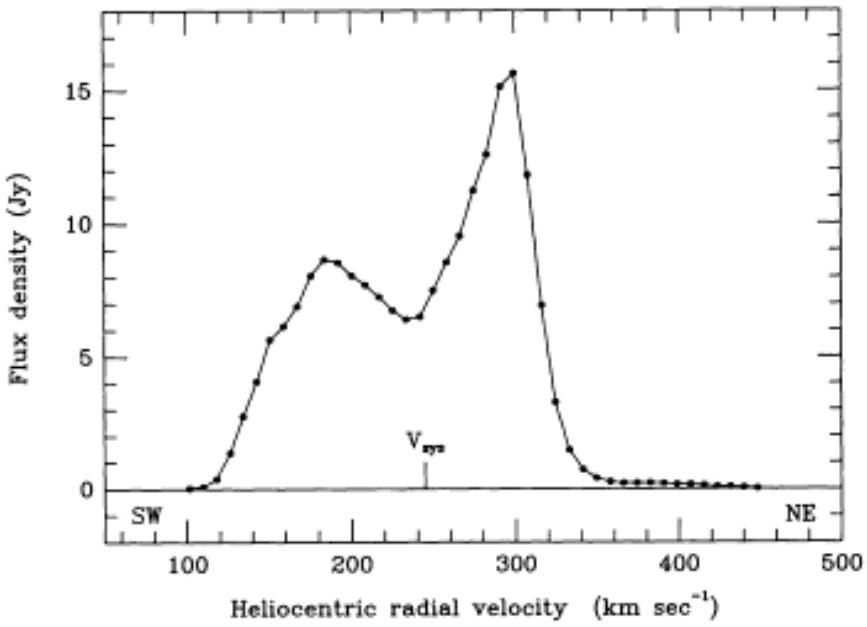

Figure 1.6: Global HI profile of M101. This profile is asymmetric (Richter & Sancisi, 1994)

the asymmetries due to spatial distribution of matter from velocity asymmetries, spectral line observations alone cannot be used. For this purpose, in this work, we have adopted the surface density maps (momnt 0 maps) and velocity field maps (momnt 1) from the HI 21 cm-line observations.

The first step in assessing the lopsidedness is to evolve a method for quantifying it. In this work, we have used the Fourier series technique to estimate the lopsidedness. This is the first time that such a technique is being used to analyse the HI 21cm-line emission radio maps (surface density maps) of spiral galaxies. The next step in this progression is to compare the lopsidedness seen in HI maps with that detected in the stellar disks of spiral galaxies. As a result of our analysis, it is demonstrated that for those galaxies where HI disk overlaps with the stellar disk, the lopsidedness of HI disk is comparable to that seen in the stellar disk. Although theoretical

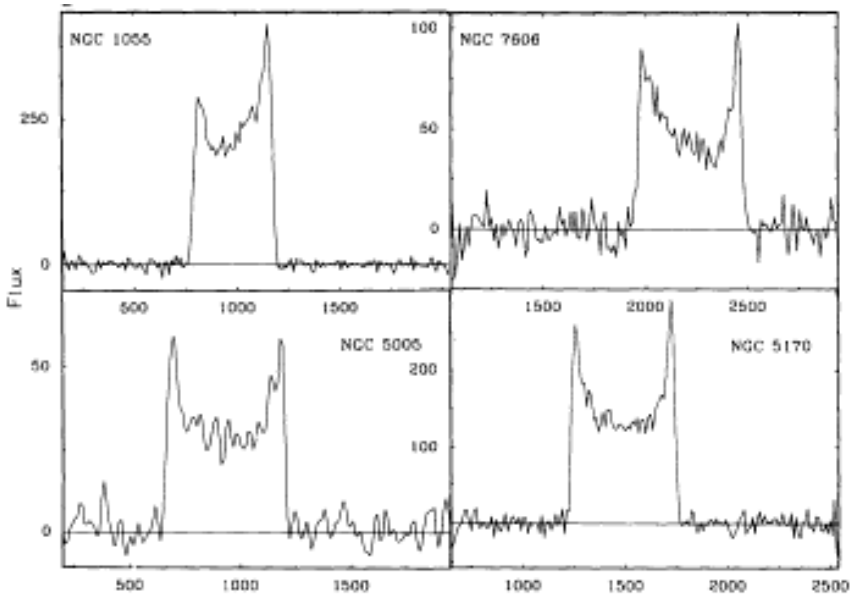

Figure 1.7: Global HI profiles of lopsided and normal galaxies. The top two HI profiles are those of lopsided galaxies, while the bottom two galaxies show the normal global HI profiles (Richter & Sancisi, 1994)

arguments exist to show that lopsidedness of gaseous disk is comparable to that of the stellar disk, it is the first time that this has been observationally confirmed. Performing the lopsidedness analysis on HI maps also has an added advantage. In many galaxies, HI extends far beyond the stellar disk. Hence lopsidedness analysis on HI maps makes us capable of studying and understanding the cause of lopsidedness far beyond the stellar disk.

Although lopsidedness is seen in many galaxies, its physical origin is not clearly understood. The cause of disk lopsidedness has been attributed to a variety of physical processes such as the disk response to halo lopsidedness which could arise due to tidal interactions (Jog, 1997) or due to mergers with satellite galaxies (Zaritsky& Rix, 1997) or asymmetric gas accretion

(Bournaud et al., 2005). The asymmetry can also be generated due to the stellar disk being offset in a spherical halo (Noordermeer et al., 2001). A study of HI asymmetry in the outer parts as done in this thesis using HI as a tracer can give a direct handle on the halo asymmetry.

Galaxies in groups were selected for lopsidedness analysis due to the following reasons. Galaxy groups generally have larger fraction of gas-rich spirals compared to clusters. This is because the velocity dispersion of galaxies and the Intra-group Medium (IGM) density in groups is low which makes ram-pressure stripping and the gas loss due to the effect of transport processes like the turbulent and viscous stripping inefficient. The above argument is further aided by the observation that IGM, if it exists, also has low X-ray luminosity and low temperature in a group environment. This implies that the dominant physical process to be concerned about is the tidal interaction.

1.4 Groups Selected for Lopsidedness Analysis and Further Observations

Lopsidedness studies on galaxies belonging to two loose groups *viz.*, Eridanus and Ursa Major and six Hickson Compact Groups (HCGs) were carried out.

1.4.1 Eridanus Group of Galaxies

The Eridanus group was identified during the Southern Sky Redshift Survey (SSRS; da Costa et al., 1988). This group of galaxies are at a mean distance of $\sim 23 \pm 2$ Mpc and is a gravitationally bound structure (Pellegrini et al., 1989; Willmer et al., 1989). The velocity dispersion of this group is $\sim$ 240km s^{-1}(Omar & Dwarakanath, 2005a) . This velocity

dispersion is lesser than the typical cluster velocity dispersion of $\sim$ 1000 km s^{-1}. In the case of hierarchical structure formation scenario, it is believed that galaxy clusters result from the mergers of groups whose gravitational potential well is smaller compared to that of clusters. Hence the low velocity dispersion implies that Eridanus is dynamically a younger system compared to clusters. This group is expected to be in the process of forming a cluster. If we compare the fraction of S0+E type galaxies in the Eridanus group (0.5)(Omar & Dwarakanath, 2005a), it lies in between a compact cluster like Fornax(0.6) (Tully et al. 1996) and a loose group like the Ursa Major(0.1)(Tully et al. 1996). This factor aids the argument that galaxies in the Eridanus group are interacting with their neighbouring galaxies.

Using the GMRT, about fifty of the galaxies belonging to the Eridanus group have been observed in HI 21 cm line emission (Omar & Dwarakanath, 2005a). Out of these, 18 galaxies were selected based on their inclination and regular appearance for lopsidedness study by us. Four galaxies from this group were used to show the correlation between lopsidedness in their respective HI and stellar disks. As a result of the lopsidedness analysis, it is seen that the estimated lopsidedness in this group is about 3 times higher than that observed in the field galaxies. It is also seen that early type spirals show more lopsidedness compared to the late type galaxies. This trend is opposite to what is observed in the case of field galaxies. Based on the argument that ram-pressure stripping is ineffective in this group, the cause for observed lopsidedness is ascribed to tidal interactions.

1.4.2 Ursa Major Group of Galaxies

Ursa Major group of galaxies which is at a mean distance of $\sim$ 15.5 Mpc has 79 galaxies associated with it (Tully et al. 1996). This group has a velocity dispersion of $\sim$150km s^{-1}. In this group no HI deficiency is seen (Verheijen & Sancisi, 2001). This might be partially due to the fact that the tidal interactions between the galaxies may not be strong enough to cause the deficiency.

The Ursa Major group was imaged in HI 21cm line emission by Verheijen (Verheijen & Sancisi, 2001) using the Westerbork Synthesis Radio Telescope (WSRT). Eleven galaxies belonging to Ursa Major group were studied for lopsidedness. Here also, galaxies show significant lopsidedness; albeit to a lesser degree compared to the galaxies of the Eridanus group. This group is much more loosely bound than Eridanus. Hence tidal interactions are expected to be much weaker. This might explain the observed lopsidedness. Using the velocity maps available for galaxies belonging to the Ursa Major group, the kinematical lopsidedness was also estimated. For galaxies of this group, we have also estimated the ellipticity of dark matter halo potential from the surface density lopsidedness value. It is observed that the ellipticity of dark matter halo obtained from velocity maps is comparable to that derived from surface density maps.

1.4.3 Hickson Compact Group of Galaxies

HCGs are isolated compact groups that contain typically $\sim$ 5 galaxies. From early x-ray observations of HCGs using ROSAT, it is known that most of the HCGs are gravitationally bound structures. They show a velocity dispersion of $\sim$ 150 km s^{-1}. By virtue of the high number densities in HCGs which are comparable to a cluster environment, they provide us with a laboratory

where the effect of high galaxy density on lopsidedness could be studied. The six HCGs, observed using the GMRT, Pune, India, were selected mainly based on the suitability of their galaxies for lopsidedness analysis and the group size. Based on the earlier studies on Eridanus and Ursa Major group of galaxies, the lopsidedness of HCGs were expected to be much higher than what was seen in a typical group or field galaxies. However, due to the constraints imposed by the Fourier series analysis procedure, the lopsidedness could be estimated only for one galaxy. This galaxy shows a higher degree of lopsidedness compared to the group galaxies. The HI deficiency studies and Far Infra-Red (FIR) - Radio correlation studies on these HCG galaxies were also carried out.

1.5 Thesis Structure

This thesis is mainly divided into five chapters, which will deal with various aspects of Kinematical and Spatial Lopsidedness. The layout of this thesis is as follows:

In Chapter 2 we discuss the nature of kinematical lopsidedness seen in galaxies belonging to Eridanus and Ursa Major groups. Kinematical lopsidedness is an important asymmetry seen in many galaxies which can, in principle, give information about the ellipticity of the dark matter halo potential. In recent times, a similar procedure as adopted here in this thesis has been used to estimate flows in the bars of spiral galaxies.

Chapter 3 will be devoted to the details of the spatial lopsidedness analysis carried out on galaxies of the Eridanus and Ursa Major groups. It is for the first time that such an analysis has ever been carried out using atomic hydrogen as the tracer. In this chapter, we will also show how the spatial lopsidedness derived from optical images compare with that of the atomic

hydrogen distribution. Interestingly, the early type spirals in group environment seems to be showing more lopsidedness compared to late type spiral galaxies. This trend is seen both in the Eridanus as well as Ursa Major group galaxies.

In Chapter 4 we will be mainly describing our observations of Hickson Compact Group of galaxies using the GMRT and the subsequent analysis. Hickson compact group of galaxies are gravitationally bound systems which are tidally interacting. The study of six selected HCG galaxies have given us information about lopsidedness, HI deficiency and FIR and Radio continuum correlations of these galaxies. This work will be discussed in greater details here.

In Chapter 5, we will discuss our main results and plans for future work. The results can be summarised as follows:

- Spatial and kinematical lopsidedness of spiral galaxies in groups have been estimated using HI as a tracer. The lopsidedness analysis which we carried out quantified asymmetry as a function of galacto-centric radius.

- In spiral galaxies belonging to groups, the early type spirals showed higher spatial lopsidedness than the late type galaxies, measured in the same disk scale length range. Opposite trend, however, is seen in the field galaxies.

- We have shown that the spatial and kinematical lopsidedness are comparable to each other.

- Assuming that the spatial and kinematical lopsidedness stem from lopsided dark matter halo potential, we have estimated the ellipticity of the potential.

In this chapter we also give the preliminary results of the N-body simulations of galaxies which we carried out. In this analysis particles were allowed to evolve in a back ground dark matter halo potential. In addition we have given some information about the on going research and future work planned.

All men by nature desire knowledge.

–Aristotle (384 BC - 322 BC)

2

Kinematical Lopsidedness in Spiral Galaxies

2.1 Introduction

A typical spiral galaxy consists of a nucleus and a stellar disk which is embedded in a dark matter halo. The stellar mass in a spiral galaxy is of the order of $10^8 - 10^{12}$ $M_\odot$(Burstein & Rubin, V.C. 1985). The nucleus is mainly made up of old stellar population, which is often termed as classical bulges (Athanassoula, 2005). It also has little amount of gas and dust and has a typical radial extent of ~ 2 kpc in optical. The stellar disk consists of young stellar population and $\sim 10\%$ of it's mass in the form of gas (atomic Hydrogen (HI), molecular hydrogen H_2 etc.)(Spitzer, 1978). In addition the disk contains $\sim 1\%$ its mass in the form of dust (mainly graphites and silicates). The radial extent of the stellar disk is typically 10kpc.

Spiral galaxies are usually modelled as cylindrically symmetric objects with the symmetry axis perpendicular to the stellar disk and centred on the bulge. The stellar disk of the spiral galaxies exhibits a systematic rotational

motion. The axis of rotation is often taken to be the same as the axis of symmetry. When observations of spiral galaxies in non-optical bands began it was noticed that the symmetric distribution and motion of matter around the nucleus of a spiral galaxy is an exception rather than a norm. In a pioneering study, Baldwin et al. (1980) pointed out the large scale spatial asymmetry in the HI gas distribution of four nearby spirals M 101, NGC 891, NGC 2841 and IC 342. Their study, which used the atomic hydrogen [HI] as the tracer for matter distribution, showed that HI distribution in these galaxies is asymmetric or lopsided.

A large fraction ($\sim$ 50%) of spirals show asymmetry. This has been deduced for much larger samples by studying the asymmetry in the global HI profiles (Richter & Sancisi, 1994; Matthews et al., 1998; Haynes et al., 1998) as a function of heliocentric radial velocity. These studies revealed that the HI profiles of the receding and approaching sides of many galaxies were asymmetric (Fig. 1.6). Such studies might indicate only a lower limit for the fraction of galaxies showing lopsidedness or asymmetry. For example, the global HI profile of an axisymmetric galaxy gives a symmetric double horn profile as shown in Fig. 1.7. The double horned profile is symmetric about the systemic velocity, with both the horns having equal HI flux density. An asymmetric galaxy, with its asymmetric axis along the minor axis will also show a symmetric double horn profile about the systemic velocity as the integrated flux along the minor axis will not reveal the asymmetry.

Such large fraction of galaxies showing asymmetry indicate that the lopsidedness is sustainable over at least one rotation period of the galaxies. Yet its physical origin is not clearly understood. The cause of disk lopsidedness has been attributed to a variety of physical processes such

as the disk response to lopsided dark matter halo which could arise due to tidal interactions (Jog, 1997) or due to mergers with satellite galaxies (Zaritsky& Rix, 1997). Due to tidal interactions with a neighbouring galaxy or mergers with satellite galaxies, it is possible to disturb the dark matter halo. Since the disk of the spiral galaxy lies within the dark matter halo, the disk can reflect the asymmetry of the halo. Since a perturbed dark matter halo can retain the perturbed shape for a long period time (compared to the rotation period of the galaxy), lopsidedness of galactic disk can also persist. It is also postulated that the asymmetry can also be the result of a disk being offset in a spherical dark matter halo (Noordermeer et al., 2001) or due to asymmetric external gas accretion and subsequent star formation (Bournaud et al., 2005).

The global HI studies indicate the result of lopsidedness caused jointly by the spatial and velocity distribution. For a given galaxy, these two effects could be decoupled only by separately studying the two dimensional velocity and surface density maps resulting from an interferometric imaging observation. The existence of asymmetry in the velocity domain, i.e., kinematical lopsidedness, has been detected in spiral galaxies. These studies are based on the analysis of asymmetry of the rotation curves on the approaching and receding sides of a galaxy (Swaters et al., 1999) and also by analysing the HI velocity field of a spiral galaxy (Schoenmakers et al., 1997). It is postulated that the same perturbation potential that gives rise to spatial lopsidedness will also unavoidably give rise to kinematical lopsidedness (Jog, 1997; Jog, 2002). However this has not been observationally verified yet.

From theoretical arguments, it is also postulated that the scatter in the Tully-Fisher relation ($L \propto v_{circular}^4$, where L is the luminosity and $v_{circular}$

is the circular velocity (Tully & Fisher, 1977)) can also be explained if the perturbations in gas motion generated due to ellipticity of DM halo potential is taken into account (Franx & de Zeeuw, 1992). Franx et al. (1992) showed that an ellipticity of dark matter potential of ≤ 0.10 can generate perturbations in the circular velocity which corresponds to an uncertainty of ~ 0.46 magnitudes in luminosity. Thus a study of HI asymmetry based on the velocity maps in the outer parts can give a direct handle on the dark matter halo asymmetry if the disc lopsidedness arises due to halo asymmetry.

In this work we are analysing the kinematical lopsidedness of galaxies belonging to two groups, *viz.* Eridanus and Ursa Major Group. Both these groups are loose groups (Omar & Dwarakanath, 2005a; Verheijen & Sancisi, 2001) , where tidal interactions between galaxies are expected to dominate. This implies that groups of galaxies will be an ideal environment to study the effect of tidal interactions on lopsidedness and on the ellipticity of the dark matter halo potential.

2.2 Data

The data used in this analysis were obtained using the Giant Meterwave Radio Telescope (GMRT) and the Westerbork Synthesis Radio Telescope (WSRT) by Omar & Dwarakanath (2005) and Verheijen & Sancisi (2001) respectively. Although details of these two facilities are given elsewhere (Swarup et al., 1991; Raimond & Genee, 1996) (or from the following web addresses: For GMRT `http://www.gmrt.ncra.tifr.res.in/gmrt_hpage/GMRT/intro_gmrt.html` and for WSRT `http://www.astron.nl/wsrt/wsrtGuide/`), for completeness sake a brief description of both telescopes are given here.

2.2.1 Giant Meterwave Radio Telescope

GMRT consists of 30 fully steerable parabolic dish antennas. Each of these antennas are of 45 m diameter. These antennas are distributed in the shape of a `Y` which is optimised for having high angular resolution as well as sensitivity to extended emission. A large fraction of these antennas (14 of them) are randomly distributed in the central 1 square kilometer and the remaining 16 antennas are almost equally distributed along the arms of the `Y`. The shortest separation between the antennas is $\sim$ 100 meters and the longest is $\sim$ 25 kilometers. Such a distribution of antennas makes GMRT sensitive to structures in the range of $2''$ - $7'$ at 21 cm wavelength. Since the galaxies in the Eridanus Group have typical sizes of 1-5$'$, GMRT is an ideal instrument to effectively image them in HI 21 cm-line.

2.2.2 Westerbork Synthesis Radio Telescope

Westerbork Synthesis Radio Telescope (WSRT) consists of fourteen, 25-m diameter dishes. They are arranged in the East-West direction. Ten of the antennas are fixed while the remaining four can be moved in the East-West direction on rails. The separation between any two of the 10 fixed antennas is 144m. The movable antennas are grouped into 2 groups consisting of 2 antennas each. Both these groups are also arranged in the East-West direction. The first group is at a distance of 36 m from the Eastern-most fixed telescope, while the other group is at a distance of $\sim$ 1.4 km away from the first group of movable antennas. As a result of such a distribution of antennas, WSRT has the shortest baseline of 36 meters. Inspite of its sensitivity to extended structures, due to its east-west arrangement, a full synthesis imaging of an object in the sky will require $\sim$ 12 hours or more.

2.2.3 The Eridanus Group of Galaxies

The Eridanus group is a loose group of galaxies at a mean distance of $\sim 23\pm2$ Mpc in the southern hemisphere ($\sim 3^h \leq \alpha \leq 4.5^h$, $\sim -10^\circ \geq \delta \geq -30^\circ$). From the redshift values, ~ 200 galaxies are associated with this group with heliocentric velocities in the range of $\sim 1000 - 2200$ km s^{-1}. The observed velocity dispersion is $\sim$ 240 km s^{-1}. Even though there are sub-groups within the system, the overall population mix of the galaxies in the Eridanus group was found to be $\sim 30\%$ ellipticals and lenticulars and $\sim 70\%$ spirals and irregulars (Omar & Dwarakanath, 2005a). Though HI was detected in 31 galaxies out of the 57 selected for observation by Omar and Dwarakanath using the Giant Meter-wave Radio Telescope (GMRT), the spiral galaxies under consideration here form a subset of these. These spiral galaxies were chosen on the basis of their inclination, with inclinations in the range of 20° and 80°. This criterion was adopted so as to get good velocity maps. If a galaxy is face on, the circular velocity of the galaxy will not have any component along the line of sight direction. As a result it will not be possible for the observer to have any information about the circular velocity of the galaxy. In addition to this, we eliminated those galaxies where the detection in HI was patchy such as NGC 1415.

The positions and Heliocentric velocities of selected galaxies are given in Table 2.1.

The HI surface density and velocity maps of the selected galaxies used in this analysis were derived out of image cubes which were convolved to a common resolution of$20'' \times 20''$. A 3σ HI column density sensitivity of 10^{20} cm^{-2} was obtained for $20''$ resolution surface density images. The velocity resolution was ~ 13.4 km s^{-1}. A typical HI surface density contour map and velocity contour map superposed on the DSS image are shown in

Table 2.1: The Type, RA & DEC values, inclination and position angle of Eridanus Group of galaxies selected for kinematical analysis

Galaxy	Type	α(J2000) h m s	δ(J2000) ° ′ ″	cz (km/s)	Inclin(i) (Deg)	PA (Deg)
NGC 1309	SAbc	03 22 06.5	-15 24 00	2135	20	210
UGCA 068	SABcdm	03 23 47.2	-19 45 15	1838	34	35
NGC 1325	SAbc	03 24 25.4	-21 32 36	1589	71	232
NGC 1345	SBc	03 29 31.7	-17 46 40	1529	34	88
NGC 1347	SBcd	03 29 41.8	-22 16 45	1759	26	328
UGCA 077	SBdm	03 32 19.2	-17 43 05	1961	66	149
IC 1953	SBd	03 33 41.9	-21 28 43	1867	37	129
NGC 1359	SBcm	03 33 47.7	-19 29 31	1966	53	325
NGC 1371	SABa	03 35 02.0	-24 55 59	1471	49	136
ESO 548- G 049	S?	03 35 28.1	-21 13 01	1510	71	128
ESO 482- G 013	Sb	03 36 53.9	-24 54 46	1835	63	65
NGC 1385	SBcd	03 37 28.3	-24 30 05	1493	40	181
NGC 1390	SB0/a	03 37 52.2	-19 00 30	1207	60	24
NGC 1414	SBbc	03 40 57.0	-21 42 47	1681	80	357
ESO 482- G 035	SBab	03 41 15.0	-23 50 10	1890	49	185
NGC 1422	SBab	03 41 31.1	-21 40 54	1637	80	65
MCG -03-10-041	SBdm	03 43 35.5	-16 00 52	1215	57	343
ESO 549- G 035	Sc	03 55 04.0	-20 23 01	1778	56	30

Fig. 2.1.

2.2.4 The Ursa Major Group

The Ursa Major group is defined as the group of galaxies seen within a circle of radius 7.5° centred at RA $11^h56.9'$ and DEC $+49°22'$ (Tully et al. 1996). The systemic velocity of this group is 950 km s^{-1} with a dispersion of 150km s^{-1} (Verheijen & Sancisi, 2001). Seventy nine galaxies have been associated with this group (Tully et al. 1996) and this group had a projected density of 3 galaxies per Mpc^{-2}. Due to the small velocity dispersion, it is not yet clear whether it can be classified as a cluster as mentioned in Tully

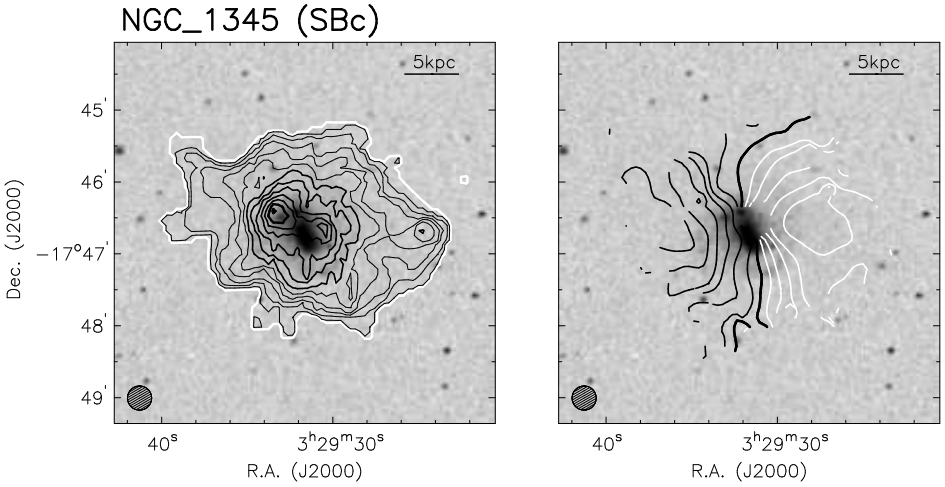

Figure 2.1: Typical HI and velocity map of a galaxy in the Eridanus group. The contours are superposed on DSS gray scale image. The beam is shown at the bottom left hand corner. The surface density map contour levels are separated by 2×10^{20} cm^{-2}. The first contour, shown in white, is at a column density of 1×10^{20} cm^{-2}. The first thick contour begins at 1.2×10^{21} cm^{-2} and the second one is at 2.2×10^{21} cm^{-2}. The velocity contours for the approaching side are shown in white while that for the receding side are shown in black. The velocity contours differ from each other by 10 km s^{-1}. The thick dark line near the centre of the galaxy denotes the systemic velocity (Omar & Dwarakanath 2005a).

et al.(1996). In addition this group contains a smaller fraction of early-type galaxies ($\sim$ 14% (E+S0) and a larger fraction of late-type galaxies $\sim$ 86% (Sp+Irr)(Tully et al. 1996)) This system does not show a central concentration (Verheijen & Sancisi, 2001) which is atypical for a cluster and more similar to that found in a group.

Out of the 49 galaxies observed using the Westerbork Synthesis Radio Telescope (WSRT) by Verheijen and Sancisi (2001) , we have selected 11 galaxies on the basis of their inclination and quality of HI maps (galaxies, whose HI maps were patchy were rejected) for further analysis. The right ascension (α), declination (δ), systemic velocity (V_{sys}), inclination (i) and Position Angle (PA) of these galaxies are given in Table 2.2. After rejecting

galaxies which had patchy appearance, galaxies in the sample available to us had inclinations in the range 45° to 70°. As mentioned earlier, this inclination range ensured the availability of good quality HI velocity maps, essential for the analysis (Block et al. 2002; Bournaud et al., 2005). Details of the observation and the preliminary data reduction are given elsewhere (Verheijen & Sancisi, 2001).

Table 2.2: The sample of galaxies selected for kinematical lopsidedness analysis from the Ursa Major group of galaxies (Verheijen & Sancisi, 2001)

Name	Type	α**(J2000)**	δ**(J2000)**	V_{sys}	Inclin	PA
		h m s	° ′ ″	(km s^{-1})	(°)	(°)
UGC 6446	Sd	11 26 40.4	53 44 48	644.3	54	200
NGC 3726	SBc	11 33 21.2	47 01 45	865.6	54	194
NGC 3893	Sc	11 48 38.2	48 42 39	967.2	49	352
NGC 3949	Sbc	11 53 41.4	47 51 32	800.2	54	297
NGC 3953	SBbc	11 53 48.9	52 19 36	1052.3	62	13
UGC 6917	SBd	11 56 28.8	50 25 42	910.7	59	123
NGC 3992	SBbc	11 57 36.0	53 22 28	1048.2	58	248
UGC 6983	SBcd	11 59 09.3	52 42 27	1081.9	50	270
NGC 4051	SBbc	12 03 09.6	44 31 53	700.3	50	311
NGC 4088	Sbc	12 05 34.2	50 32 21	756.7	71	231
NGC 4389	SBbc	12 25 35.1	45 41 05	718.4	50	276

For the sake of completeness, a summary of the data reduction procedure is given here. The observations were carried out using the WSRT radio telescope. The FWHM of the primary beam of the telescope is $37.4'$. This resulted in having more than one Ursa Major group galaxy being present in the field of view. Each pointing on the Ursa Major group had a typical duration of 12 to 60 hours. The raw UV data so obtained were calibrated, interactively flagged and Fast Fourier Transformed using the NEWSTAR software developed at the NFRA, Dwingeloo specifically meant for WSRT data reduction. The resulting data cubes were further processed using the

Groningen Image Processing SYstem (GIPSY)(van der Hulst et al. 1992). All the data cubes were smoothed to $30'' \times 30''$ and continuum subtraction was carried out. The resulting cubes were used to obtain the HI-surface density (Moment 0) and HI-velocity (Moment 1) maps. The typical 3σ column density of $10^{20}\mathrm{cm}^{-2}$ was obtained for the moment 0 maps. The moment 1 maps had typical velocity resolution of $\sim 19\mathrm{kms}^{-1}$. It should be emphasised that the galaxies in the Eridanus group were convolved to a common angular resolution of $\sim 20''$ (~ 2.24kpc) and had a velocity resolution (~ 10 km s^{-1}) (Omar & Dwarakanath, 2005a). These values were comparable to that of galaxies belonging to the Ursa Major.

2.3 Harmonic Analysis of Radio Data

We have adopted the harmonic analysis for analysing the data. In HI, where both velocity maps and surface density maps are available, the analysis technique is different from that adopted in optical analysis. The procedure assumes that in an ideal galaxy, HI is in pure circular motion. Hence we have,

$$V(x,y) = V_0 + V_c\cos(\phi')\sin(i) + V_r\sin(\phi')\sin(i) \qquad (2.1)$$

where $V(x,y)$ is the velocity at the rectangular coordinate (x,y),V_0 is the systemic velocity, V_c is the rotation velocity, i is the inclination and V_r is the expansion velocity which was taken to be zero. The azimuthal angle (ϕ') measured in the plane of the galaxy, is given by the equations

$$\cos(\phi') = \frac{-(x-x_0)\sin(PA) + (y-y_0)\cos(PA)}{r} \qquad (2.2)$$

$$\sin(\phi') = \frac{-(x-x_0)\cos(PA) + (y-y_0)\sin(PA)}{r\cos(i)} \qquad (2.3)$$

where $r = \sqrt{((x - x_0)^2 + (y - y_0)^2/\cos(i)^2)}$. In these equations, (x_0, y_0) is the kinematic centre of the galaxy, PA is the position angle of the galaxy measured in the anti-clockwise direction from north. Using these equations, the five unknown parameters, namely (x_0, y_0), PA, V_c and i were estimated using the GIPSY task ROTCUR (Begeman, 1989), which fits tilted rings to the velocity maps, in an iterative manner (Wong et al. 2003; Omar & Dwarakanath, 2005a). As per the algorithm of ROTCUR, initially the galaxies velocity field is divided into concentric rings where each ring separated by a synthesized beam. Approximate values of (x_0, y_0), PA, V_c and i obtained from the optical observations are given as an input to ROTCUR. ROTCUR calculates the initial estimate of the radial velocity at the sky coordinates (x, y) using the given approximate values of (x_0, y_0), i and PA and compares it with the observed value of velocity at (x, y). A least-square minimization is carried out using the calculated and observed radial velocity values taking (x_0, y_0), PA, V_c and i as the parameters. This procedure is repeated in an iterative manner. As a result of ROTCUR analysis on the velocity fields of galaxies it was observed that the dynamical centre, derived from velocity maps were less than $2''$ away from the optical centre. Hence, for all the calculations the optical centre was used.

Kinematical Lopsidedness in HI

The five parameters i.e. the coordinates of the centre (x_0, y_0), systemic velocity (V_0), circular velocity (V_c), inclination (i) and the position angle (PA), estimated from the velocity maps using the iterative use of GIPSY routine ROTCUR were given as the input to another GIPSY routine called RESWRI along with the velocity maps to obtain the harmonic coefficients.

At each radii (r), RESWRI expanded the line of sight velocity in the

form

$$v_{los}(r,\phi') = c_0 + \sum_{m=1} c_m \cos(m\phi') + s_m \sin(m\phi') \qquad (2.4)$$

where, c_m,s_m are the harmonic coefficients (see Appendix for an interpretation of these coefficients in terms of the perturbing potential), c_0 is identical to the systemic velocity V_0 and ϕ' is the azimuthal angle. These harmonic coefficients were derived at concentric radii which were separated by a synthesized beam width. In our analysis we have derived the harmonic coefficients up to the 10^{th} order. This was partially prompted by the observation that effects of bars tend to retain the strength of the Fourier coefficients even for m=10 terms (Buta et al. 2003). Typical velocity harmonic coefficients of the galaxies in the Eridanus group are shown in Fig. 2.2 to Fig. 2.12. Similarly the velocity harmonic coefficients of the Ursa Major group are shown in Fig. 2.13 to Fig. 2.23. In each of these images, the lower left hand panel shows the power in various orders of harmonic coefficients. The lower right hand panel shows the V_{sys} values for various rings.

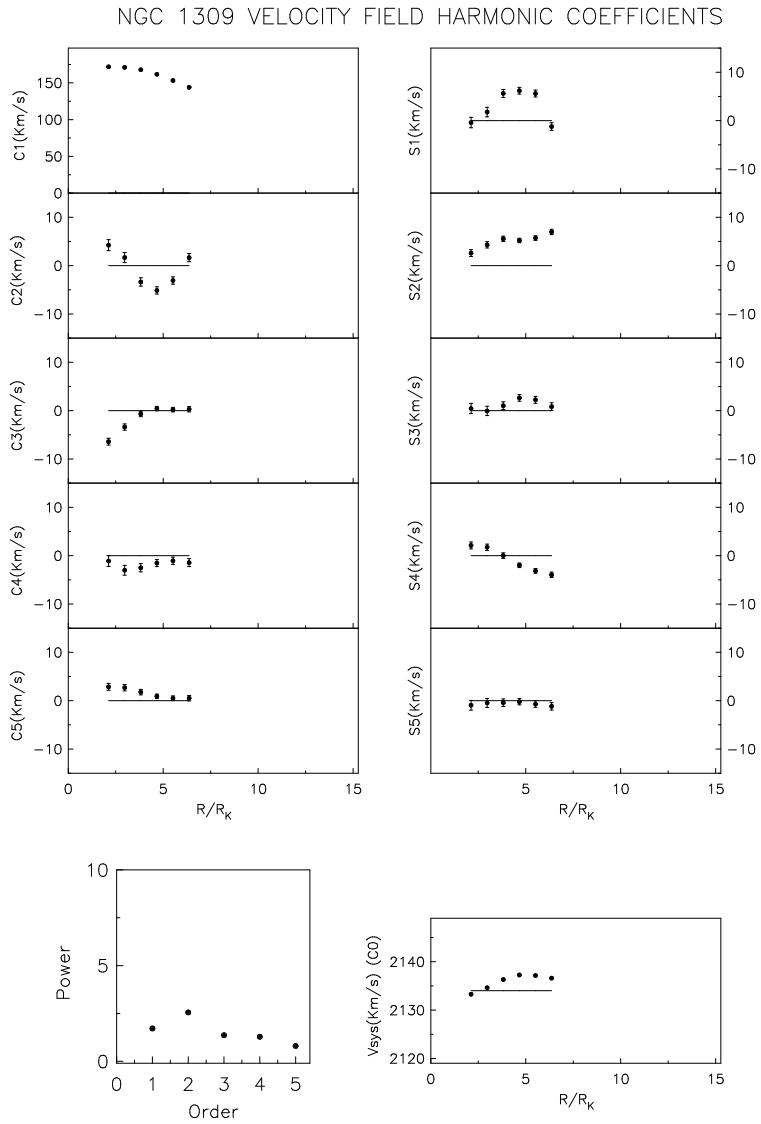

Figure 2.2: Velocity harmonic coefficients of NGC 1309 galaxy in the Eridanus group. R_k is the K-band scale length (1.32 kpc)

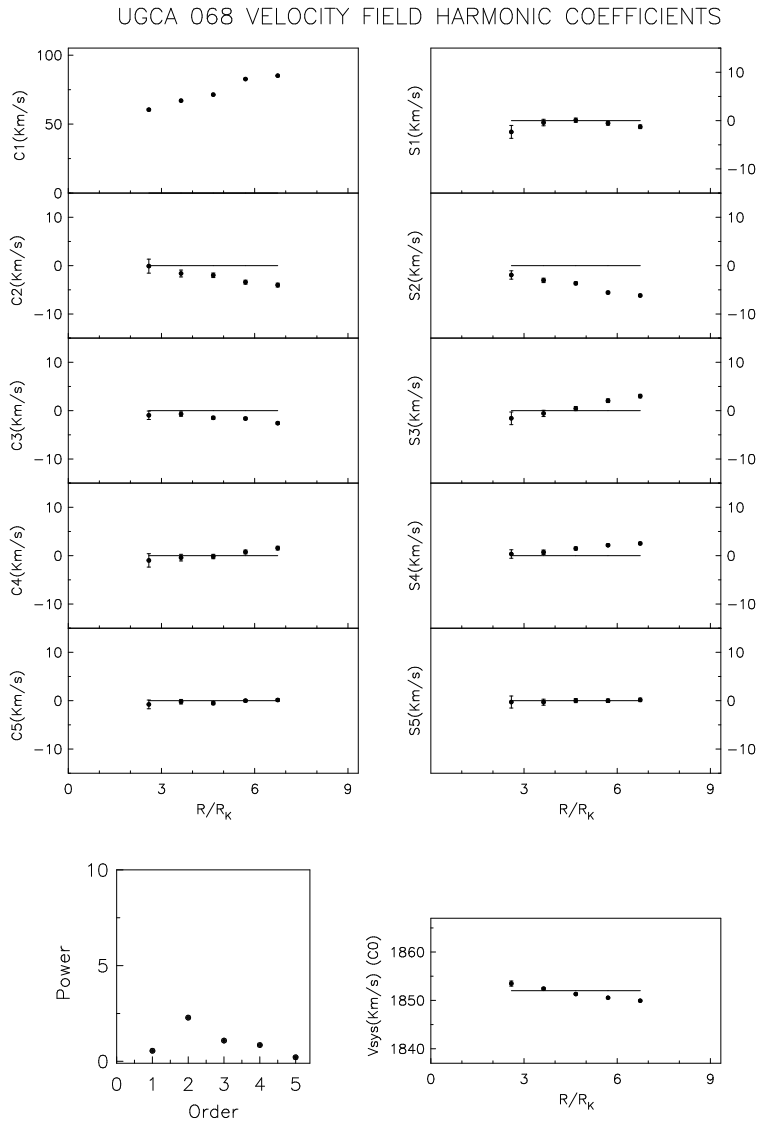

Figure 2.3: Velocity harmonic coefficients of UGC 068 galaxy in the Eridanus group. R_k is the K-band scale length (1.08 kpc)

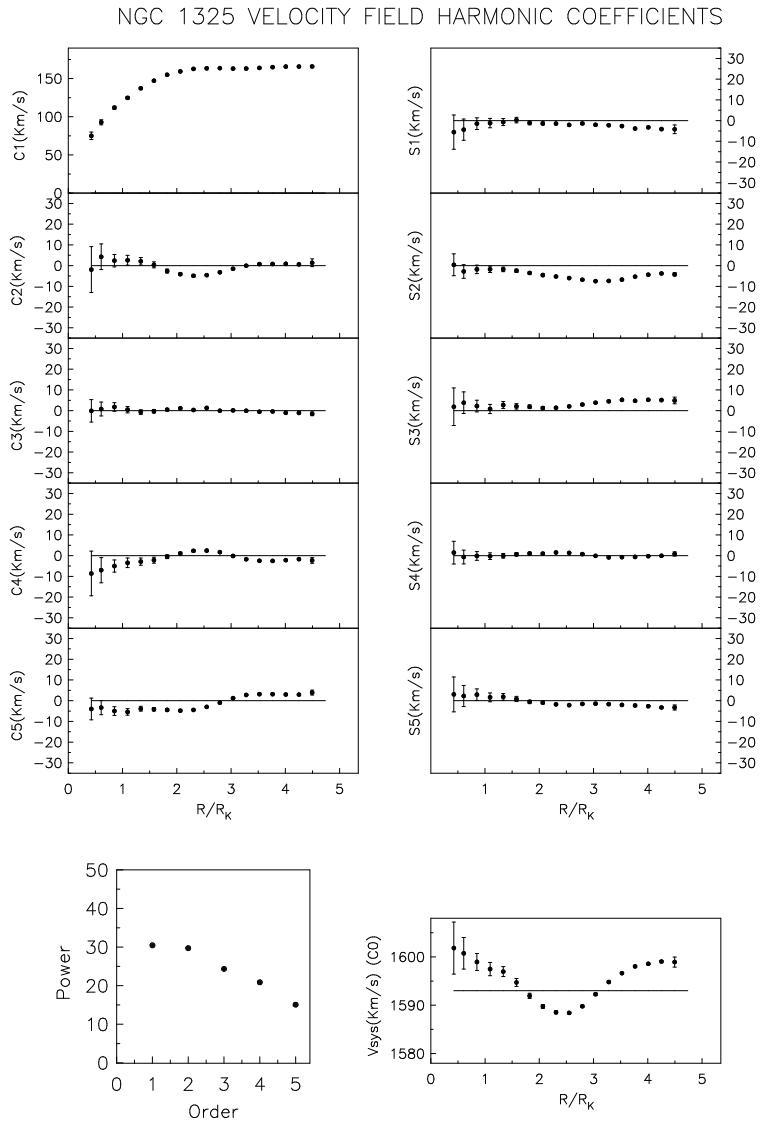

Figure 2.4: Velocity harmonic coefficients of NGC 1325 galaxy in the Eridanus group. R_k is the K-band scale length (4.61 kpc)

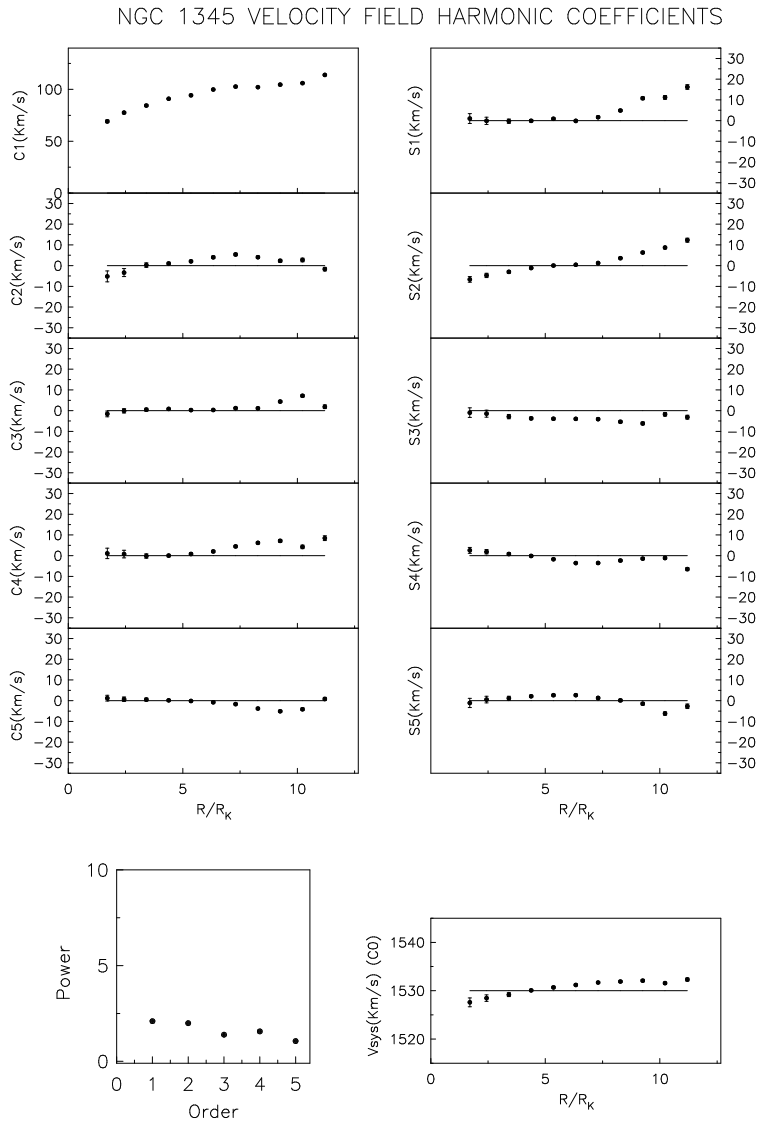

Figure 2.5: Velocity harmonic coefficients of NGC 1345 galaxy in the Eridanus group. R_k is the K-band scale length (1.15 kpc)

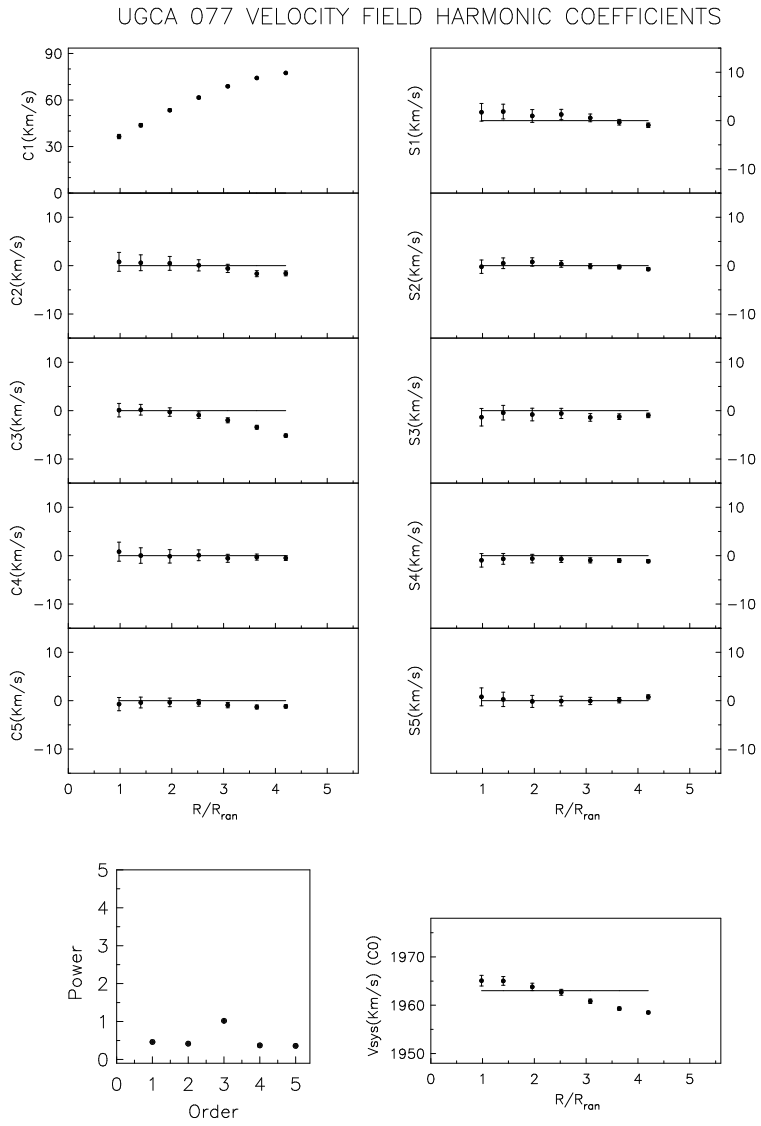

Figure 2.6: Velocity harmonic coefficients of UGC 077 galaxy in the Eridanus group. R_k is the K-band scale length (take to be 2 kpc)

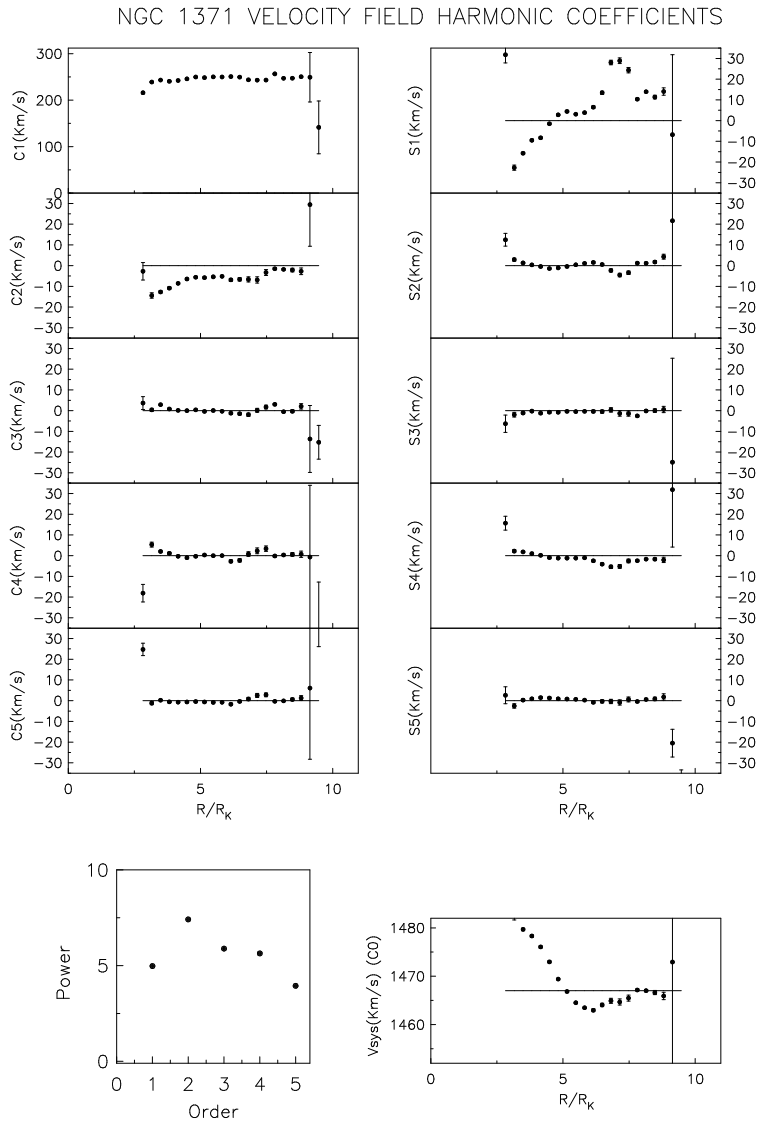

Figure 2.7: Velocity harmonic coefficients of NGC 1371 galaxy in the Eridanus group. R_k is the K-band scale length (3.37 kpc)

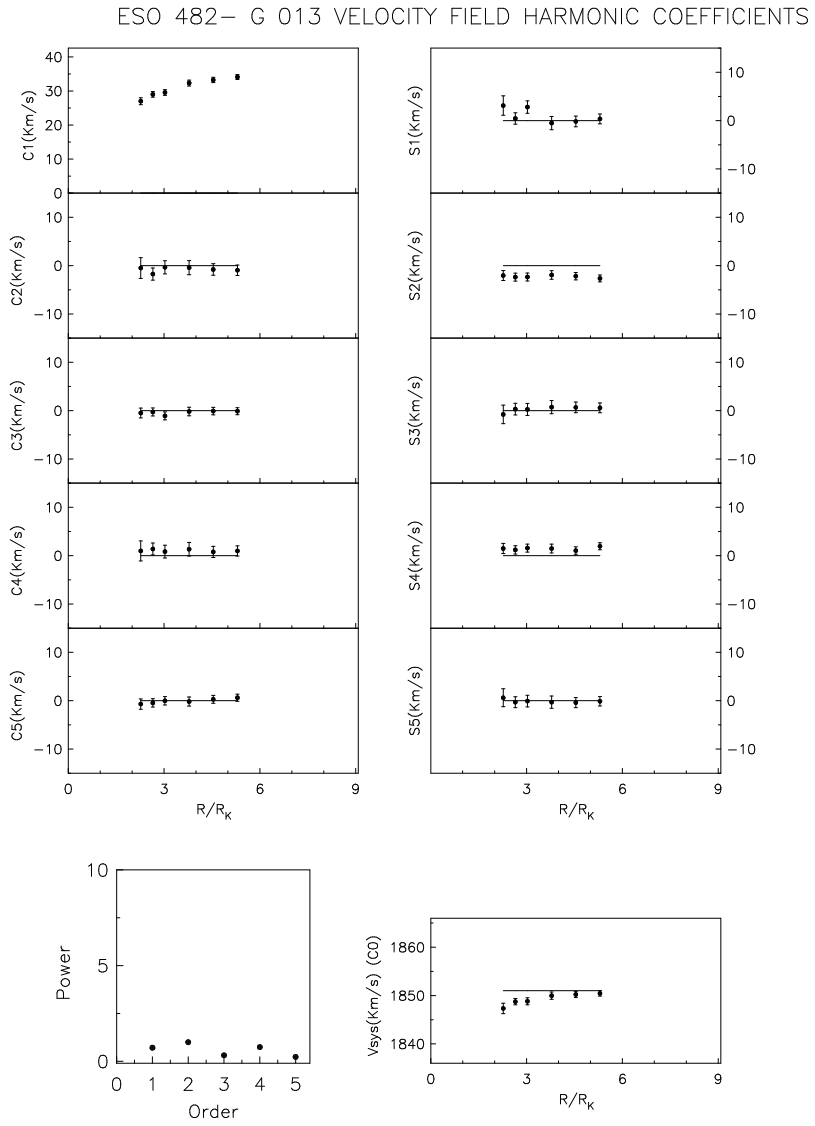

Figure 2.8: Velocity harmonic coefficients of ESO 482 -G 013 galaxy in the Eridanus group. R_k is the K-band scale length (0.74 kpc)

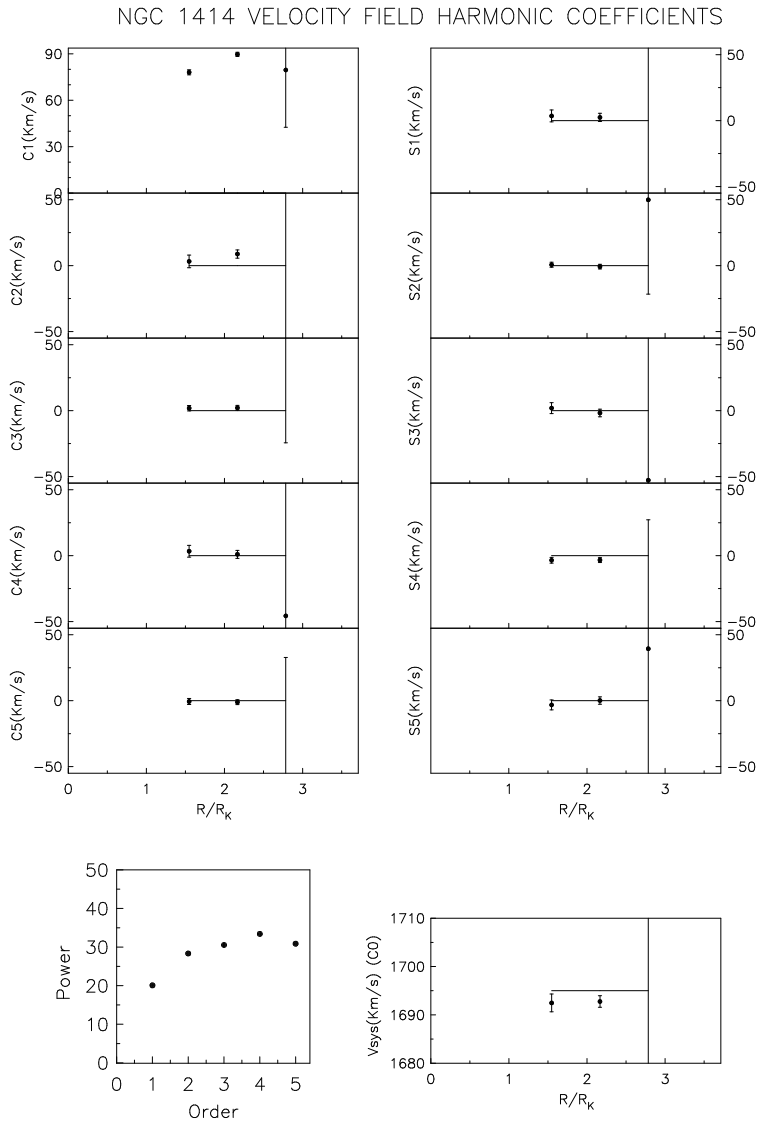

Figure 2.9: Velocity harmonic coefficients of NGC 1414 galaxy in the Eridanus group. R_k is the K-band scale length (1.81 kpc)

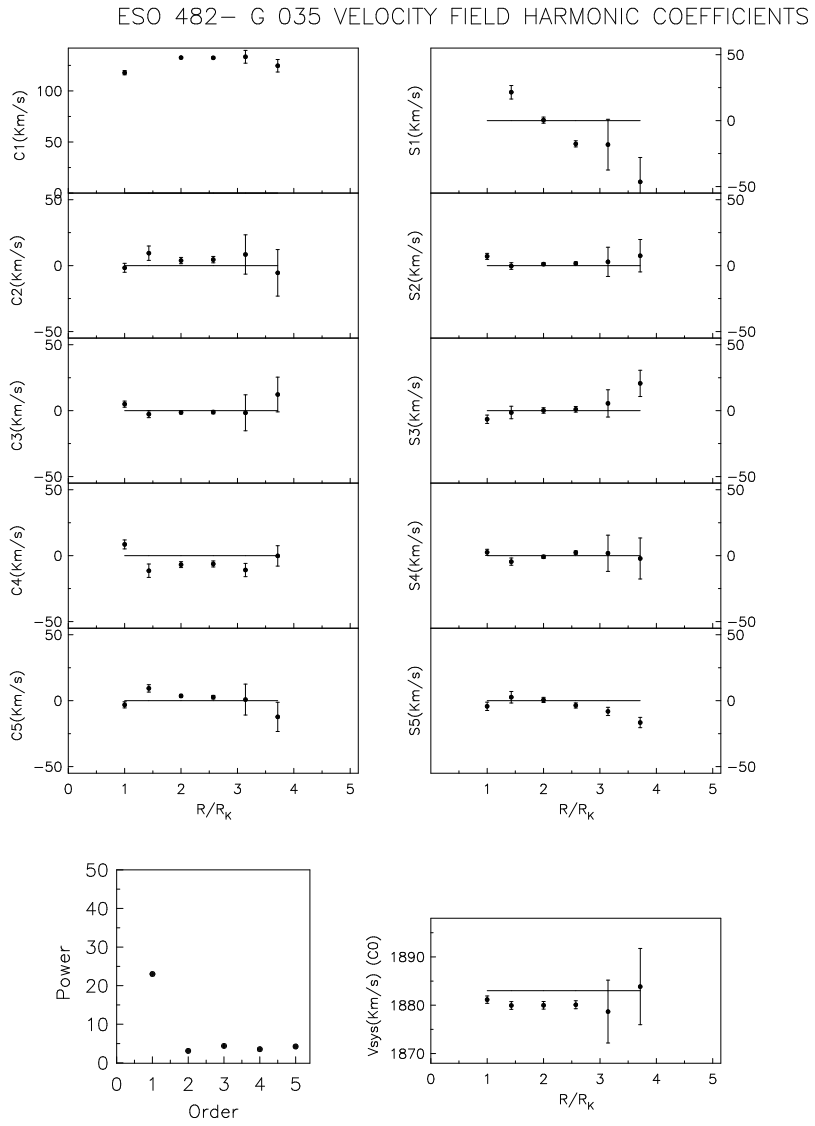

Figure 2.10: Velocity harmonic coefficients of ESO 482 -G 035 galaxy in the Eridanus group. R_k is the K-band scale length (1.96 kpc)

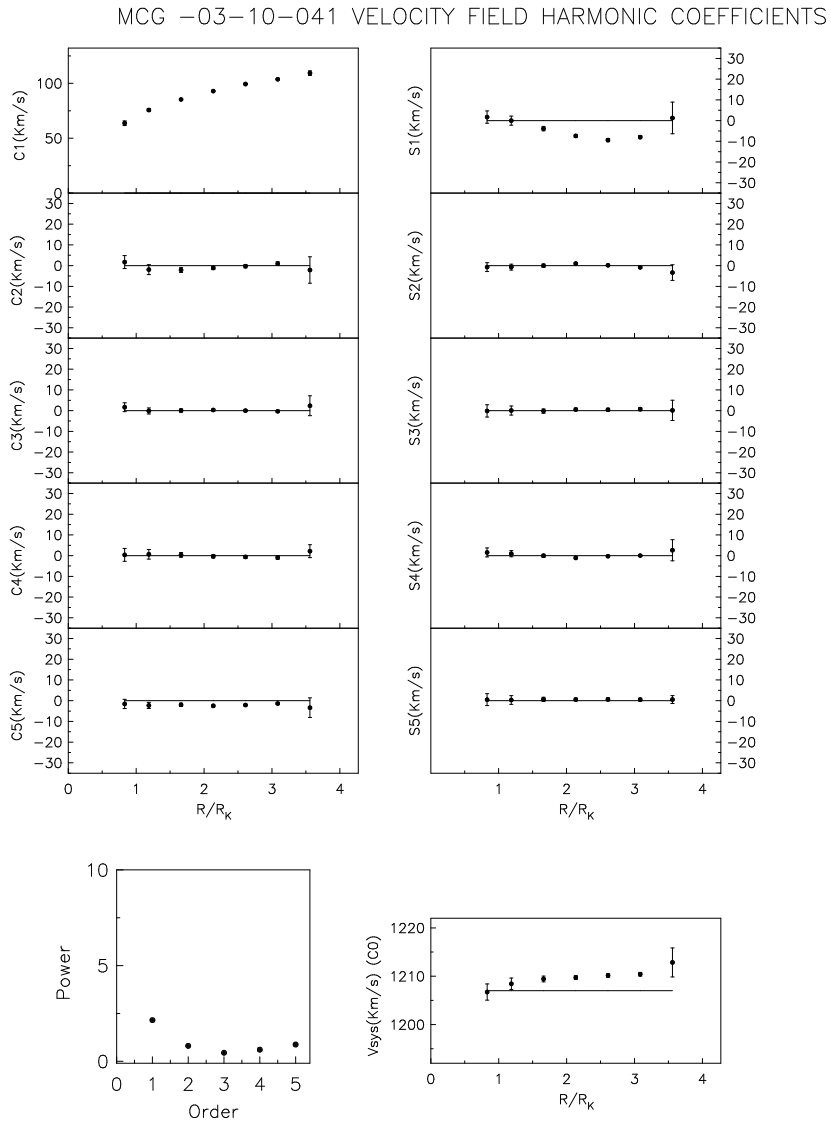

Figure 2.11: Velocity harmonic coefficients of MCG 03-10-041 galaxy in the Eridanus group. R_k is the K-band scale length (2.36 kpc)

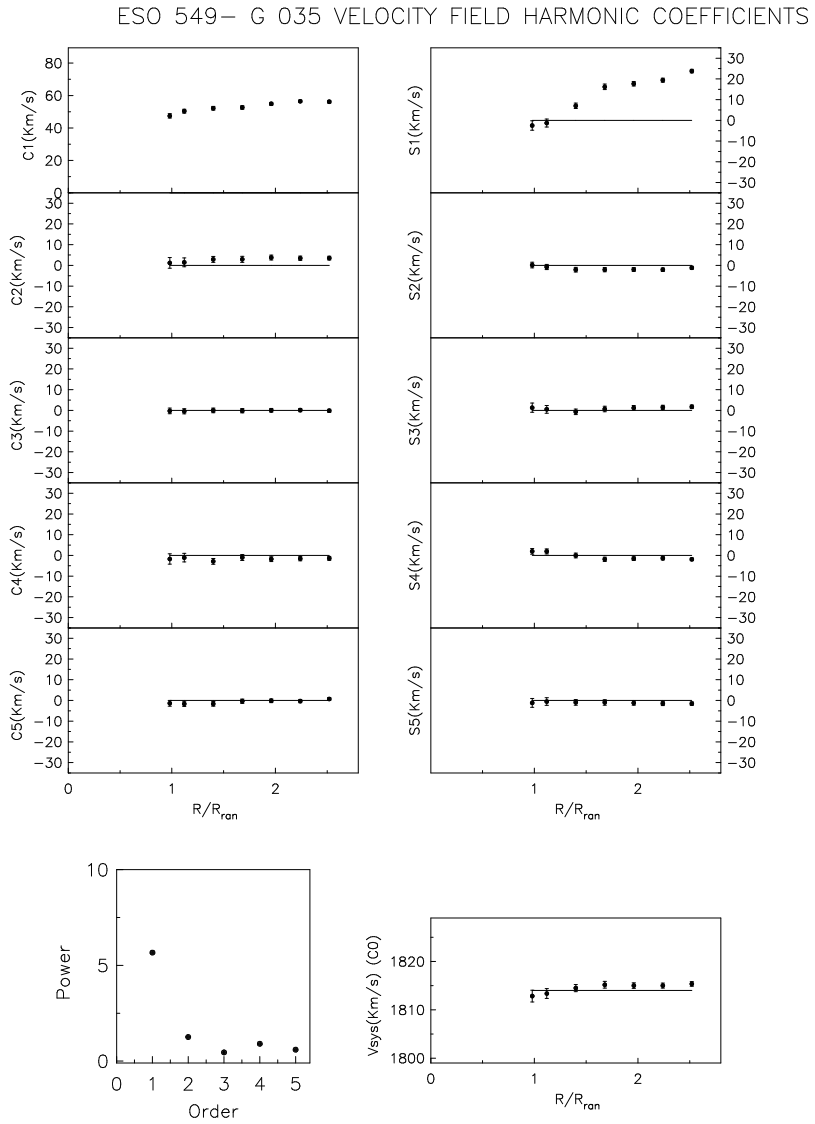

Figure 2.12: Velocity harmonic coefficients estimated for the ESO 549 -G 035 belonging to the Eridanus Group. R_k is the K-band scale length (taken to be 2 kpc)

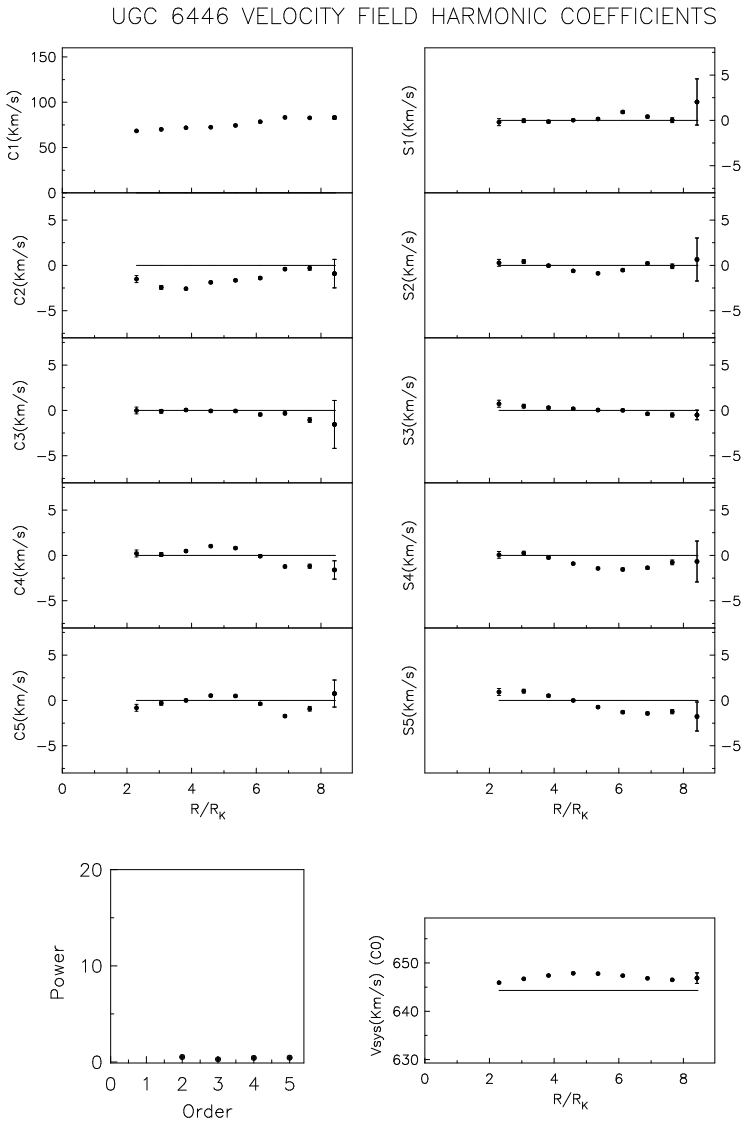

Figure 2.13: Velocity harmonic coefficients estimated for UGC 6446 galaxy belonging to the Ursa Major group. R_k is the K-band scale length (0.82 kpc)

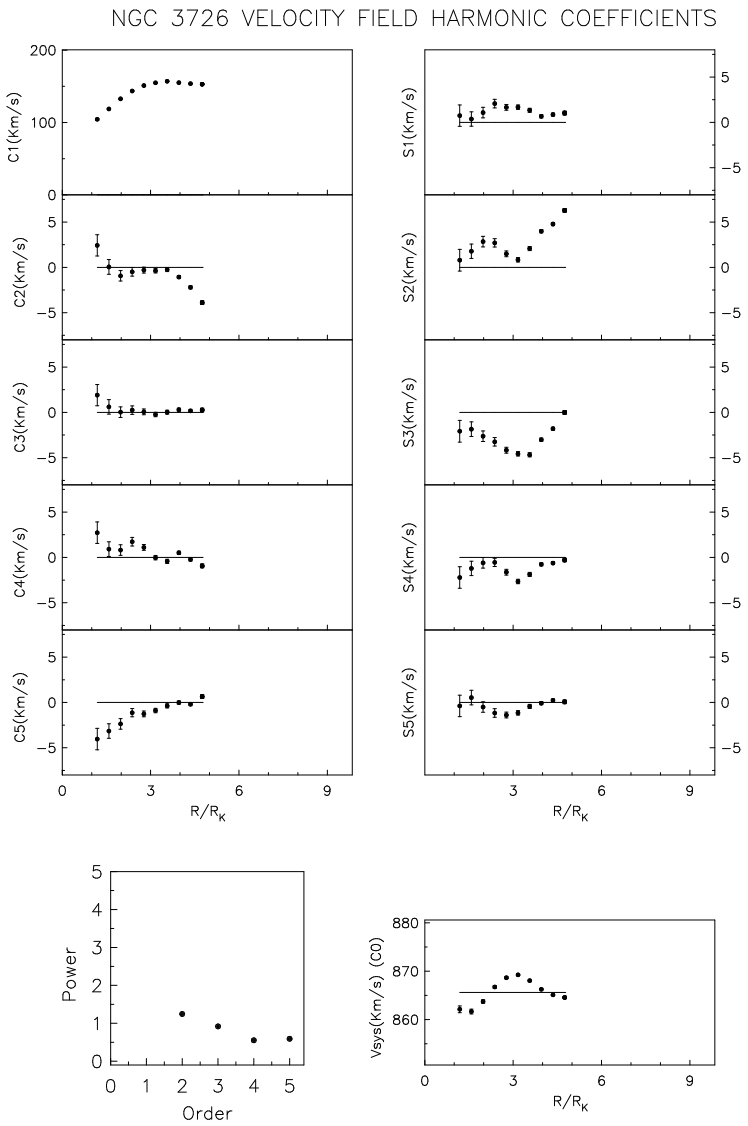

Figure 2.14: Velocity harmonic coefficients estimated for NGC 3726 galaxy belonging to the Ursa Major group. R_k is the K-band scale length (2.12 kpc)

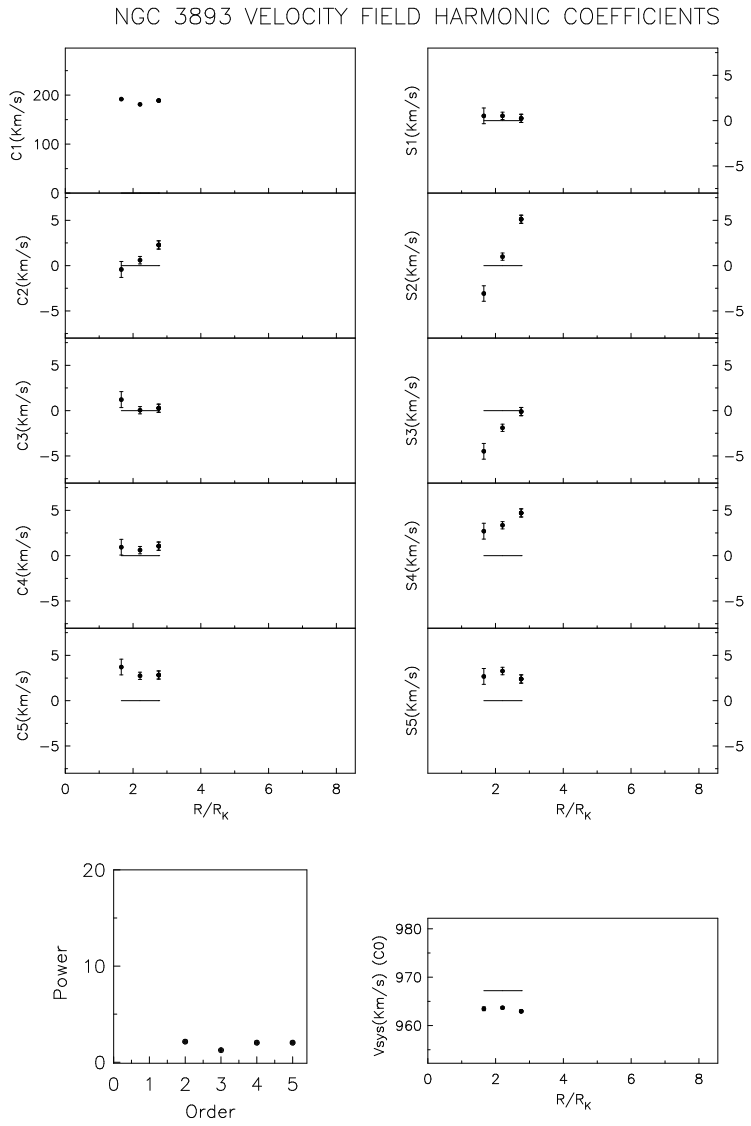

Figure 2.15: Velocity harmonic coefficients estimated for NGC 3893 galaxy belonging to the Ursa Major group. R_k is the K-band scale length (1.7 kpc)

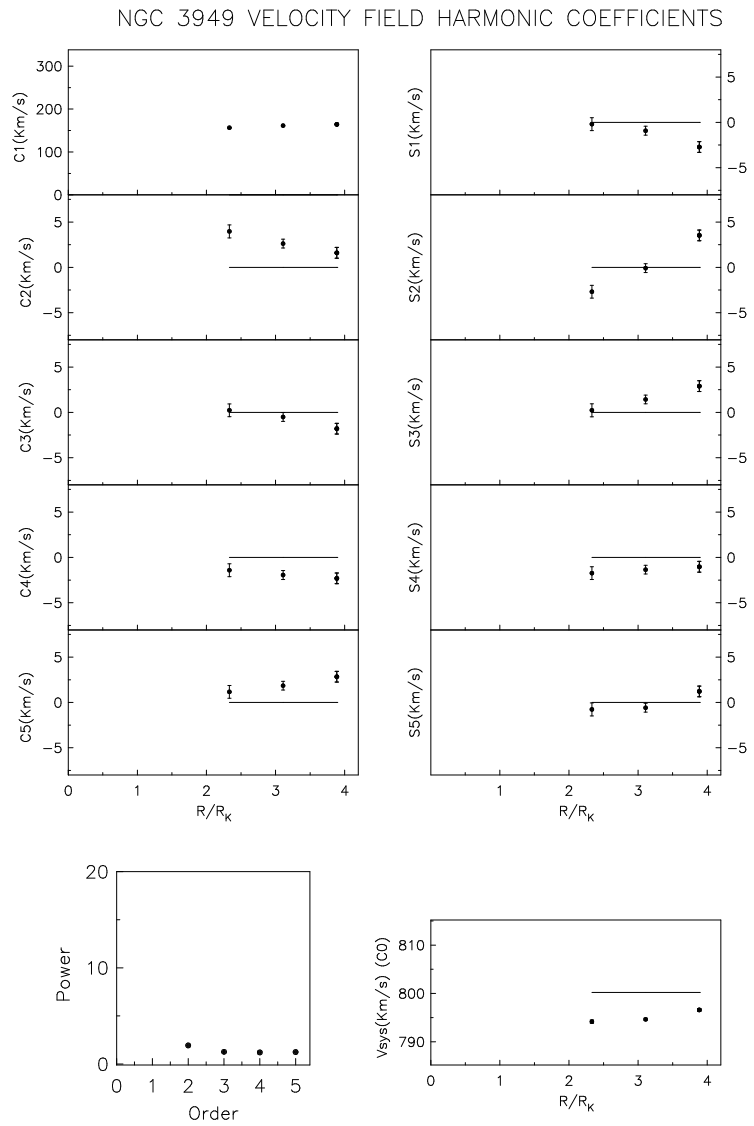

Figure 2.16: Velocity harmonic coefficients estimated for NGC 3949 galaxy belonging to the Ursa Major group. R_k is the K-band scale length (1.00 kpc)

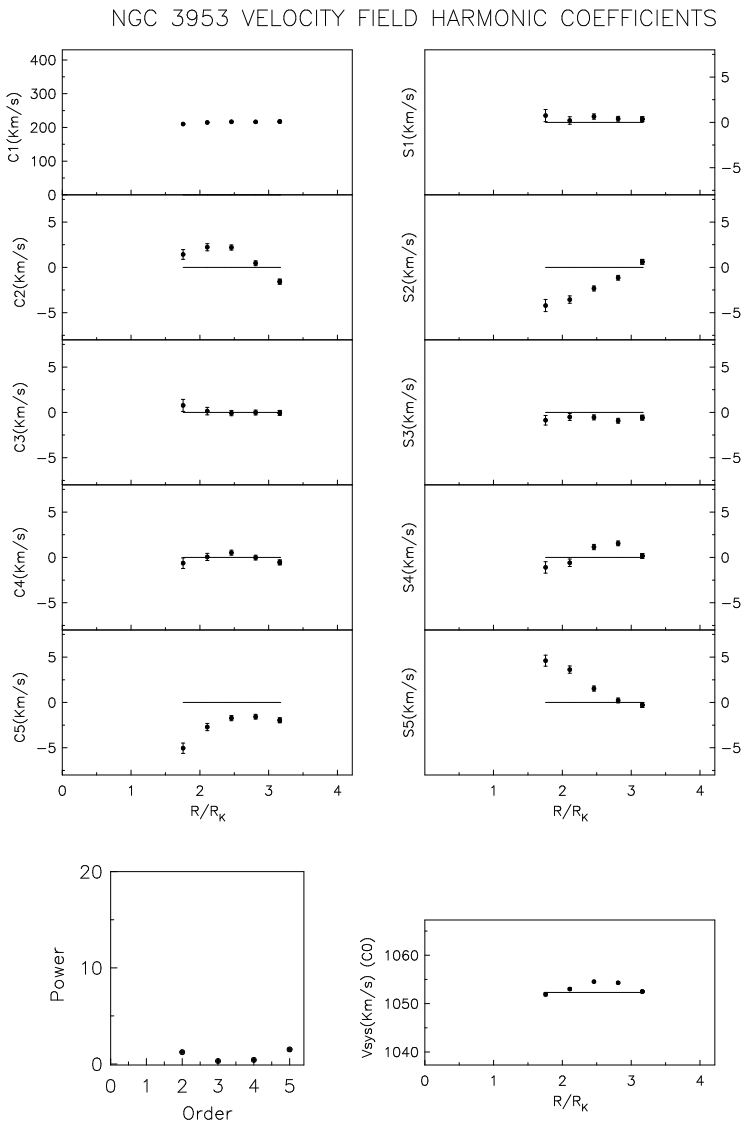

Figure 2.17: Velocity harmonic coefficients estimated for NGC 3953 galaxy belonging to the Ursa Major group. R_k is the K-band scale length (2.90 kpc)

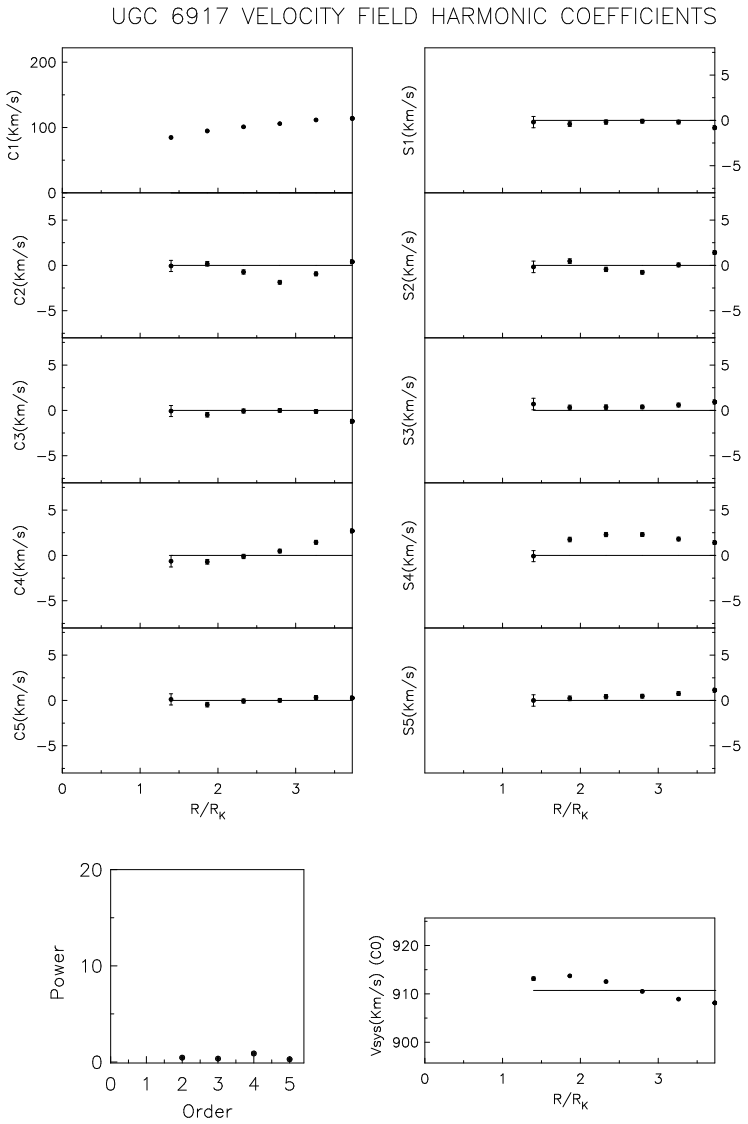

Figure 2.18: Velocity harmonic coefficients estimated for UGC 6917 galaxy belonging to the Ursa Major group. R_k is the K-band scale length (1.90 kpc)

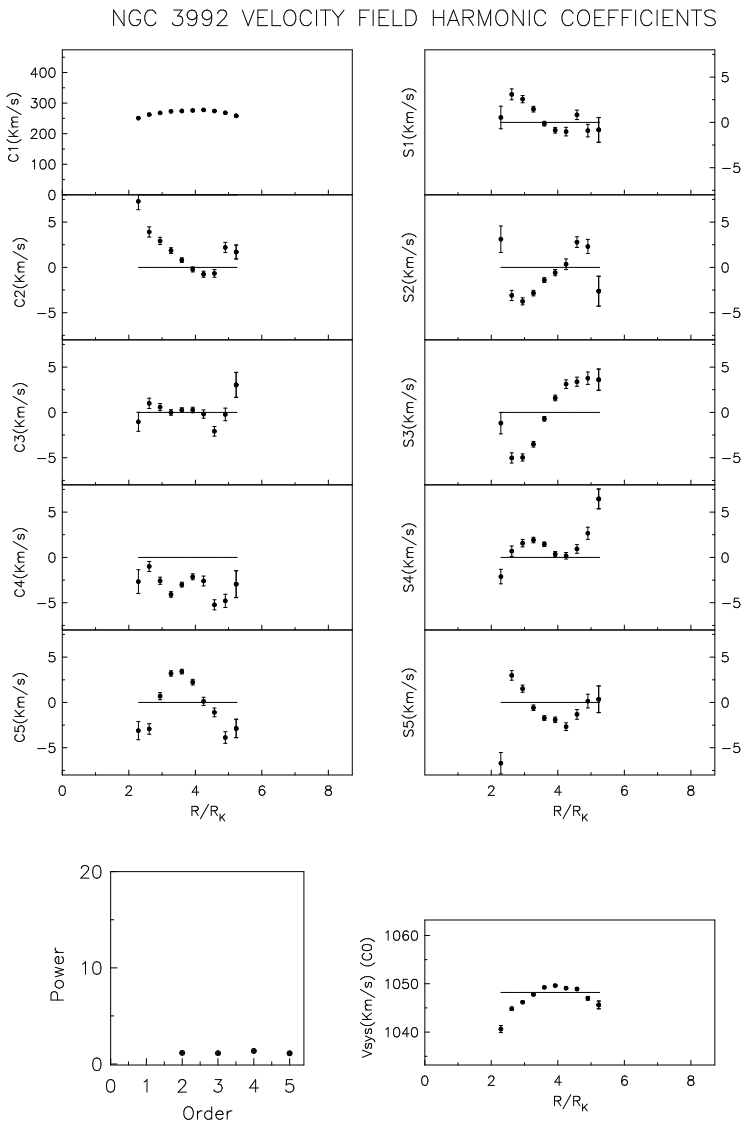

Figure 2.19: Velocity harmonic coefficients estimated for NGC 3992 galaxy belonging to the Ursa Major group. R_k is the K-band scale length (3.11 kpc)

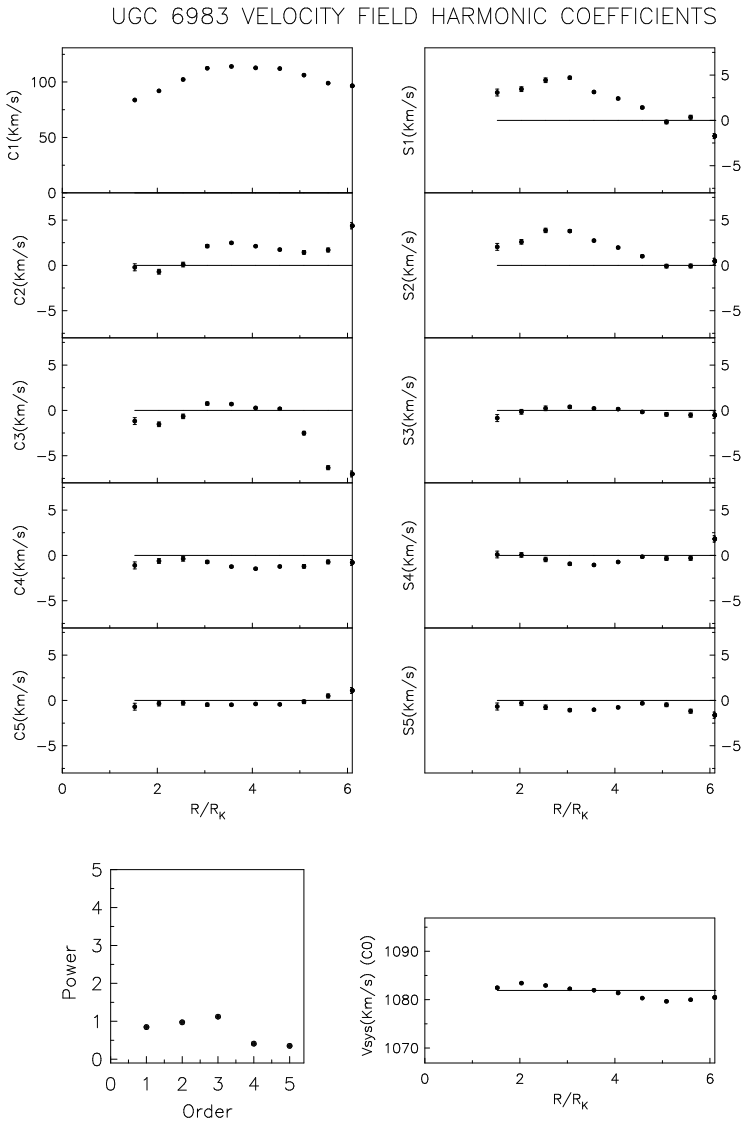

Figure 2.20: Velocity harmonic coefficients estimated for UGC 6983 galaxy belonging to the Ursa Major group. R_k is the K-band scale length (2.06 kpc)

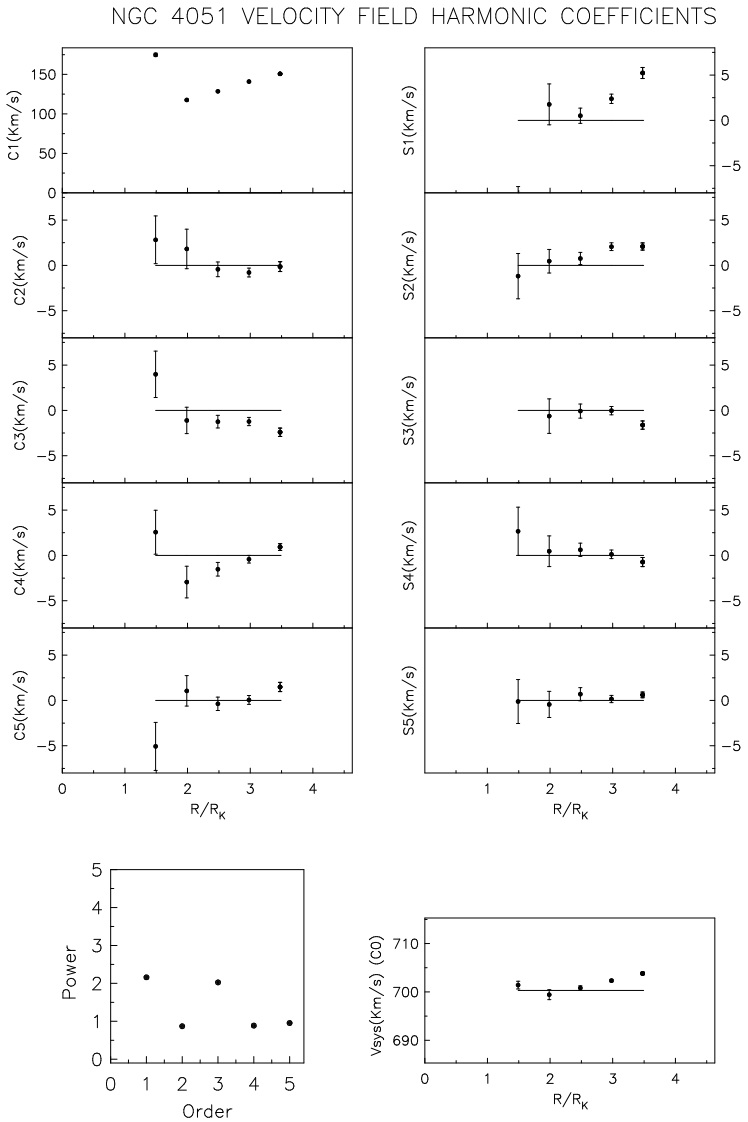

Figure 2.21: Velocity harmonic coefficients estimated for NGC 4051 galaxy belonging to the Ursa Major group. R_k is the K-band scale length (1.37 kpc)

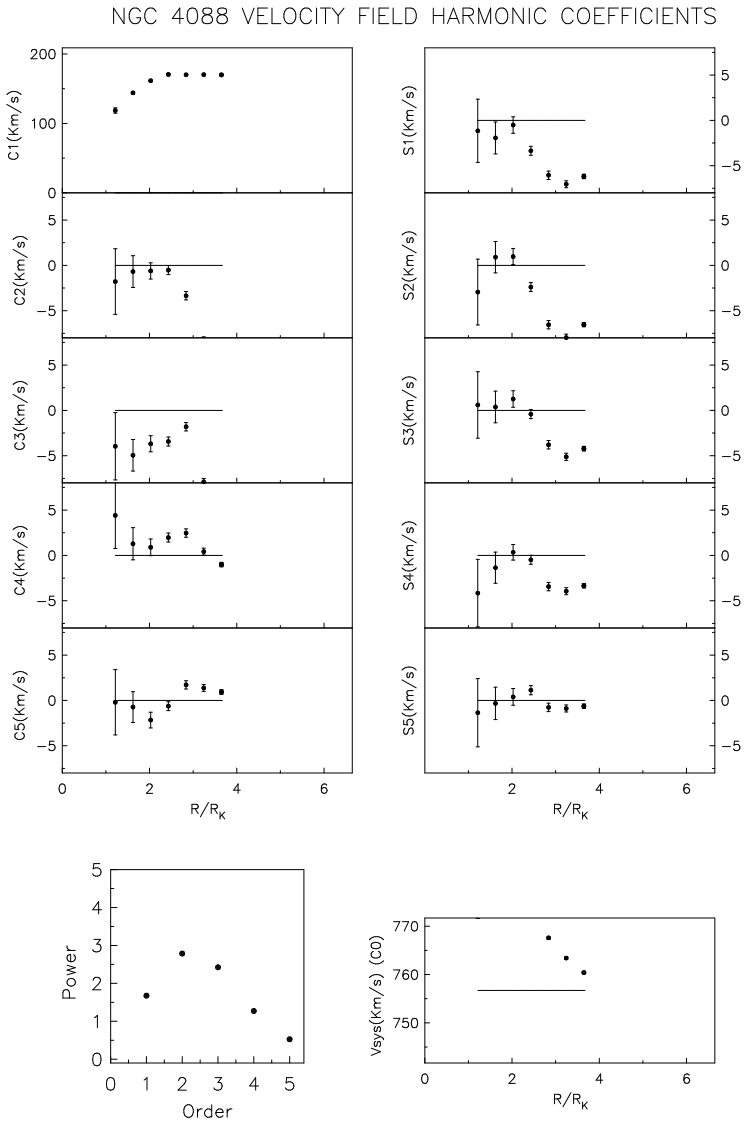

Figure 2.22: Velocity harmonic coefficients estimated for NGC 4088 galaxy belonging to the Ursa Major group. R_k is the K-band scale length (1.81 kpc)

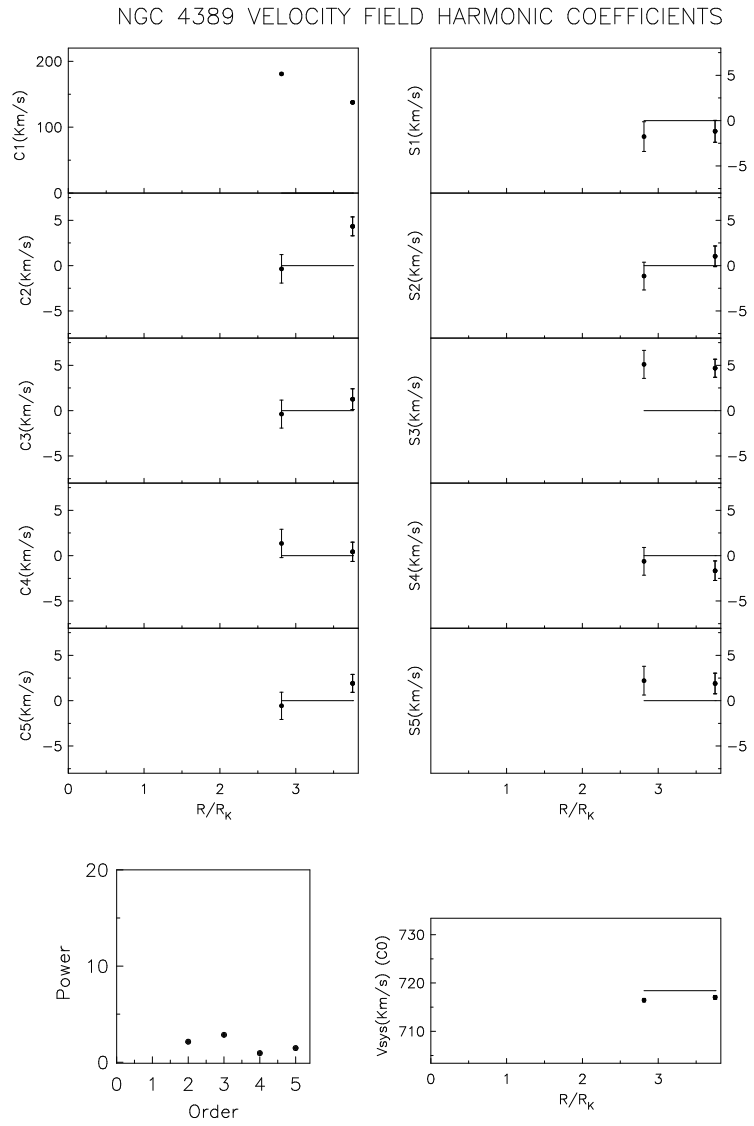

Figure 2.23: Velocity harmonic coefficients estimated for the NGC 4389 galaxy in Ursa Major group. R_k is the K-band scale length (0.74 kpc)

It can be shown that for a globally elongated potential, as in the case of a triaxial dark matter halo potential, m=2. In such a potential for a flat rotation curve as seen in many galaxies, $\alpha = 0$ (Appendix eq. A.32). In such a situation, after subtracting the systemic velocity, it can be shown that $v_{los} = c_1 \cos(\phi) + s_1 \sin(\phi) + s_3 \sin(3\phi)$ (Franx et al. 1994). In this equation $c_3 = 0$. As a result, in the region where the rotation curve is almost flat we expect $c_3 \sim 0$ which is an indication of fitting procedure converging (Schoenmakers et al., 1997). In addition, an estimate of the effects of spiral arms be estimated from the s_1 & s_3 coefficients. If the influence of spiral arms are large, s_1 and s_3 are expected to oscillate rapidly (Schoenmakers et al., 1997). Since this is not seen in Fig. 2.12 to Fig. 2.23, their contribution must be small.

From the harmonic coefficients thus obtained, it is possible to estimate the elongation in the potential of the galaxy times a factor of $\sin(2\phi_2)$, where ϕ_2 is the phase angle for $m = 2$ in the plane of the galaxy (Schoenmakers et al., 1997). The estimation of the ellipticity of the potential of an early type galaxy, IC 2006, using the velocity field for the HI ring in it was first carried out by Franx et al. (1994). This was later generalised to include spiral galaxies (Schoenmakers et al., 1997). In this procedure, with the assumptions of flat rotation curve in the outer regions of the galaxy and constant phase ($\phi_2(r)$), the ellipticity of potential (ϵ_{pot}) is obtained as

$$\epsilon_2 \sin(2\phi_2(r)) = (s_3 - s_1)\frac{1 + 2\cos^2(i) + 5\cos^5(i)}{c_1(1 - \cos^4(i))} \qquad (2.5)$$

(Schoenmakers et al., 1997). We have carried out similar analysis for all the sample galaxies in the Eridanus and the Ursa Major group. The asymmetry or the elongation in the potential for the Eridanus and the Ursa Major group

galaxies are shown in Fig. 2.24 - 2.33 and Fig.2.34 - 2.44 respectively.

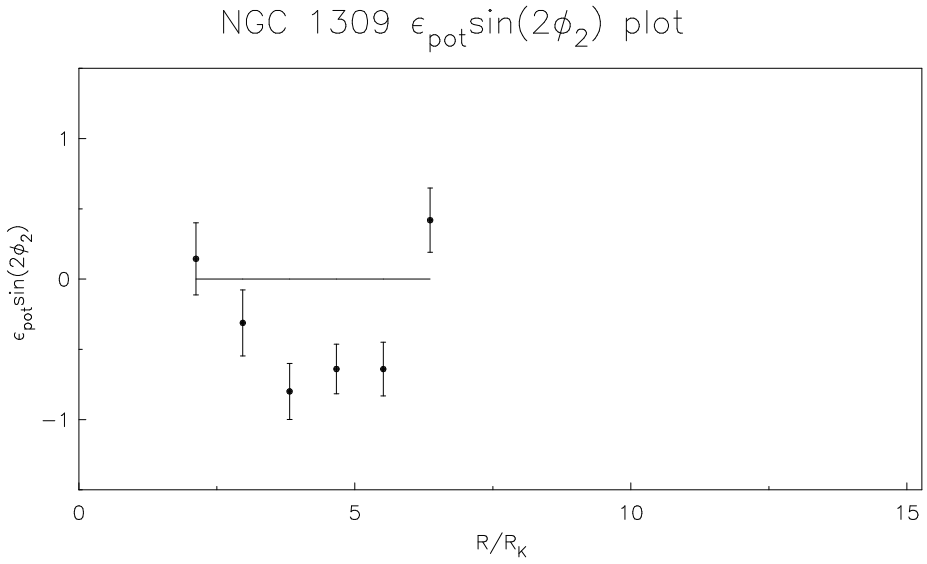

Figure 2.24: Elongation in the potential ϵ_{pot} derived from the velocity harmonic coefficients for NGC 1309 galaxy in the Eridanus group as a function of normalized radius

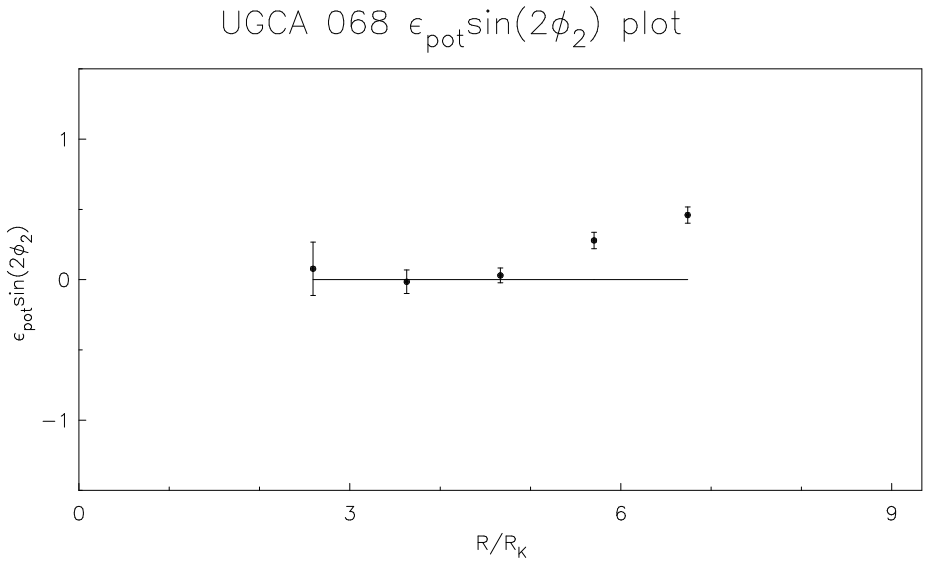

Figure 2.25: Elongation in the potential ϵ_{pot} derived from the velocity harmonic coefficients for UGC 068 galaxy in the Eridanus group as a function of normalized radius

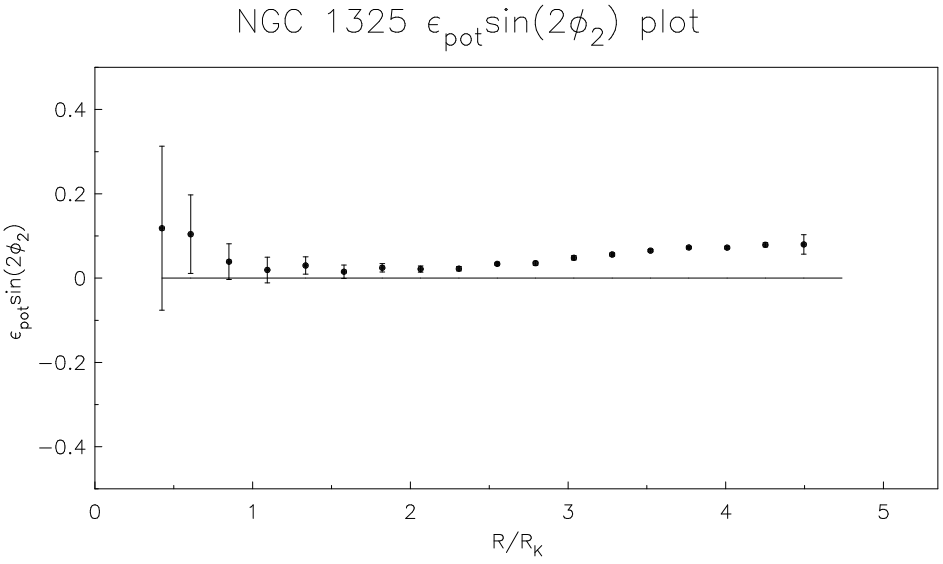

Figure 2.26: Elongation in the potential ϵ_{pot} derived from the velocity harmonic coefficients for NGC 1325 galaxy in the Eridanus group as a function of normalized radius

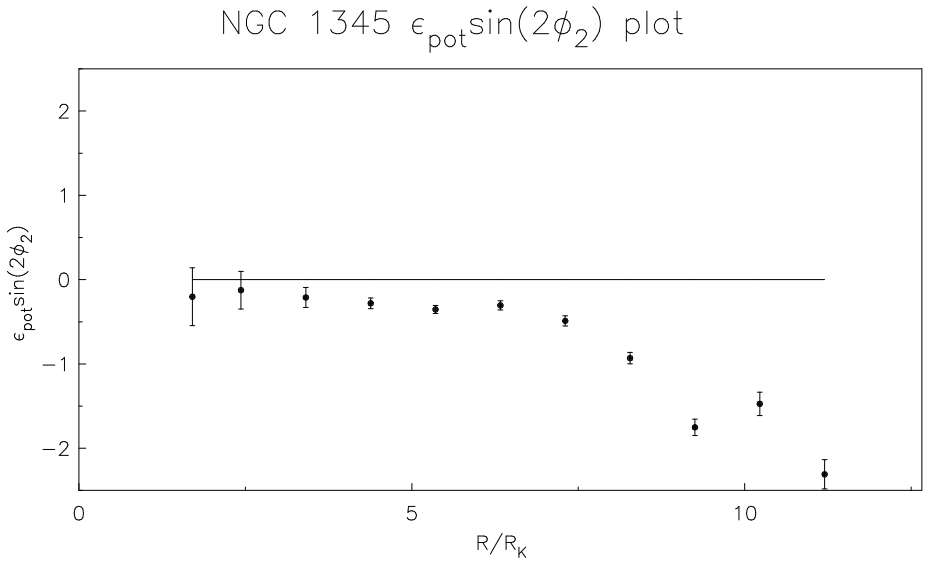

Figure 2.27: Elongation in the potential ϵ_{pot} derived from the velocity harmonic coefficients for NGC 1345 galaxy in the Eridanus group as a function of normalized radius

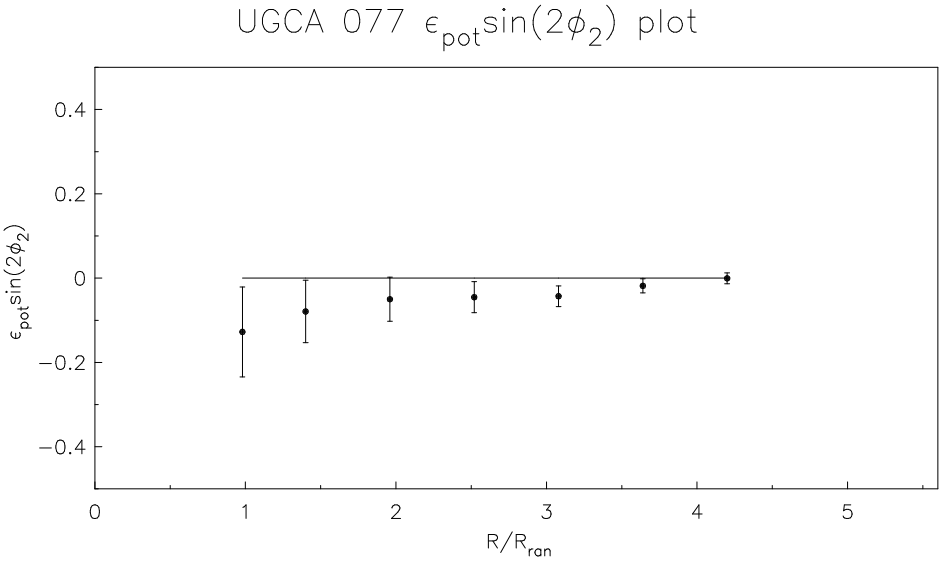

Figure 2.28: Elongation in the potential ϵ_{pot} derived from the velocity harmonic coefficients for UGC 077 galaxy in the Eridanus group as a function of normalized radius

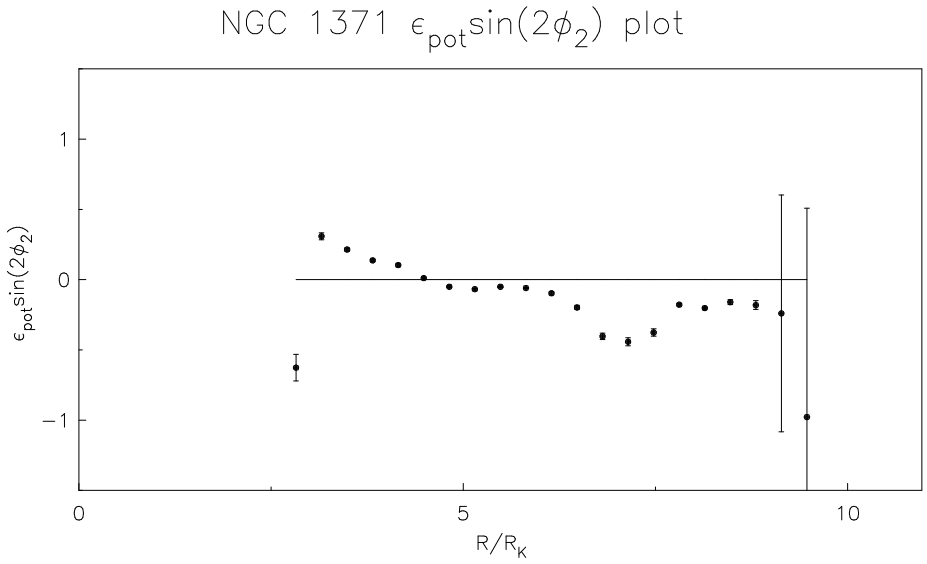

Figure 2.29: Elongation in the potential ϵ_{pot} derived from the velocity harmonic coefficients for NGC 1371 galaxy in the Eridanus group as a function of normalized radius

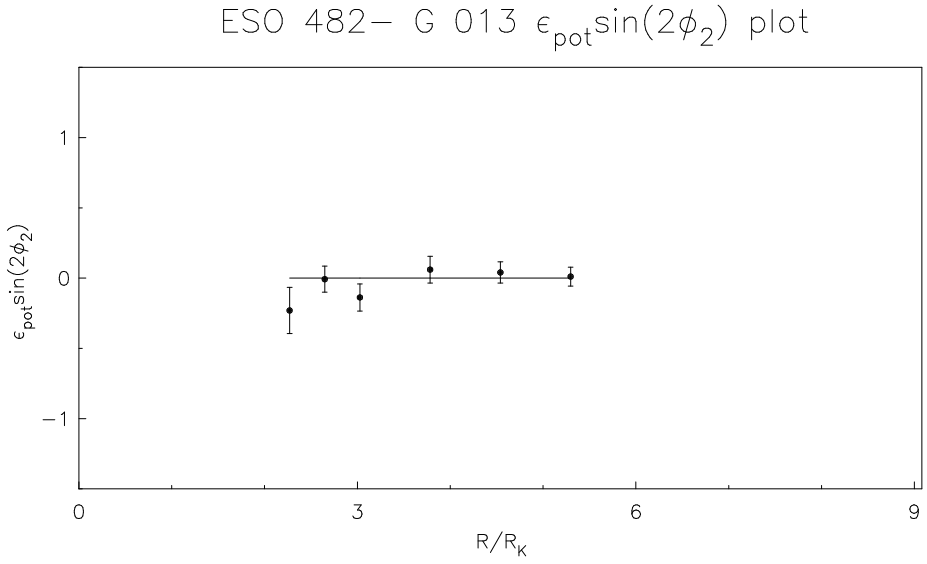

Figure 2.30: Elongation in the potential ϵ_{pot} derived from the velocity harmonic coefficients for ESO 482 -G 013 galaxy in the Eridanus group as a function of normalized radius

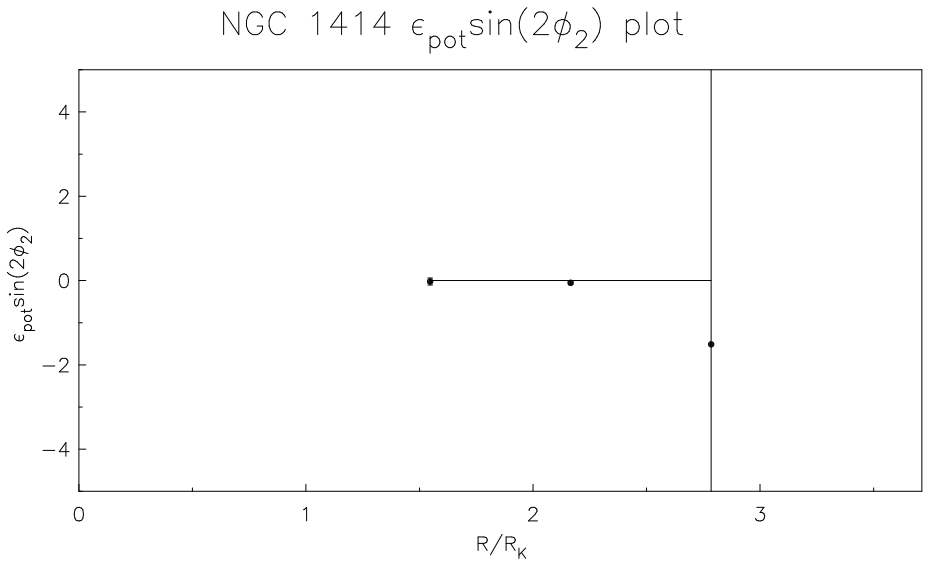

Figure 2.31: Elongation in the potential ϵ_{pot} derived from the velocity harmonic coefficients for NGC 1414 galaxy in the Eridanus group as a function of normalized radius

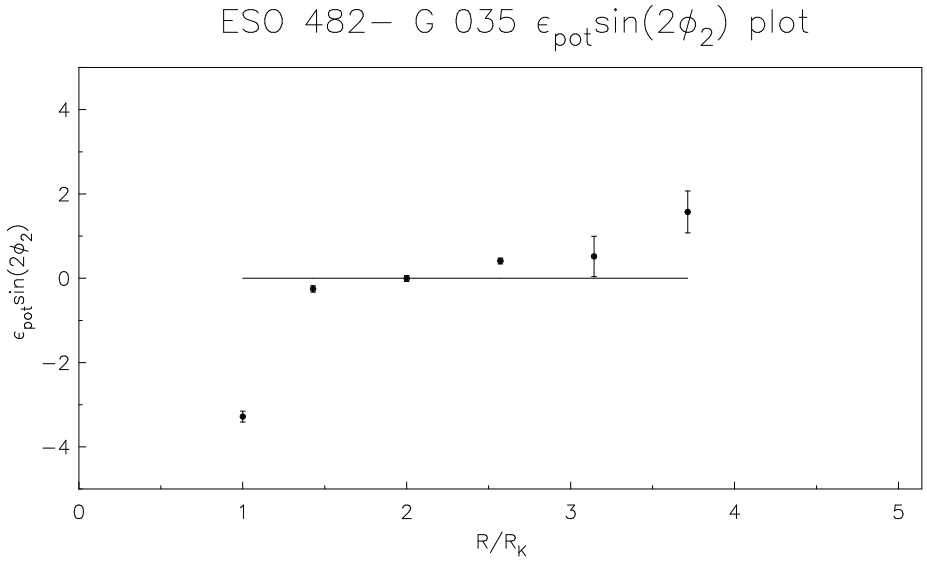

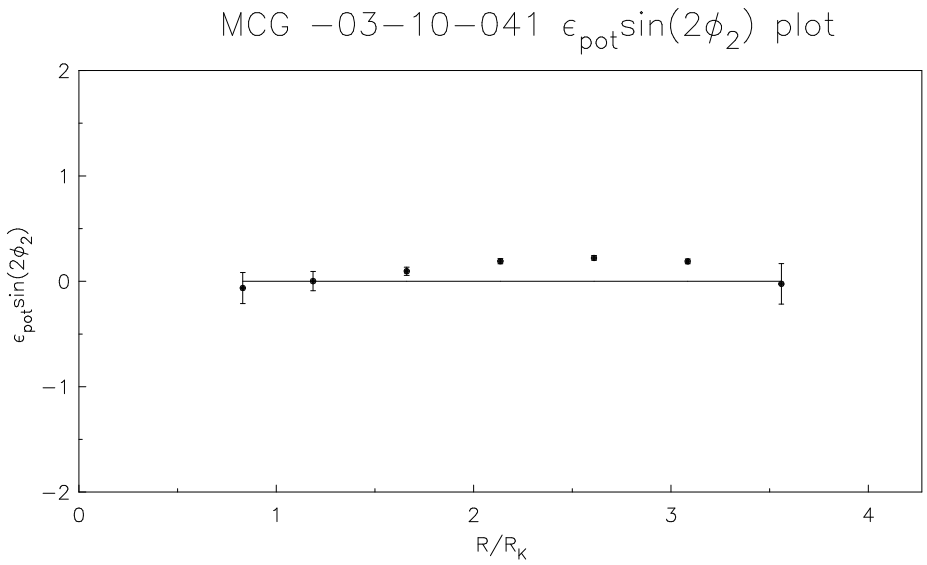

Figure 2.32: Elongation in the potential ϵ_{pot} derived from the velocity harmonic coefficients for MCG -03-10-041 galaxy in the Eridanus group as a function of normalized radius

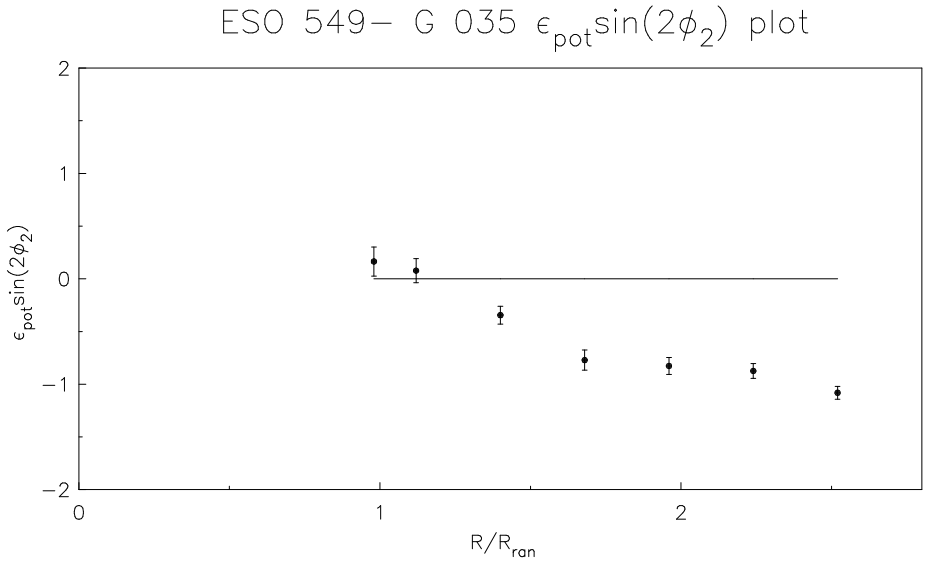

Figure 2.33: Elongation in the potential ϵ_{pot}) derived from the velocity harmonic coefficients for ESO -549 -G 035 galaxy in the Eridanus group

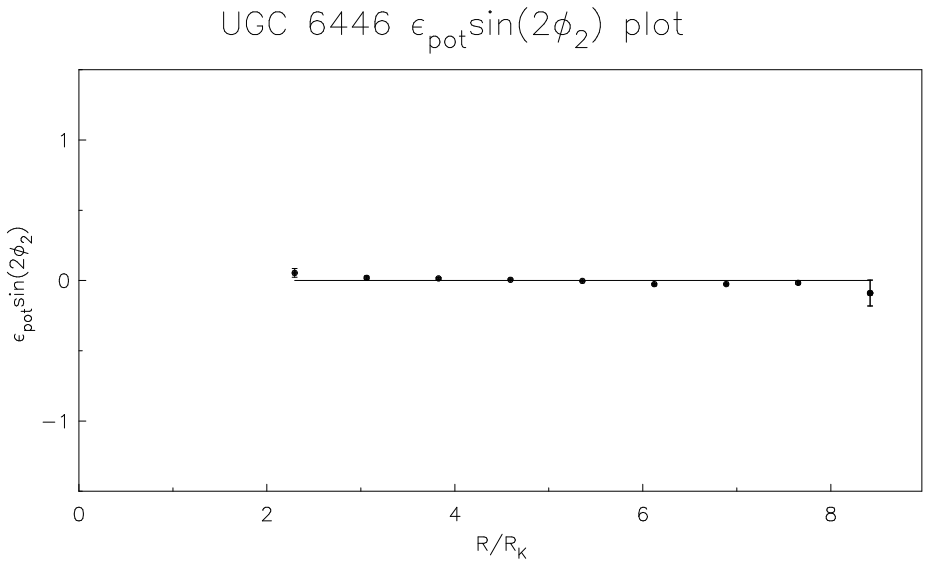

Figure 2.34: Elongation in the potential ϵ_{pot} derived from the velocity harmonic coefficients for UGC 6446 galaxy in the Ursa Major group as a function of normalized radius

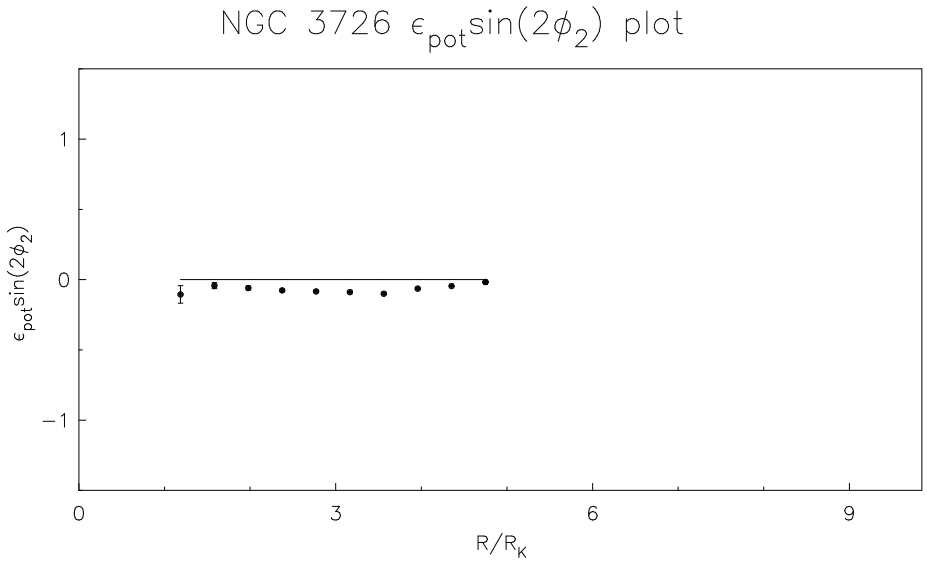

Figure 2.35: Elongation in the potential ϵ_{pot} derived from the velocity harmonic coefficients for NGC 3726 galaxy in the Ursa Major group as a function of normalized radius

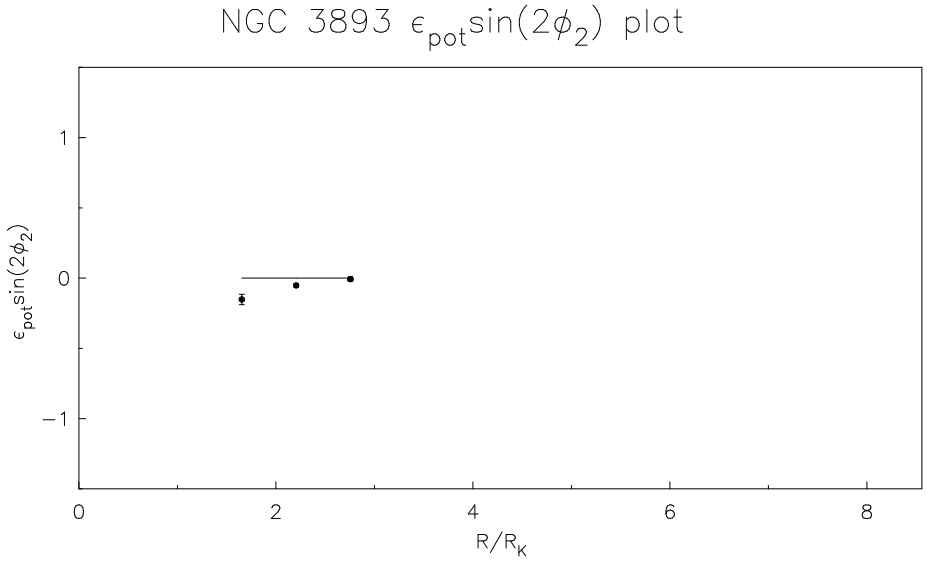

Figure 2.36: Elongation in the potential ϵ_{pot} derived from the velocity harmonic coefficients for NGC 3893 galaxy in the Ursa Major group as a function of normalized radius

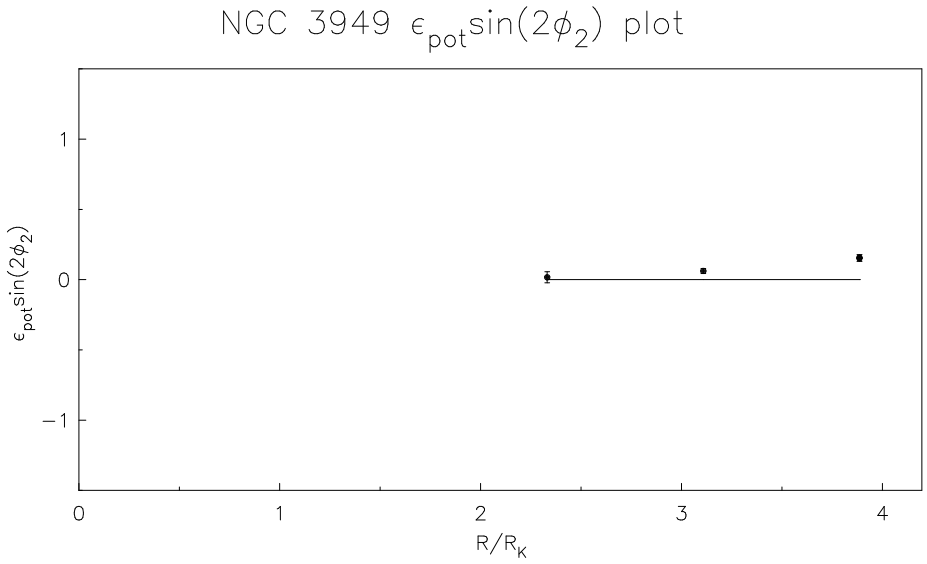

Figure 2.37: Elongation in the potential ϵ_{pot} derived from the velocity harmonic coefficients for NGC 3949 galaxy in the Ursa Major group as a function of normalized radius

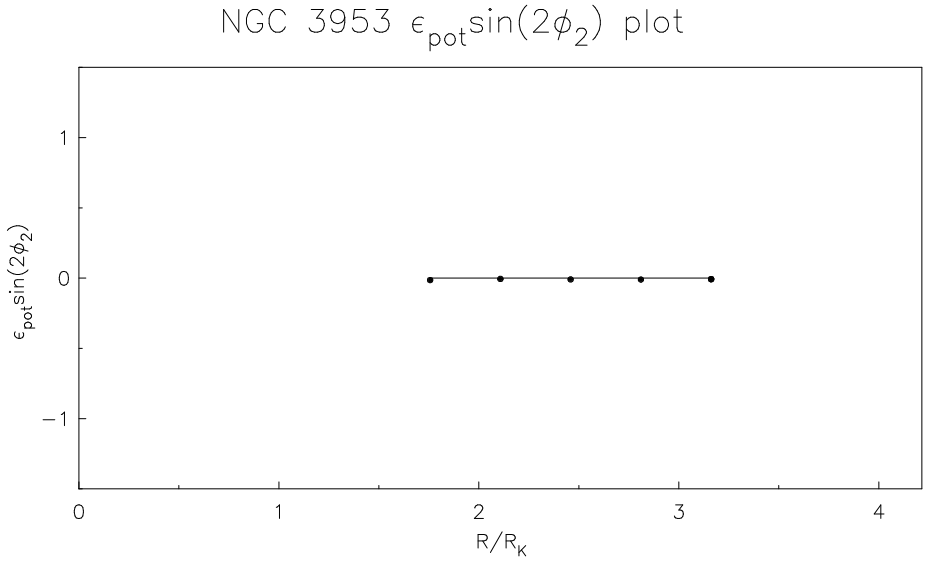

Figure 2.38: Elongation in the potential ϵ_{pot} derived from the velocity harmonic coefficients for NGC 3953 galaxy in the Ursa Major group as a function of normalized radius

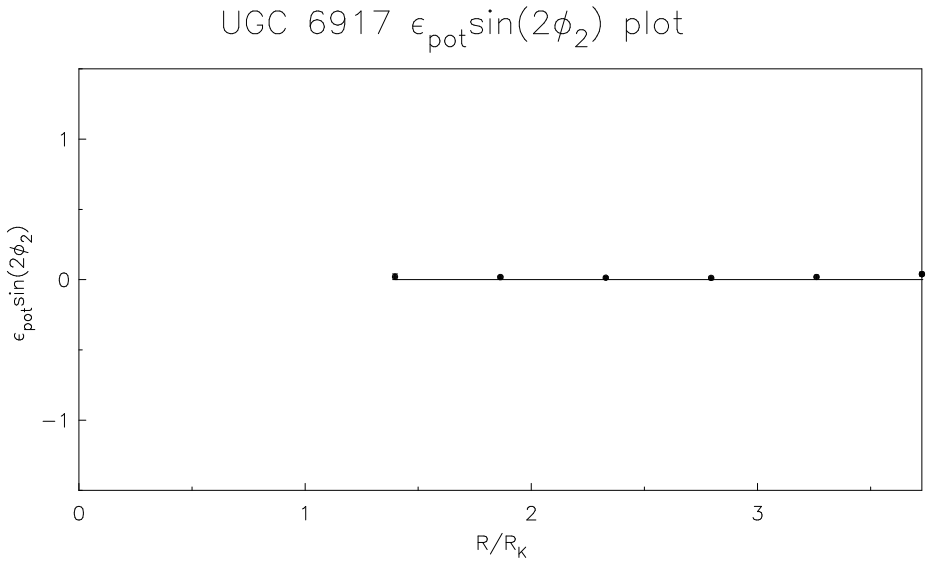

Figure 2.39: Elongation in the potential ϵ_{pot} derived from the velocity harmonic coefficients for UGC 6917 galaxy in the Ursa Major group as a function of normalized radius

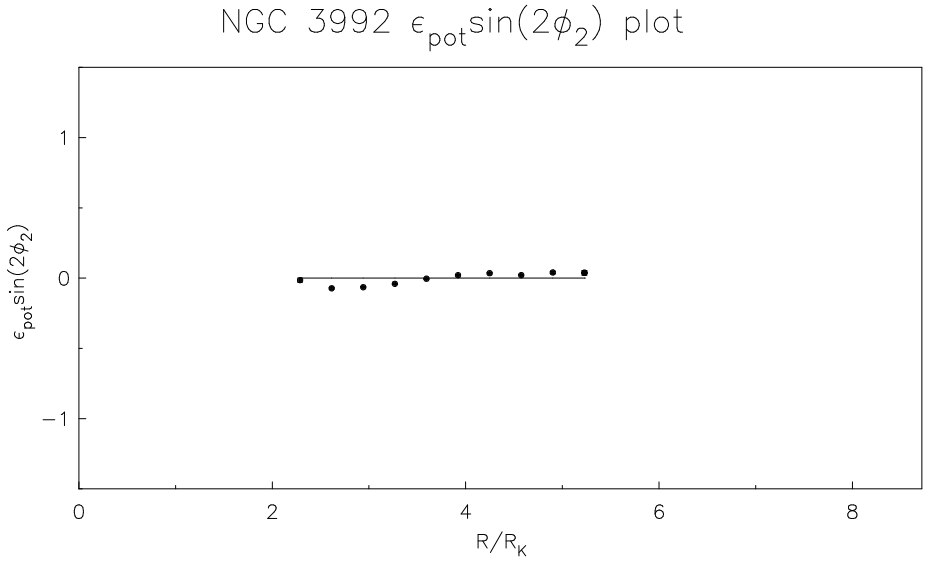

Figure 2.40: Elongation in the potential ϵ_{pot} derived from the velocity harmonic coefficients for NGC 3992 galaxy in the Ursa Major group as a function of normalized radius

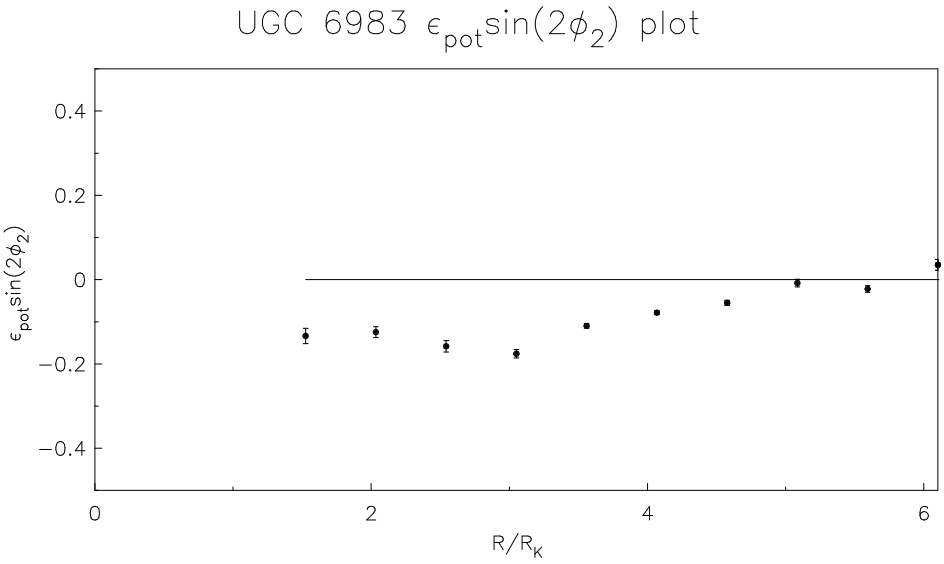

Figure 2.41: Elongation in the potential ϵ_{pot} derived from the velocity harmonic coefficients for UGC 6983 galaxy in the Ursa Major group as a function of normalized radius

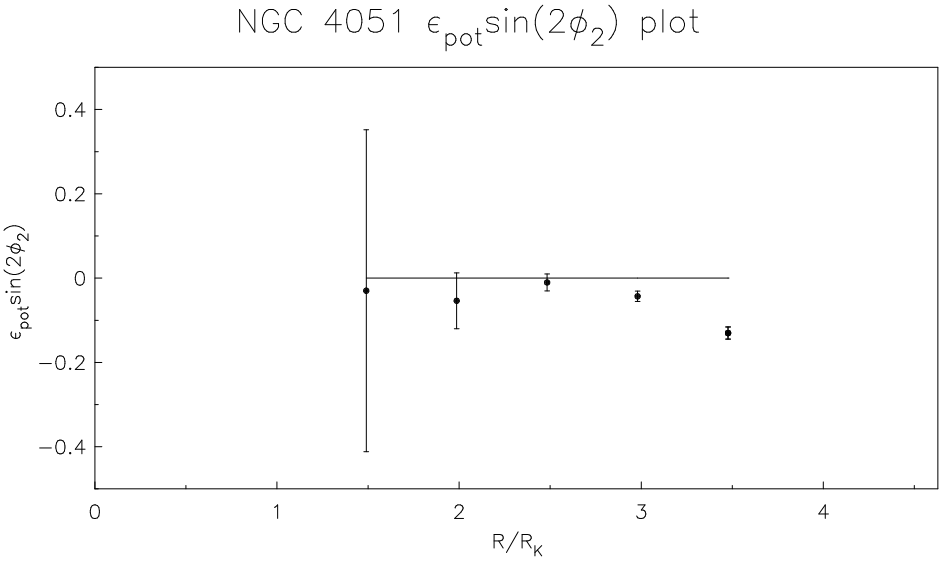

Figure 2.42: Elongation in the potential ϵ_{pot} derived from the velocity harmonic coefficients for NGC 4051 galaxy in the Ursa Major group as a function of normalized radius

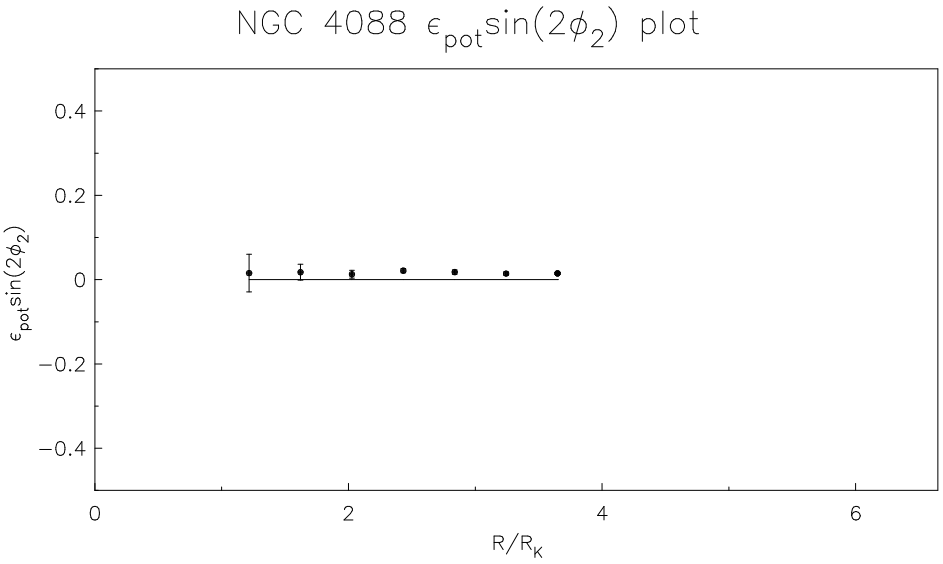

Figure 2.43: Elongation in the potential ϵ_{pot} derived from the velocity harmonic coefficients for NGC 4088 galaxy in the Ursa Major group as a function of normalized radius

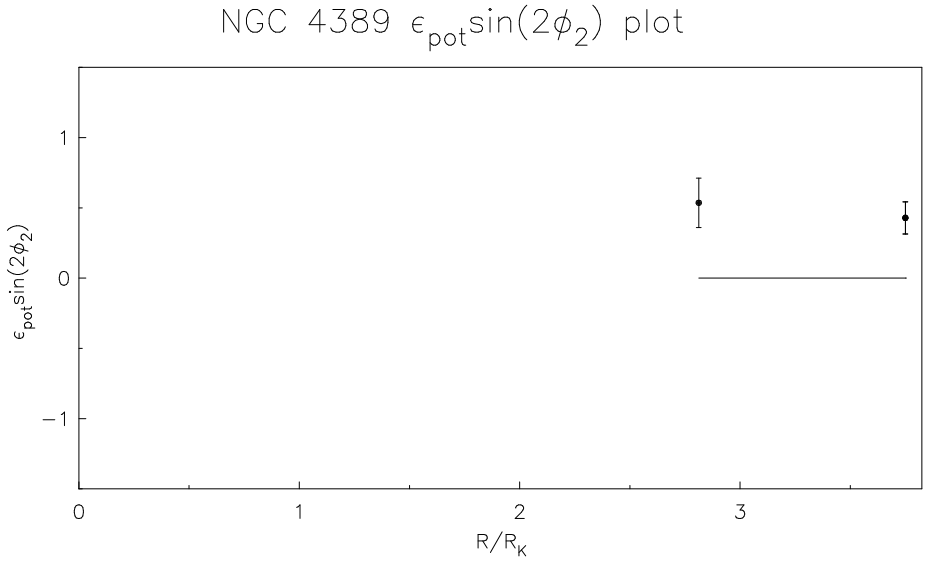

Figure 2.44: Elongation in the potential ϵ_{pot} derived from the velocity harmonic coefficients for NGC 4389 galaxy in the Ursa Major group as a function of normalized radius

Table 2.3: Eridanus group galaxies: J, K band scale lengths (R_J,R_K), *HI scale length (R_w)* and the average kinematical lopsidedness in the 1-2 HI Scale length of galaxies selected for kinematical lopsidedness analysis

Galaxy	R_J (kpc)	R_K (kpc)	R_w (kpc)	$< \epsilon_2 \sin(2\phi_2) >$
NGC 1309	1.42	1.32	4.76	-0.621
UGCA 068	1.29	1.08	3.59	0.113
NGC 1325	4.6	4.61	6.18	0.030
NGC 1345	0.93	1.15	6.95	-0.984
UGCA 077	*	*	4.55	-0.029
NGC 1371	3.34	3.37	*	*
ESO 482- G 013	0.65	0.74	2.95	0.032
NGC 1414	1.96	1.81	8.40	*
ESO 482- G 035	1.95	1.96	3.22	0.203
MCG -03-10-041	3.13	2.36	5.15	-0.025
ESO 549- G 035	*	*	3.73	-0.951

Using the formula mentioned above we have estimated the ellipticity of the potential in both Eridanus and Ursa Major group galaxies. The average values of the ellipticity of potential in the outer regions are tabulated in Table 2.3 and Table 2.4 respectively. As these galaxies typically have a Gaussian profile for the surface density, we have decided to estimate the average value of the ellipticity of the potential in the 1 to 2 *Gaussian scale lengths*. The Gaussian scale length was estimated by fitting a Gaussian profile to the surface density maps of the selected galaxies and is shown in the 4th column of Table 2.3 and column 3 of Table 2.4. It should be pointed out that the ellipticity of potential is valid only within a factor of $\sin(2\phi_2)$ only.

Table 2.4: Ursa Major group: K band scale length (R_K), *HI scale length (R_w)* and the average kinematical lopsidedness in the 1-2 HI Scale length of galaxies selected for kinematical lopsidedness analysis

Galaxy	R_K (kpc)	R_w (kpc)	$< \epsilon_2 \sin(2\phi_2) >$
UGC 6446	0.82	3.19	-0.173
NGC 3726	2.12	4.08	-0.392
NGC 3893	1.70	*	*
NGC 3949	1.00	2.69	0.178
NGC 3953	2.90	3.96	-0.171
UGC 6917	1.90	3.80	0.007
NGC 3992	3.11	*	*
UGC 6983	2.06	4.43	-0.213
NGC 4051	1.37	2.86	-0.087
NGC 4088	1.81	4.13	0.001
NGC 4389	0.74	*	*

2.4 Discussion and Conclusion

We have carried out the kinematical lopsidedness calculation proposed by Franx (Franx et al. 1994) and Schoenmakers et al. (Schoenmakers et al., 1997) to Eridanus and Ursa Major group of galaxies. Ellipticity of potential was also estimated for the galaxies belonging to these two groups. In estimating this value we have used those galaxies, whose rotation curve appears to be flat in the outer regions. In order to estimate the ellipticity of the halo potential, we assumed that the halo potential for each of the galaxies has a bi-symmetric nature (m=2) and the phase $\phi(R) \sim 0$ (Schoenmakers et al., 1997).

On the whole, most of the galaxies selected on the basis of their inclination and quality of velocity maps from the Eridanus and the Ursa Major group of galaxies show kinematical lopsidedness. If one considers the ab-

solute magnitude of $\epsilon_2 \sin(2\phi_2)$ in the 1-2 R_w range, Ursa Major group of galaxies have an average kinematical lopsidedness ~ 0.15 compared to ~ 0.33 for the galaxies belonging to the Eridanus group. The same trend is seen in the spatial lopsidedness part also, which is discussed in detail in chapter 3. The average values of kinematical lopsidedness in these groups are higher than the typical values seen in nearby isolated galaxies, where the values are ~ 0.06 (Schoenmakers et al., 1997). Hence group galaxies show more kinematical lopsidedness compared to the field galaxies. This may indicate that the group environment is conducive in producing kinematical lopsidedness. This argument is also supported by the spatial lopsidedness analysis carried out by us (see Chapter 3).

Intuition isn't the enemy, but the ally, of reason.

–John Kord Lagemann

3

Spatial Lopsidedness in Spiral Galaxies

3.1 Introduction

It is known that a large fraction of spiral galaxies exhibit spatial lopsidedness or asymmetry in the distribution of matter. This phenomenon was brought to the notice first by Baldwin et al. (Baldwin et al., 1980), using the radio maps of M101, NGC 891, NGC 2841 and IC 342. All these galaxies show HI gas extending out to larger radii on one side than the other.

Since then the non-axisymmetric distribution of HI gas has been deduced for much larger samples by studying the asymmetry in the global HI profiles (Richter & Sancisi, 1994; Matthews et al., 1998; Haynes et al., 1998). These studies revealed that the HI profiles on the receding and approaching sides are asymmetric. It was inferred from the sample that at least 50% of galaxies studied show HI lopsidedness. Richter & Sancisi (1994) claim that for nearby resolved galaxies like M101, there exists a correspondence between the spatial HI lopsidedness and the global HI velocity profile observed. However, a quantitative measurement of HI spatial asymmetry from 2-D maps still remains to be carried out. In this chapter we analyse the

2-D synthesis HI maps of a few galaxies belonging to the Eridanus and the Ursa Major group in order to study the HI lopsidedness. To the best of our knowledge, this is the first time such a study has been attempted.

Another important question to be addressed is regarding the similarity seen in HI lopsidedness and that of the stellar disk. With the advent of near-IR observations in recent years, spatial lopsidedness has also been detected in the distribution of old stellar population that make up the main mass component of galactic disks (Block et al. 1994, Rix& Zaritsky 1995). The harmonic analysis is used on the galaxy images, which gives a quantitative measurement of spatial lopsidedness as a function of radius. It is found that more than 30% of galaxies show strong spatial lopsidedness in the near-IR bands(Rix & Zaritsky 1995, Zaritsky & Rix 1997, Bournaud et al. 2005); but the increased sky brightness in the near-IR bands limits the measurement of Fourier components of stellar asymmetry to radii less than 2.5 exponential disk scale lengths. It is also not known whether the lopsidedness in HI and near-IR bands are correlated. If the lopsidedness is caused by a global effect which affects the galaxy as a whole, then the stellar disk asymmetry should be comparable to the HI disk lopsidedness at the same galacto-centric radius (Valluri & Jog, 1990; Jog, 1997; Jog, 2000). This is another aspect of lopsidedness which is yet to be confirmed. In this chapter we verify observationally this aspect of lopsidedness.

In the present work, we have adopted Fourier-analysis technique to study lopsidedness in the HI surface density distribution. For this analysis we have chosen a sample of eighteen galaxies in the Eridanus group (Omar & Dwarakanath 2005a) and eleven galaxies in the Ursa Major group (Verheijen & Sancisi, 2001). To our knowledge, this is the first time that an analysis of this kind has been applied for quantitative measurement of HI

spatial asymmetry. The availability of interferometric 2-D maps of galaxies has made such a study possible. Since the HI gas usually extends farther out than the stars, the disk lopsidedness can be measured up to twice or more the radial distance than it was possible using stellar light. Since the lopsidedness is observed to increase with radius (Rix & Zaritsky 1995, Bournaud et al. 2005), the Fourier amplitude measured at these distances are expected to provide better constraints on the generating mechanisms for disk lopsidedness (Valluri & Jog, 1990). In addition to this we have also compared the lopsidedness in HI with that in the near-IR band for a few galaxies belonging to both Eridanus and Ursa Major groups. It is observed that the spatial lopsidedness values obtained from near-IR band optical images are comparable to those obtained from the HI maps. We also show that the main physical mechanism for the origin of disk lopsidedness for the group galaxies is different from that of the field galaxies.

3.2 Data: The Eridanus Group of Galaxies

As discussed earlier (section 2.2.3), the Eridanus group is a loose group of galaxies at a mean distance of $\sim 23 \pm 2$ Mpc in the southern hemisphere ($\sim 3^h \leq \alpha \leq 4^h 30'$, $\sim -10^\circ \geq \delta \geq -30^\circ$). From the redshift values, $\sim$ 200 galaxies are associated with this group with heliocentric velocities in the range of $\sim 1000 - 2200$ km s^{-1} (Omar & Dwarakanath, 2005a). The observed velocity dispersion is ~ 240 km s^{-1}. Even though there are subgroups within the system, the overall population mix of the galaxies in the Eridanus group was found to be $\sim 30\%$ ellipticals and lenticulars and $\sim 70\%$ spirals and irregulars (Omar & Dwarakanath 2005a). Though HI was detected in 31 galaxies out of the 57 selected for observation by Omar and Dwarakanath using the Giant Meter-wave Radio Telescope (GMRT),

the spiral galaxies under consideration here form a subset of these. These spiral galaxies were chosen on the basis of their inclination, with inclinations in the range of 20° and 80°. This criterion was adopted so as to get good velocity and surface density maps.

If a galaxy is almost face on, the circular velocity information derived from the velocity map of the galaxy will be reduced to a great extent resulting in greater uncertainty in the inclination. Similarly, if a galaxy is viewed edge-on, the line of sight velocity information will be of good quality, but the surface density map will not be suitable for the spatial lopsidedness analysis. With these criteria, an inclination range of 20°-80° was found suitable.In addition to this, we eliminated those galaxies where the detection in HI was patchy such as NGC 1415. The positions, heliocentric velocities(, inclinations(i) and the position angle(PA) of selected Eridanus group galaxies are given in Tab. 3.1. For these galaxies the J & K-band scale length values are given in Tab. 3.2 (Omar & Dwarakanath, 2006).

The HI surface density and velocity maps of the selected galaxies used in this analysis were derived out of image cubes which were convolved to a common resolution of $20'' \times 20''$. A 3σ column density sensitivity of 10^{20} cm^{-2} was obtained for $20''$ resolution surface density images. The velocity resolution was ~ 13.4 km s^{-1}.

3.2.1 Eridanus: Optical Data

With a view to studying the spatial lopsidedness of the stellar component, the corresponding R-band images of these galaxies were analysed. The R-band images were obtained from Aryabhatta Research Institute of observational-sciencES (ARIES)using the 104 cm Sampurnanand telescope. The details of the observations and data reduction methods are given else-

Table 3.1: Hubble type, position, inclination and position angle of Eridanus group galaxies selected for spatial lopsidedness analysis

Galaxy	Type	α(J2000) h m s	δ(J2000) ° ′ ″	V_{sys} (km/s)	Inclin(i) (Deg)	PA (Deg)
NGC 1309	SAbc	03 22 06.5	-15 24 00	2135	20	210
UGCA 068	SABcdm	03 23 47.2	-19 45 15	1838	34	35
NGC 1325	SAbc	03 24 25.4	-21 32 36	1589	71	232
NGC 1345	SBc	03 29 31.7	-17 46 40	1529	34	88
NGC 1347	SBcd	03 29 41.8	-22 16 45	1759	26	328
UGCA 077	SBdm	03 32 19.2	-17 43 05	1961	66	149
IC 1953	SBd	03 33 41.9	-21 28 43	1867	37	129
NGC 1359	SBcm	03 33 47.7	-19 29 31	1966	53	325
NGC 1371	SABa	03 35 02.0	-24 55 59	1471	49	136
ESO 548- G 049	S?	03 35 28.1	-21 13 01	1510	71	128
ESO 482- G 013	Sb	03 36 53.9	-24 54 46	1835	63	65
NGC 1385	SBcd	03 37 28.3	-24 30 05	1493	40	181
NGC 1390	SB0/a	03 37 52.2	-19 00 30	1207	60	24
NGC 1414	SBbc	03 40 57.0	-21 42 47	1681	80	357
ESO 482- G 035	SBab	03 41 15.0	-23 50 10	1890	49	185
NGC 1422	SBab	03 41 31.1	-21 40 54	1637	80	65
MCG -03-10-041	SBdm	03 43 35.5	-16 00 52	1215	57	343
ESO 549- G 035	Sc	03 55 04.0	-20 23 01	1778	56	30

where (Omar & Dwarakanath, 2006).The final re-gridded images had a typical resolution of $1''.0 \times 1''.0$ and a limiting surface brightness of ~ 26.0 mag arcsec^{-2}.

3.3 Ursa Major Group of Galaxies

Out of the 49 galaxies observed using the Westerbork Synthesis Radio Telescope (WSRT) by Verheijen and Sancisi (2001) , we have selected 11 galaxies on the basis of their inclination and quality of HI maps (galaxies, whose HI maps were patchy were rejected) for further analysis. The right ascension (α), declination (δ), systemic velocity (V_{sys}), inclination (i) and

Table 3.2: The scale lengths in J, K-bands of galaxies belonging to the Eridanus group selected for spatial lopsidedness analysis (Omar & Dwarakanath, 2006)

Galaxy	R_J (kpc)	R_K (kpc)
NGC 1309	1.42	1.32
UGCA 068	1.29	1.08
NGC 1325	4.6	4.61
NGC 1345	0.93	1.15
NGC 1347	1.46	1.44
UGCA 077	*	*
IC 1953	3.78	4.19
NGC 1359	2.67	*
NGC 1371	3.34	3.37
ESO 548- G 049	1.18	*
ESO 482- G 013	0.65	0.74
NGC 1385	3.21	2.98
NGC 1390	0.74	0.87
NGC 1414	1.96	1.81
ESO 482- G 035	1.95	1.96
NGC 1422	2.44	1.84
MCG -03-10-041	3.13	2.36
ESO 549- G 035	*	*

Table 3.3: The Hubble type, position (RA, DEC) , systemic velocity (V_{sys}), inclination (i) and the position angle (PA) of galaxies selected for spatial lopsidedness analysis belonging to the Ursa Major group (Verheijen & Sancisi, 2001)

Name	Type	α**(J2000)**	δ**(J2000)**	V_{sys}	Inclin.(i)	PA
		h m s	° ′ ″	(km s^{-1})	(°)	(°)
UGC 6446	Sd	11 26 40.4	53 44 48	644.3	54	200
NGC 3726	SBc	11 33 21.2	47 01 45	865.6	54	194
NGC 3893	Sc	11 48 38.2	48 42 39	967.2	49	352
NGC 3949	Sbc	11 53 41.4	47 51 32	800.2	54	297
NGC 3953	SBbc	11 53 48.9	52 19 36	1052.3	62	13
UGC 6917	SBd	11 56 28.8	50 25 42	910.7	59	123
NGC 3992	SBbc	11 57 36.0	53 22 28	1048.2	58	248
UGC 6983	SBcd	11 59 09.3	52 42 27	1081.9	50	270
NGC 4051	SBbc	12 03 09.6	44 31 53	700.3	50	311
NGC 4088	Sbc	12 05 34.2	50 32 21	756.7	71	231
NGC 4389	SBbc	12 25 35.1	45 41 05	718.4	50	276

Position Angle (PA) of these galaxies are given in Tab. 3.3. All the selected galaxies had good velocity and HI maps, both of which were essential for the analysis (Block et al. 2002; Bournaud et al., 2005). Details of the observation and the preliminary data reduction are given elsewhere (Verheijen & Sancisi, 2001) (see section 2.2.4 for a brief summary).

3.3.1 Optical and Near-IR Data

The K′-Band and R-Band images of a few of the largest galaxies having a typical diameter of $3' - 6'$ in the inclination range of $49° - 62°$ were sourced from the Canadian Astronomy Data Centre (CADC)[1] archives. These images were obtained using various telescopes and CCD cameras by Tully et al. (1996) and are kept in the archives after the initial data reductions like

[1]This research used the facilities of the Canadian Astronomy Data Centre operated by the National Research Council of Canada with the support of the Canadian Space Agency.

cosmic ray removal, dark subtraction, and flat fielding were carried out. The typical resolution of the images were $1''$ (R-Band) and $\sim 2''$ (K-Band). These images were analysed to obtain the asymmetry in the stellar distribution of the galaxies.

3.3.2 Harmonic Analysis of Radio Data

In HI, where both velocity maps and surface density maps are available, the analysis technique is different from that adopted in optical analysis. The procedure assumes that in an ideal galaxy, HI is in pure circular motion. Hence we have,

$$V(x,y) = V_0 + V_c\cos(\phi')\sin(i) + V_r\sin(\phi')\sin(i) \tag{3.1}$$

where $V(x,y)$ is the velocity at the rectangular coordinate (x,y), V_0 is the systemic velocity, V_c is the rotation velocity, i is the inclination and V_r is the radial velocity which was taken to be zero. The azimuthal angle (ϕ') measured in the plane of the galaxy, is given by the equations

$$\cos(\phi') = \frac{-(x-x_0)\sin(PA) + (y-y_0)\cos(PA)}{r} \tag{3.2}$$

$$\sin(\phi') = \frac{-(x-x_0)\cos(PA) + (y-y_0)\sin(PA)}{r\cos(i)} \tag{3.3}$$

where $r = \sqrt{((x-x_0)^2 + (y-y_0)^2/\cos(i)^2)}$. In these equations, (x_0, y_0) is the kinematic centre of the galaxy, PA is the position angle of the galaxy measured in the anti-clockwise direction from the north direction. Using these equations, the five unknown parameters, namely (x_0, y_0), PA, V_c and i were estimated using the GIPSY task ROTCUR (Baldwin et al., 1980) in an iterative manner (Wong et al. 2003; Omar & Dwarakanath, 2005a) as mentioned in section 2.3 for both sets of galaxies belonging to Eridanus and

Ursa Major group. It was observed that the dynamical centre, derived from velocity maps were less than $2''$ away from the optical centre. Hence, for all the calculations the optical centre was used.

To derive the surface density harmonic coefficients, values obtained for (x_0, y_0), PA, V_c and i by ROTCUR (see section 2.3) as well as the surface density and velocity maps were given to the GIPSY task RESWRI, a task which is an offshoot of ROTCUR based on the harmonic analysis idea developed by Schoenmakers et al.(1997). The radii of each of the rings were separated by half the synthesized beam width and the width of each ring was one synthesized beam width for the Eridanus and the Ursa Major group galaxies to satisfy the Nyquist sampling condition (Shannon, 1949). To avoid beam smearing along the minor axis, a cone of $10'$ about the minor axis of the galaxy was not included in the analysis for the galaxies in the Eridanus group. This value was $15'$ for Ursa Major group galaxies. A uniform weightage was given for each of the points within one annulus. At each of these rings, with the same values of PA and inclination obtained from the velocity map analysis, the surface density values were extracted from the surface density map, which were Fourier expanded. The programme parameters were set to return ten Fourier harmonic coefficients in the spatial domain. The resulting harmonic coefficients were recast so that the surface density could be modelled as

$$\sigma(R,\phi) = \sigma_0(R) + \sum_m a_m(R)\cos(m\phi - \phi_m(R)) \qquad (3.4)$$

Here $\sigma_0(R)$ is the mean surface density at a given radius R. ϕ is the azimuthal angle in the plane of the galaxy and ϕ_m is the phase of the m^{th} Fourier coefficient. From this analysis, the harmonic coefficients $a_1(R)$ were extracted out and the normalized harmonic coefficients

$A_1(R) = a_1(R)/\sigma_0(R)$ were calculated for various rings. $\phi_1(R)$ for various rings were also determined. The errors in each of these coefficients were determined assuming that the coefficients $a_1(R), \sigma_0(R), \phi_1(R)$ to be independent of each other. This procedure was adopted to facilitate the comparison of the A_1, ϕ_1 values with the values derived from a similar analysis of the near-IR data for stars (Rix & Zaritsky 1995, Bournaud et al. 2005).

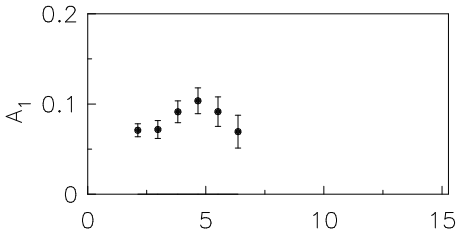

NGC 1309
A_{1max} =0.10
A_{1mean} =0.08±0.01

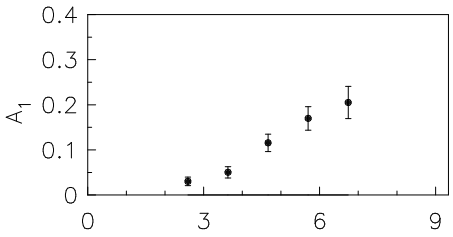

UGCA 068
A_{1max} =0.21
A_{1mean} =0.11±0.02

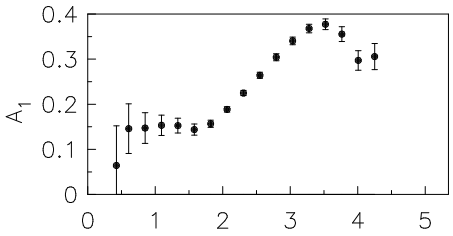

NGC 1325
A_{1max} =0.38
A_{1mean} =0.23±0.03

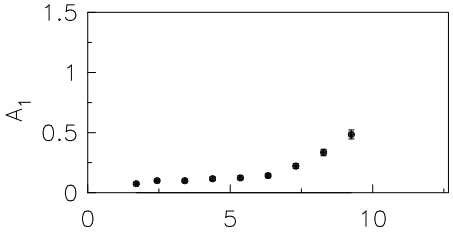

NGC 1345
A_{1max} =0.48
A_{1mean} =0.19±0.02

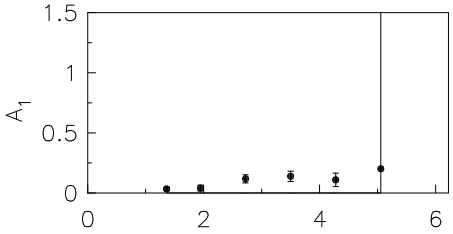

NGC 1347
A_{1max} =0.20
A_{1mean} =0.11±0.84

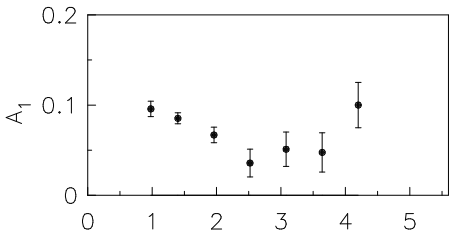

UGCA 077
A_{1max} =0.10
A_{1mean} =0.07±0.02

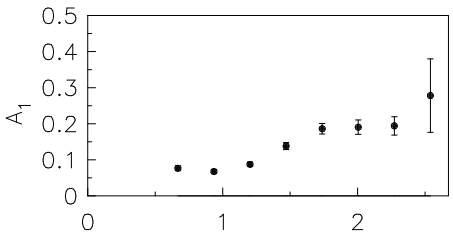

IC 1953
A_{1max} =0.28
A_{1mean} =0.15±0.04

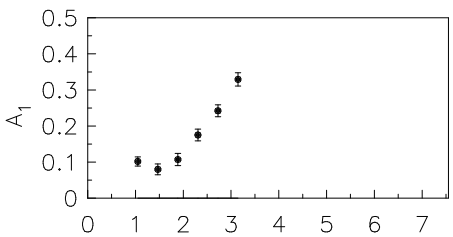

NGC 1359
A_{1max} =0.33
A_{1mean} =0.17±0.02

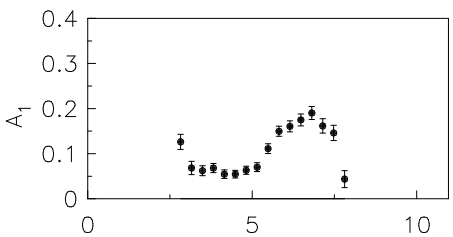

NGC 1371
A_{1max} =0.19
A_{1mean} =0.11±0.01

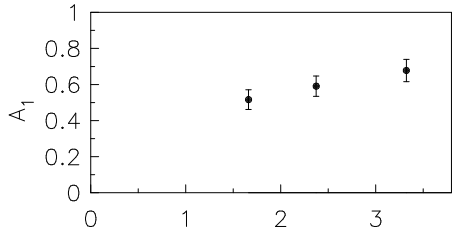

ESO 548− G 049
A_{1max} =0.80
A_{1mean} =0.65±0.06

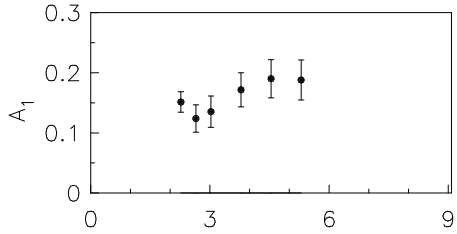

ESO 482− G 013
A_{1max} =0.19
A_{1mean} =0.16±0.03

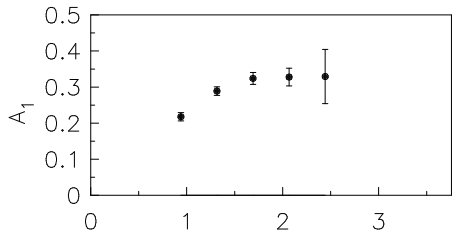

NGC 1385
A_{1max} =0.33
A_{1mean} =0.30±0.04

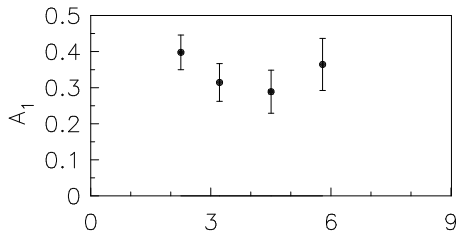

NGC 1390
A_{1max} =0.40
A_{1mean} =0.34±0.06

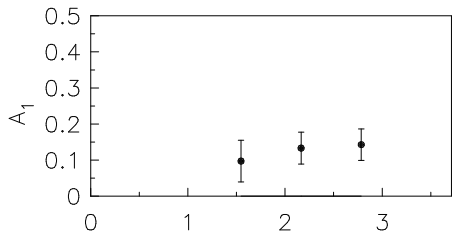

NGC 1414
A_{1max} =0.14
A_{1mean} =0.12±0.05

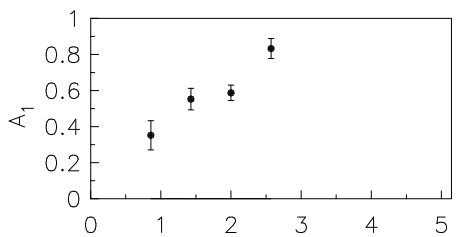

ESO 482− G 035
A_{1max} =0.83
A_{1mean} =0.58±0.06

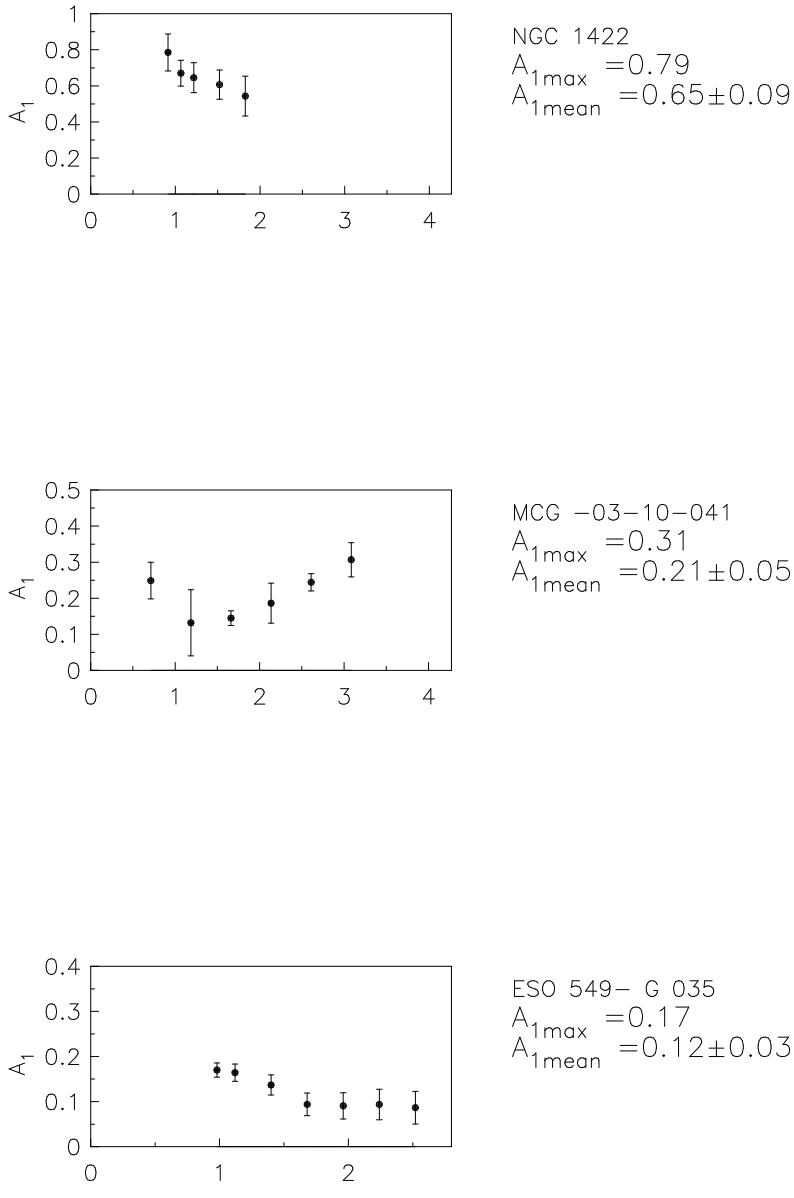

Figure 3.1: A_1 coefficients of galaxies in the Eridanus group as a function of R/R_K.For NGC 1359 and ESO 548 -G 049 the J band scale length is used. For UGCA 077 & ESO 549 -G 035, a scale length of 2kpc is used.Here A_{1mean} is the mean value of A_1 over the whole HI disk

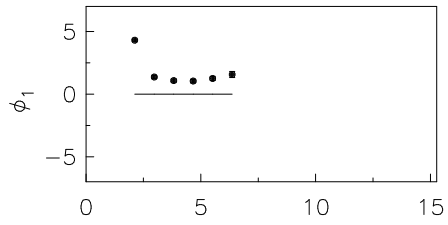

NGC 1309
ϕ_{1max} =4.3(rad)
ϕ_{1mean} =1.8±0.2(rad)

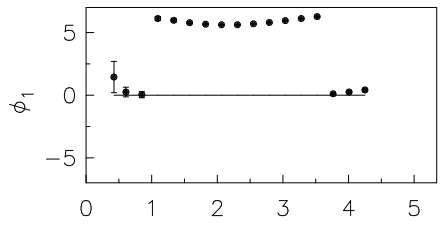

NGC 1325
ϕ_{1max} =6.3(rad)
ϕ_{1mean} = 4.0±0.3(rad)

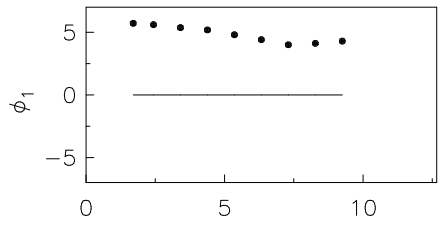

NGC 1345
ϕ_{1max} =5.7(rad)
ϕ_{1mean} =4.8±0.1(rad)

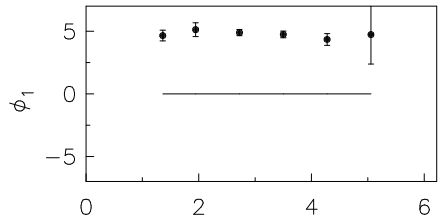

NGC 1347
ϕ_{1max} =5.1(rad)
ϕ_{1mean} =4.7±1.0(rad)

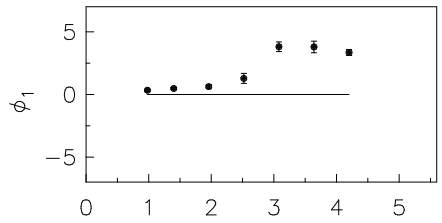

UGCA 077
ϕ_{1max} =3.8(rad)
ϕ_{1mean} =2.0±0.3(rad)

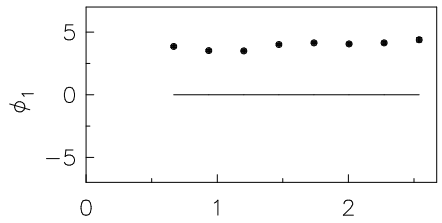

IC 1953
ϕ_{1max} =4.4(rad)
ϕ_{1mean} =4.0±0.1(rad)

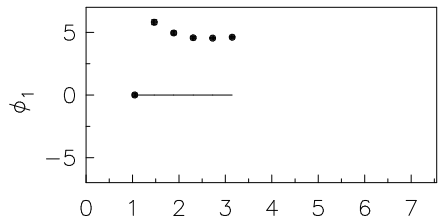

NGC 1359
ϕ_{1max} =5.8(rad)
ϕ_{1mean} =4.1±0.1(rad)

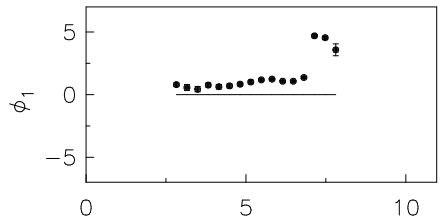

NGC 1371
ϕ_{1max} =4.7(rad)
ϕ_{1mean} = 1.5±0.2(rad)

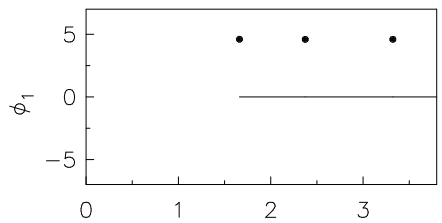

ESO 548− G 049
ϕ_{1max} =4.6(rad)
ϕ_{1mean} =4.6±0.1(rad)

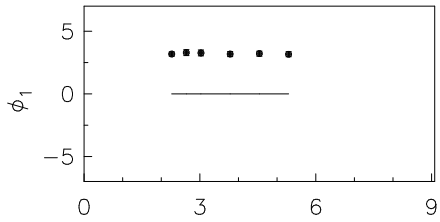

ESO 482− G 013
ϕ_{1max} =3.3(rad)
ϕ_{1mean} =3.2±0.2(rad)

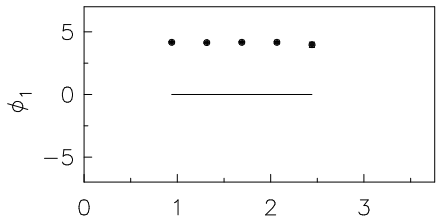

NGC 1385
ϕ_{1max} =4.2(rad)
ϕ_{1mean} =4.1±0.1(rad)

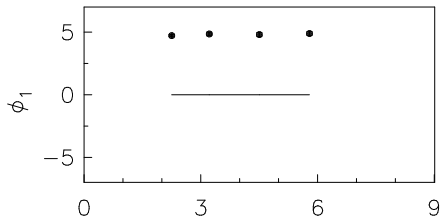

NGC 1390
ϕ_{1max} =4.9(rad)
ϕ_{1mean} =4.8±0.1(rad)

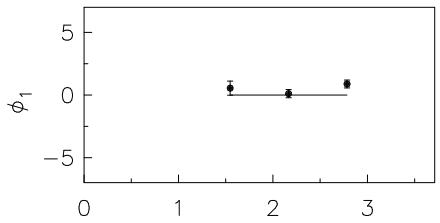

NGC 1414
ϕ_{1max} =0.9(rad)
ϕ_{1mean} =0.5±0.4(rad)

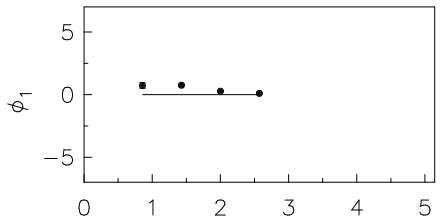

ESO 482− G 035
ϕ_{1max} =0.8(rad)
ϕ_{1mean} =0.5±0.1(rad)

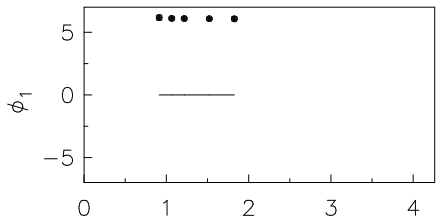

NGC 1422
ϕ_{1max} =6.2(rad)
ϕ_{1mean} =6.1±0.1(rad)

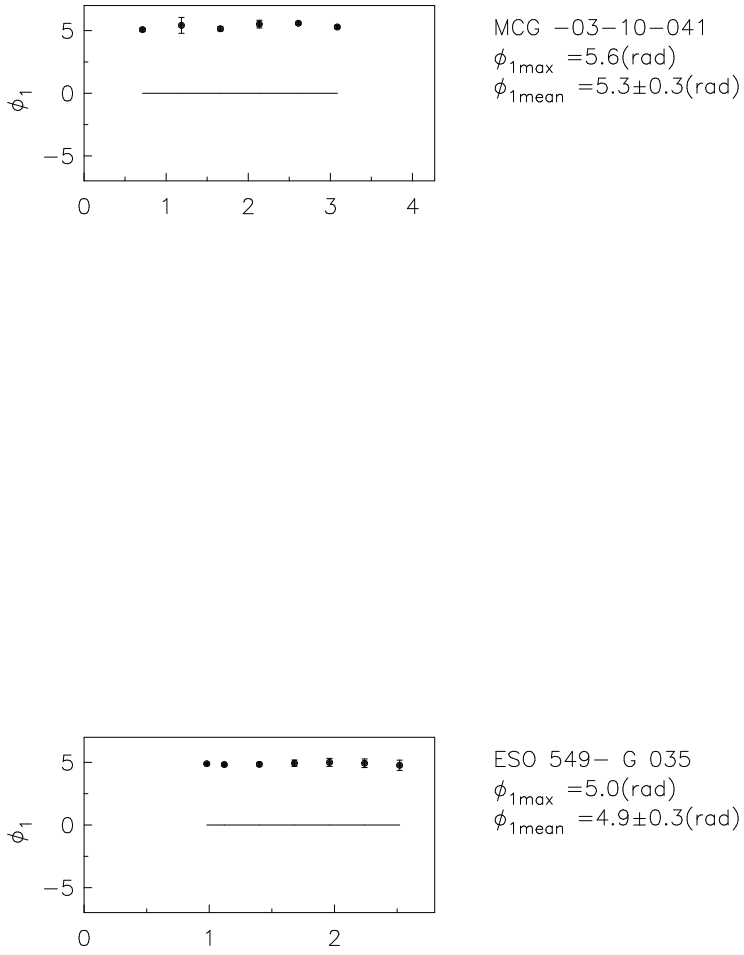

Figure 3.2: ϕ_1 coefficients of galaxies in the Eridanus group as a function of R/R_K.For NGC 1359 and ESO 548 -G 049 the J band scale length is used. For UGCA 077 & ESO 549 -G 035, a scale length of 2kpc is used.

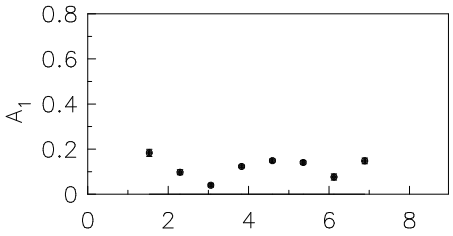

UGC 6446
A_{1max} =0.18
A_{1mean} =0.12±0.01

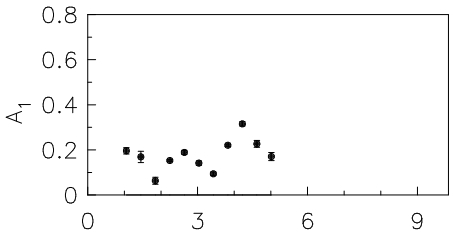

NGC 3726
A_{1max} =0.32
A_{1mean} =0.18±0.01

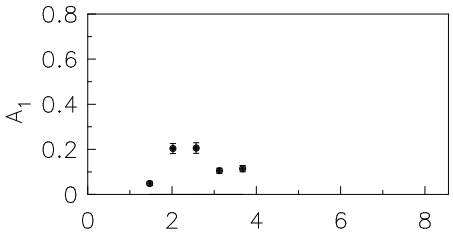

NGC 3893
A_{1max} =0.21
A_{1mean} =0.14±0.02

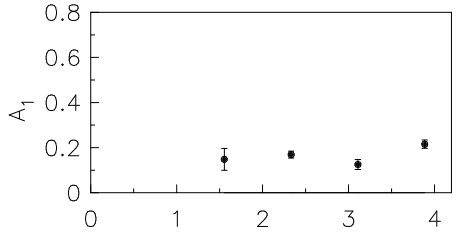

NGC 3949
A_{1max} =0.22
A_{1mean} =0.16±0.03

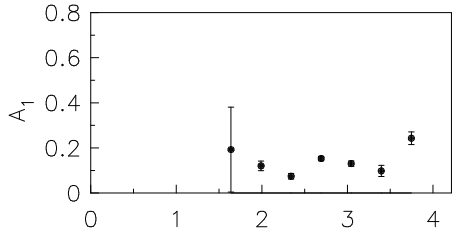

NGC 3953
A_{1max} =0.24
A_{1mean} =0.14±0.07

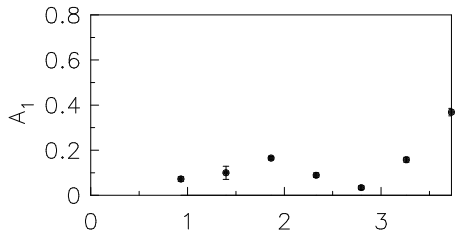

UGC 6917
A_{1max} =0.37
A_{1mean} =0.14±0.01

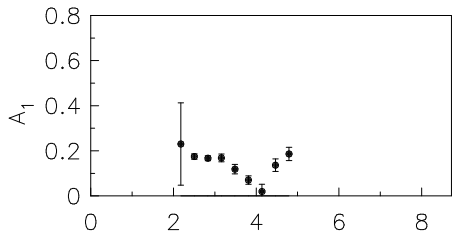

NGC 3992
A_{1max} =0.23
A_{1mean} =0.14±0.06

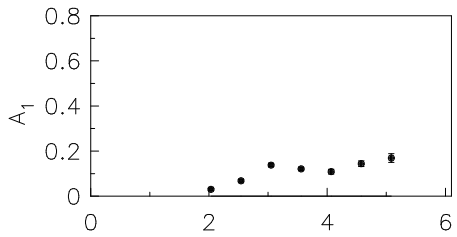

UGC 6983
A_{1max} =0.17
A_{1mean} =0.11±0.01

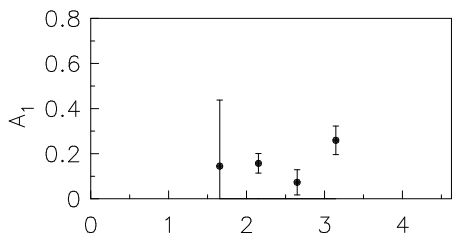

NGC 4051
A_{1max} =0.26
A_{1mean} =0.16±0.15

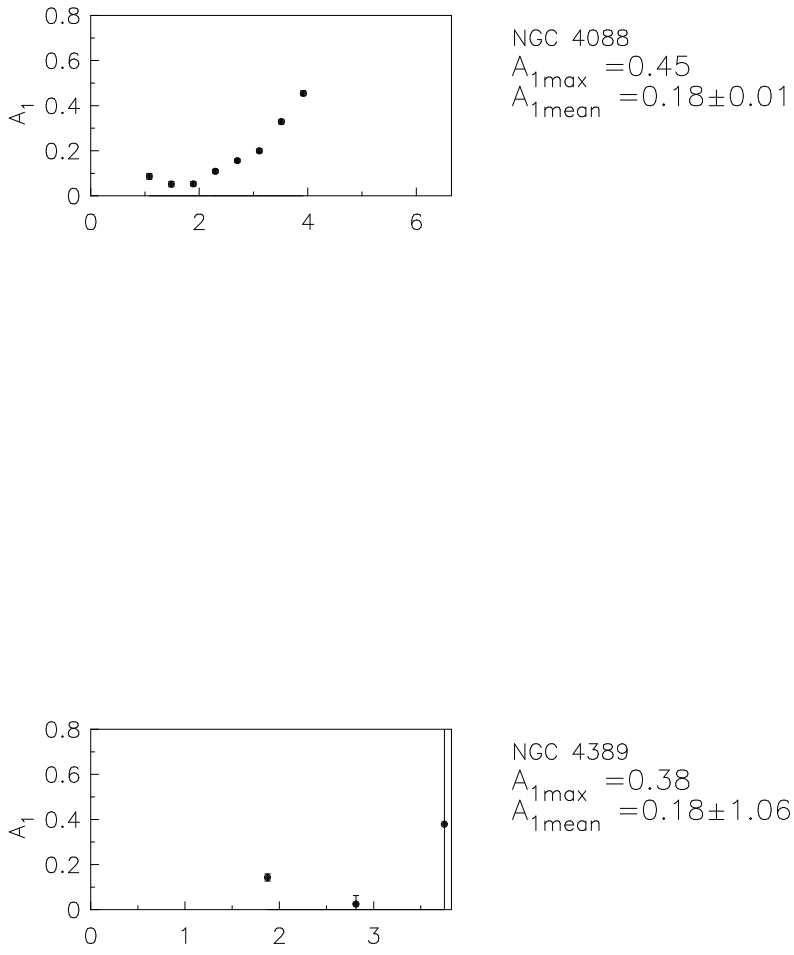

Figure 3.3: The asymmetry parameter derived from the surface density maps (moment 0) of galaxies belonging to the Ursa Major group. In each of the maps, the radius is in the units of K'-band scale length. The mean value estimated is for the complete range.

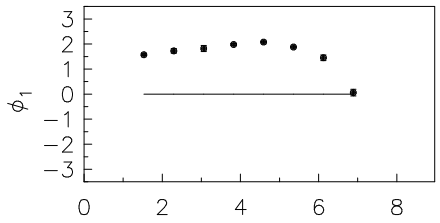

UGC 6446
$|\phi_{1max}|$ =2.1(rad)
$|\phi|_{1mean}$ =1.6±0.1(rad)

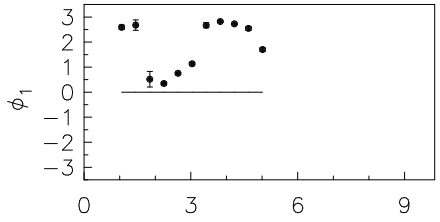

NGC 3726
$|\phi_{1max}|$ =2.8(rad)
$|\phi|_{1mean}$ =1.9±0.1(rad)

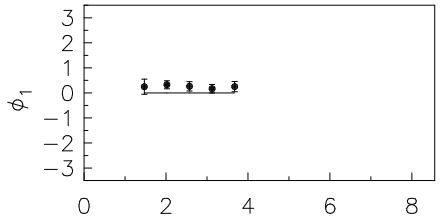

NGC 3893
$|\phi_{1max}|$ =0.3(rad)
$|\phi|_{1mean}$ =0.3±0.2(rad)

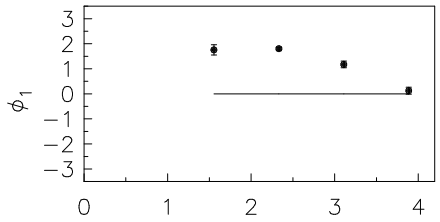

NGC 3949
$|\phi_{1max}|$ =1.8(rad)
$|\phi|_{1mean}$ =1.2±0.1(rad)

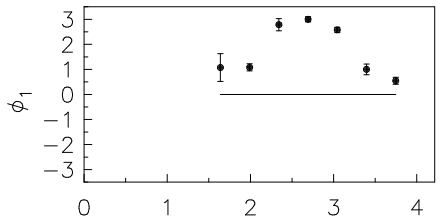

NGC 3953
$|\phi_{1max}|$ =3.0(rad)
$|\phi|_{1mean}$ =1.7±0.3(rad)

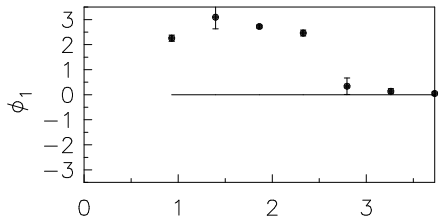

UGC 6917
$|\phi_{1max}|$ =3.1(rad)
$|\phi|_{1mean}$ =1.6±0.2(rad)

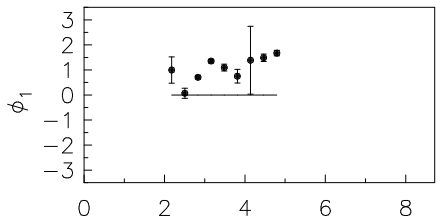

NGC 3992
$|\phi_{1max}|$ =1.7(rad)
$|\phi|_{1mean}$ =1.1±0.5(rad)

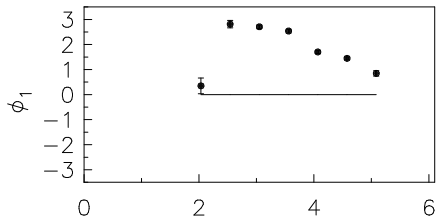

UGC 6983
$|\phi_{1max}|$ =2.8(rad)
$|\phi|_{1mean}$ =1.8±0.1(rad)

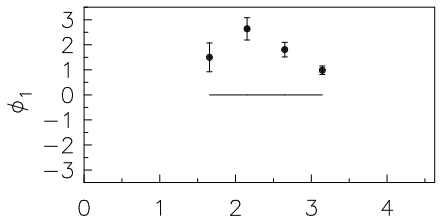

NGC 4051
$|\phi_{1max}|$ =2.6(rad)
$|\phi|_{1mean}$ =1.7±0.4(rad)

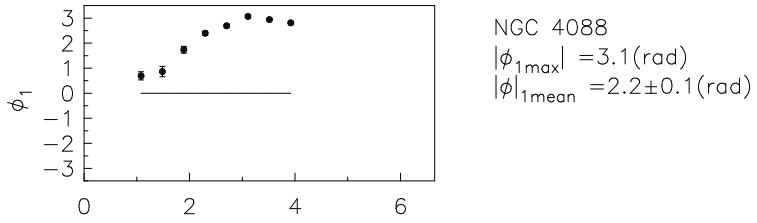

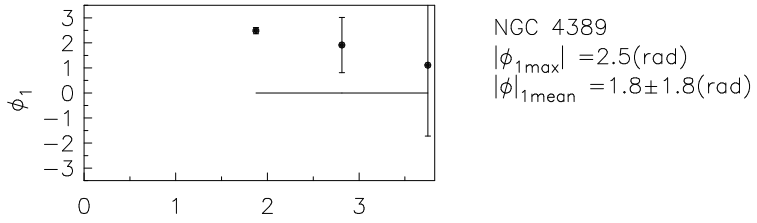

Figure 3.4: The asymmetry phase parameter derived from the surface density maps (moment 0) of galaxies selected from the Ursa Major group. In each of the maps, the radius is in the units of K'-band scale length.

The resulting A_1 and ϕ_1 values are plotted as a function of the radius scaled in terms of the near-IR scale lengths R_K or R_J are shown in Fig. 3.1, Fig. 3.2, Fig. 3.3 and Fig. 3.4 respectively. This scaling was done in order to facilitate a direct comparison with the near-IR values of stellar asymmetry over the same radial range as given in the earlier literature. In the case of some of the Eridanus group of galaxies, where no scale lengths were available (denoted by $*$ in the last two columns in Tab. 3.2), a mean scale length of $\sim$ 2kpc was taken. For the Eridanus group galaxies, the mean values for A_1 obtained over the range of 1.5 to 2.5 stellar exponential disk scale lengths (R_K values are preferred) are given in column 3, Tab. 3.6. The average A_1 values in the 1.5 to 2.5 R_K range of Ursa Major group galaxies are given in the column 3 of Tab. 3.5. For easy comparison of these two group A_1 values, we display them in the form of a histogram also (Fig. 3.5). In order to check whether the A_1 values of these two groups are similar, we have carried out Kolmogorov-Smirnov (KS) test on the data samples, including 3 values of A_1 estimated from the R-Band analysis (see section 3.3.3). The D statistics value was estimated to be 0.357. The probability that the two samples come from the same distribution is 23.6%. Hence the KS test indicates that the A_1 coefficients of the two groups come from different sets. This points to different physical origins for the lopsidedness seen in these two groups.

The typical HI radial surface density profile of the galaxies belonging to Eridanus group and the Ursa Major group are far from exponential and was close to a Gaussian (Omar & Dwarakanath, 2005a; Verheijen & Sancisi, 2001). This is unlike the Virgo cluster, where many galaxies have exponentially decreasing HI surface density in the outer regions (Warmels, 1988). Hence we determined a scale length, R_w, associated with a Gaussian profile for the various galaxies in these groups. This was

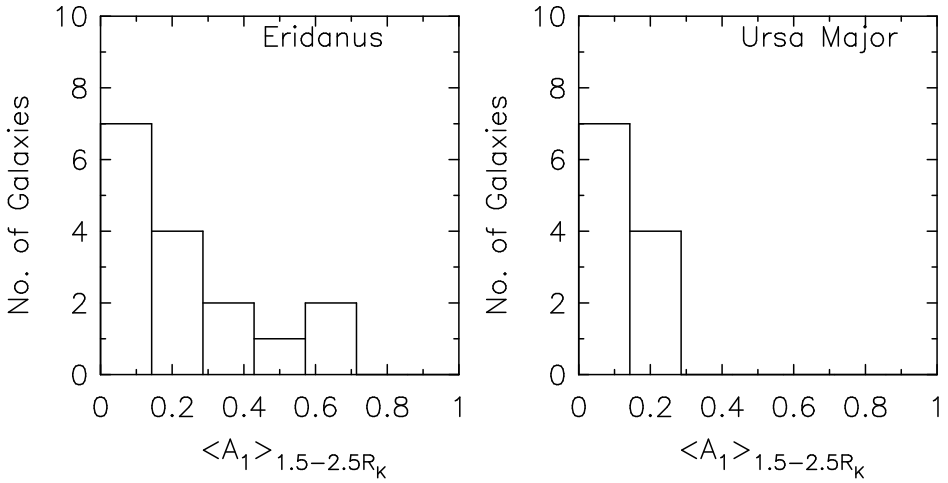

Figure 3.5: Histograms showing the number of galaxies Vs. $< A_1 >$ in the 1.5-2.5 R_K range for the Eridanus group (left-hand panel) and the Ursa Major group (right-hand panel) of galaxies.

done by performing a χ^2 fit to the radial surface density profile. A face-on radial surface density profile was obtained for each galaxy after integrating along concentric annuli. This surface density profile was fitted with a curve of the form $S_0 \exp(-(R-b)^2/2R_w^2)$ using a χ^2-fitting technique with S_0, b and R_w as the best fit parameters. The R_w values of Eridanus group of galaxies are given in column 4, Tab. 3.3 and those of the Ursa Major group galaxies are given in column 5, Tab. 3.5. For the Ursa Major group galaxies, we have estimated the A_1, A_2 and A_3 values in the 1 to 2 R_w range. These values are also tabulated in Tab. 3.5.

3.3.3 Harmonic Analysis of Optical Images

As a result of the HI harmonic analysis described earlier, we are at a unique position to compare the lopsidedness observed in the stellar disk with that of the observed HI asymmetry. Even though a theoretical model for the origin of lopsidedness based on the linear disk response to a distorted halo predicts similar values for the A_1 coefficients from the stellar and gaseous components

(Jog, 1997; Jog, 2000), this point is not yet verified by observations. Here we analyse the R-band images of some of the sample galaxies obtained of the Eridanus group of galaxies using the Sampurnanand Telescope, ARIES, Nainital,India. Details of the observations and the basic image processing are dealt with elsewhere (Omar & Dwarakanath, 2006). In a similar vein, we have also made use of the R-band images of some of the galaxies belonging to the Ursa Major group to study the lopsidedness seen in them. These images were obtained from the CDAC.

The reduced images were de-projected using the IRAF[2] STSDAS [3] task IMLINTRAN (Buta et al., 1998). The mean inclination and position angle derived from the HI velocity field were used in de-projection. Since our interest was in the outer regions of the galaxies the bulge-disk decomposition was not performed before the de-projection. In this region ($\sim$ 3kpc from the centre), the effect due to the bulge and the bar are unimportant.

From the de-projected images, the isophotal intensities along concentric annuli of width $1''$ were extracted as a function of azimuthal angle. The ELLIPSE[4] task was used for this purpose. A χ^2 fit on the extracted intensities was carried out by NFIT1D routine of STSDAS using the function

$$I(R,\phi) = a_0(R) + \sum_m a_m(R)\cos(m\phi) + b_m(R)\sin(m\phi) \qquad (3.5)$$

Here, $I(R,\phi)$ is the intensity at the ring radius R and azimuthal angle ϕ in the plane of the galaxy. a_m and b_m were the harmonic coefficients. From the resulting a_1,b_1 coefficients the normalized A_1 coefficients for various rings

[2]IRAF is distributed by the National Optical Astronomy Observatories,which are operated by the Association of Universities for Research in Astronomy, Inc., under cooperative agreement with the National Science Foundation.

[3]Space Telescope Science Data Analysis System

[4]ELLIPSE is a product of the Space Telescope Science Institute, which is operated by AURA for NASA.

were determined.

The values so derived for four galaxies belonging to the Eridanus group: NGC 1309, NGC 1347, IC 1953, and NGC 1359, are shown in Fig. 3.6. Similarly, the A_1 coefficients of two galaxies belonging to the Ursa Major group, namely NGC 3726 and NGC 4051, are shown in Fig. 3.7. For easy comparison, we have also plotted the corresponding A_1 coefficients derived from the HI data. It is seen that A_1 coefficients derived from R-band images and those from HI analysis are comparable in the radial region where the data overlap, although we caution that the region of overlap is small. From Fig. 3.6 it can be seen that in one case, the stellar asymmetry values are slightly higher than the HI values while the reverse is true in two cases, and in NGC 1359 they overlap. Thus in general, the A_1 values for stars show the same general trend as do the HI values. In these graphs HI is the only available tracer in the outer regions.

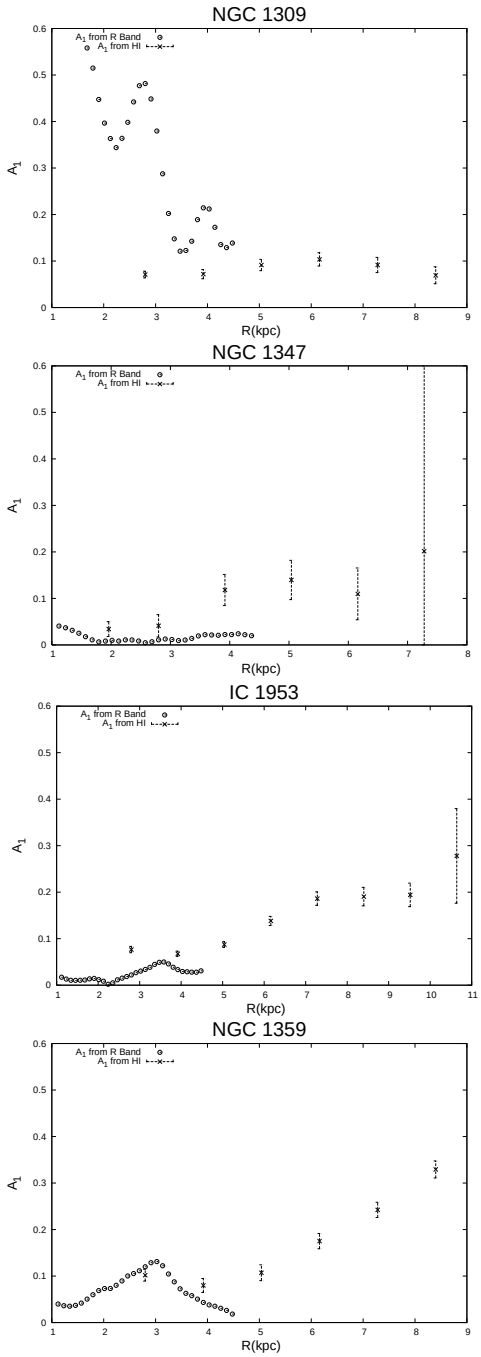

Figure 3.6: A_1 coefficients derived from R-band images of a few Eridanus group of galaxies along with those derived from HI analysis as a function of distance.

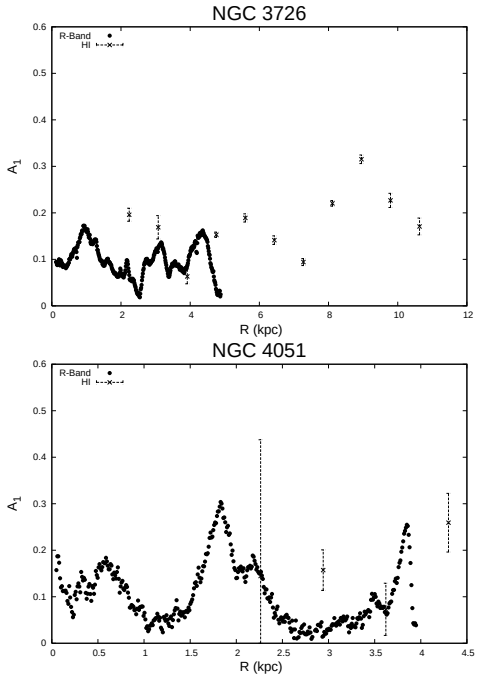

Figure 3.7: The A_1 coefficients derived from R-Band images of two Ursa Major group of galaxies, which are compared with that obtained from HI surface density maps. Note that the values are comparable in the inner regions of radial overlap.

3.3.4 Spatial Lopsidedness and Galaxy Morphology

As a result of our analysis of spatial lopsidedness of the galaxies belonging to the Eridanus and Ursa Major groups, we are capable of comparing the spatial lopsidedness of galaxies as a function of the Hubble type. The B-band images and corresponding Hubble classification of the galaxies belonging to the two groups, namely the Eridanus and the Ursa Major groups, are available from the NASA Extra-galactic Data Archives (NED) and the Digitized Sky Survey (DSS). For each of the galaxies, we have used the average A_1 value in the 1.5 to 2.5 K-band scale length range and the associated Hubble type value to check for correlations. As mentioned earlier, in the scale length range mentioned above we expect the effect of bars and the associated shocks and perturbations to be minimal.

Consequent to our analysis, we found that in the Eridanus group, early type spirals have higher spatial lopsidedness compared to its late type spiral galaxies. Such a trend is seen in the Ursa Major group galaxies also, although in a much weaker scale. We postulate that the group compactness and the associated strength of tidal interactions to be the major cause for the early type spiral galaxies to be more lopsided compared to the late type spiral galaxies. This postulate is buttressed by three other observations. The first of them is that in the field galaxies the asymmetry parameter Vs. Hubble type shows an opposite trend (Bournaud et al., 2005) to that seen in group galaxies. The cause of asymmetry in this case, where tidal and ram-pressure effects are small, is ascribed to asymmetric accretion of gas from the cosmological filaments. Secondly the asymmetry of early type spirals seen in the Eridanus group galaxies is on the average larger than that seen in the case of Ursa Major group. It is known from the earlier studies that Eridanus group is more compact compared to the Ursa Major group

(Omar & Dwarakanath, 2005a). Recent work on Ursa Major group seems to indicate that this group is close to the field galaxies.

3.3.5 Estimation of the halo perturbation

Assuming that the disk lopsidedness arises as a disk response to the halo perturbation, we use the observed A_1 coefficients to determine the halo asymmetry or the perturbation potential (Jog, 2000). We assume that the potential $\psi(R,\phi)$ at a radius R for a galaxy to be composed of an unperturbed part $\psi_0(R,\phi)$ and a perturbed part $\psi_1(R,\phi)$. It is known that most spiral galaxies have flat rotation curves in the outer regions. Choosing $\psi_0 \propto \ln(R)$ as the unperturbed potential can explain this result. The perturbation potential is assumed to have a cosine dependence to represent the lopsidedness.

For computational purpose, ψ_0 and ψ_1 were taken as

$$\psi_0(R,\phi) = V_c^2 \ln(R)$$

$$\psi_1(R,\phi) = V_c^2 \epsilon_1 \cos(\phi) \tag{3.6}$$

Here, V_c is the rotational velocity, ϕ is the azimuthal angle in the plane of the galaxy and ϵ_1 is the perturbation parameter which is assumed to be constant with radius for simplicity.

Simultaneously solving the equations of motion of orbits in this net potential, the effective surface density (assuming an exponential disk) and the equation of continuity yields a relation between the A_1 values and the halo perturbation parameter ϵ_1 for an exponential disk (Jog, 2000). This is applicable for both stars and gas in the linear perturbation regime (Jog, 1997).

Taking the cue from Jog (2000) and applying the same for a Gaussian surface density distribution, we obtained the following relation between A_1 and ϵ_1, in terms of R_w :

$$\epsilon_1 = \frac{A_1(R)}{(2(\frac{R}{R_w})^2 - 1)} \tag{3.7}$$

For the Eridanus group galaxies, the values of R_w, the Gaussian scale length, $< A_1 >_w$, the mean A_1 observed over 1-2 R_w range, and $< \epsilon_1 >$, the mean perturbation parameter for the halo potential over this radial range are given in the last three columns of Tab. 3.6. The typical value of the exponential stellar disk scale length is $\sim$ 2 kpc, while that of the scale length for the HI distribution R_w is $\sim$ 6 kpc. The third column gives an average of $< A_1 >_K$ for HI measured over 1.5-2.5 exponential disk scale lengths, and can be compared directly with the values of lopsidedness measured earlier from stellar distribution over the same range of radii (Rix&Zaritsky, 1995; Bournaud et al., 2005). The last two columns denote asymmetry in the HI surface density and the mean perturbation parameter respectively, in the outer parts of a galactic disk. The mean value of $< A_1 >_K$ in the inner disk (1.5 to 2.5 R_K) is 0.24, while that in the outer disk is slightly higher =0.27 (Tab. 3.6).

In the case of galaxies belonging to the Ursa Major group, from their respective surface density maps we have also estimated the higher order normalized harmonic coefficients for m= 2 & 3 in additon to m=1. Assuming that the HI surface density can be fitted with a Gaussian curve, the associated Gaussian scale length (R_w) was also estimated as in the case of Eridanus Group Galaxies. Using this scale length the relations between ϵ_m, A_m and R_w have been derived for m = 1, 2 and 3, following the procedure in Jog (2000) where it was developed for an exponential disk distribution in

Table 3.4: The m=1 asymmetry values in the Eridanus sample.

Galaxy	A_{1Max}	$< A_1 >_K$ (1.5 to 2.5 R_K)	R_w (kpc)	$< A_1 >_w$ (1 to 2 R_w)	$< \epsilon_1 >$ (1 to 2 R_w)
NGC 1309	0.10 ± 0.01	0.07	4.76	0.09	0.04
UGCA 068	0.21 ± 0.04	$--$	3.59	0.11	0.04
NGC 1325	0.38 ± 0.01	0.18	6.18	0.20	0.06
NGC 1345	0.48 ± 0.04	0.09	6.95	0.30	0.12
NGC 1347	0.20 ± 2.1	0.04	3.23	0.12	0.04
UGCA 077	0.10 ± 0.03	0.07	4.55	0.06	0.02
IC 1953	0.28 ± 0.10	0.19	4.61	0.15	0.05
NGC 1359	0.33 ± 0.02	0.14	11.23	$--$	$--$
NGC 1371	0.19 ± 0.01	$--$	$--$	$--$	$--$
ESO 548 -G 049	0.80 ± 0.08	0.55	3.91	0.74	0.51
ESO 482 -G 013	0.19 ± 0.03	0.15	2.95	0.19	0.10
NGC 1385	0.33 ± 0.08	0.33	6.16	0.33	0.26
NGC 1390	0.40 ± 0.07	0.40	4.07	0.36	0.18
NGC 1414	0.14 ± 0.04	0.12	8.40	$--$	$--$
ESO 482-G 035	0.83 ± 0.06	0.59	3.22	0.71	0.26
NGC 1422	0.79 ± 0.10	0.58	20.45	$--$	$--$
MCG -03-10-041	0.31 ± 0.05	0.17	5.15	0.28	0.12
ESO 549-G 035	0.17 ± 0.02	0.09	3.73	0.09	0.05

Notes:

1. The A_1 mean value between 1.5 to 2.5 exponential scale lengths is given in column 3. The Gaussian scale length for HI, R_w, and the resulting $< A_1 >_w$ and ϵ_1 over 1-2 R_w are shown in columns 4 and 5 respectively.

2. The mean of $< A_1 >_K$ in the range 1.5 to 2.5 R_K is 0.24 ± 0.19 and the mean of $< A_1 >_w$ in the 1 to 2 R_w range is 0.27 ± 0.22.The mean of $< \epsilon_1 >$ is 0.13 ± 0.13.

3. These results do not change much if the galaxies with i $> 70^\circ$ and with $R_{exp} = 2$ are eliminated from the sample - in that case the mean of $< A_1 >_K = 0.22 \pm 0.17$ between 1.5 - 2.5 R_K and mean of $< A_1 >_w = 0.26 \pm 0.18$ between 1-2 R_w

Table 3.5: The mean values of A_1 in the range 1.5-2.5 R_k, and A_1, A_2, A_3 in the range 1-2 R_w

Name	Type	R_k (kpc)	$< A_1 >_k$ $1.5-2.5R_k$	R_w (kpc)	$< A_1 >_w$ $1-2R_w$	$< A_2 >_w$ $1-2R_w$	$< A_3 >_w$ $1-2R_w$
UGC 6446	7	0.82	0.14	3.19	0.17	0.23	0.08
NGC 3726	5	2.12	0.11	4.08	0.16	0.12	0.12
NGC 3893	5	1.70	0.20	$--$	$--$	$--$	$--$
NGC 3949	4	1.00	0.16	2.69	0.22	0.27	0.07
NGC 3953	4	2.90	0.13	3.96	0.17	0.28	0.17
UGC 6917	7	1.90	0.13	3.80	0.13	0.21	0.06
NGC 3992	4	3.11	0.23	$--$	$--$	$--$	$--$
UGC 6983	6	2.06	0.03	4.43	0.13	0.07	0.11
NGC 4051	4	1.37	0.15	2.86	0.17	0.25	0.14
NGC 4088	4	1.81	0.08	4.13	0.19	0.18	0.11
NGC 4389	4	0.74	0.14	$--$	$--$	$--$	$--$
Mean			0.14 ± 0.05		0.17 ± 0.03	0.20 ± 0.07	0.11 ± 0.04

a region of flat rotation curve. This yields the following relations between the perturbation parameters for the potential ϵ_m and the A_m values:

$$\epsilon_2 = \frac{A_2(R)}{(R/R_w)^2 + 1} \tag{3.8}$$

and

$$\epsilon_3 = \frac{A_3(R)}{(2/7)(R/R_w)^2 + 1} \tag{3.9}$$

The resulting mean values of the perturbation parameters are obtained using the measured values of the Fourier amplitudes A_1, A_2 and A_3. These values are given in Tab. 3.5.

It is now believed that halos of galaxies in groups are merged in the outer parts (Athanassoula et al. 1997). However, in the inner regions of 10 kpc where we studied the asymmetry, we could treat the asymmetry as if

the halo was isolated. Hence the above model of disk response to a halo is still reasonably valid and the inner regions could carry the salient features of complex tidal interactions in a group setting.

The main results from this subsection are:

- The average value of ϵ_1 or the lopsided perturbation for the potential obtained in the outer parts of Ursa Major group galaxies (in the radial range 1-2 R_w) is $\sim 6\%$. This is smaller than the value for the Eridanus group galaxies where the halo lopsided potential was derived to be 10% - This reflects the smaller observed amplitudes of lopsidedness in the galaxies of Ursa Major group sample.

  Thus if the lopsidedness is due to the response to the halo distortion, then this gives 6% as the typical halo lopsidedness for the Ursa Major galaxies.

- For the Ursa Major group galaxies the elongation in the potential or the magnitude or the amplitude of the elongation in the term ϵ_1 value is comparable (within a factor of $\sin(2\phi_2)$) with the kinematical asymmetry (see columns 3 and 6 of Tab. 3.6). This confirms the argument (Jog 1997, Jog 2002) that both spatial and kinematical asymmetry result from the same perturbation potential.

- The values of all three perturbation potentials derived for the Ursa Major group of galaxies *viz.* $\epsilon_1, \epsilon_2, \epsilon_3$ are comparable to each other(Tab. 3.6). Although this result depends on the model used, it reinforces the similar result obtained for the Fourier amplitudes *viz.* $< A_1 >$, $< A_2 >$ and $< A_3 >$ (Tab. 3.5), which are directly observed and hence are model-independent. This can be an important clue to the mechanism for generating lopsidedness in groups, and perhaps in-

Table 3.6: Ursa Major group galaxies: The HI-scale length(R_w), and the mean perturbation parameters of potentials ($< \epsilon_1 >$,$< \epsilon_2 >$ & $< \epsilon_3 >$) obtained from A_1, A_2 and A_3- the coefficients of surface densities and $< \epsilon_2 \sin(2\phi_2) >$ from velocity fields. The mean values are calculated between 1-2 R_w

Name	R_w (kpc)	$< \epsilon_1 >$	$< \epsilon_2 >$	$< \epsilon_3 >$	$< \epsilon_2 \sin(2\phi_2) >$
UGC 6446	3.19	0.046	0.040	0.065	-0.173
NGC 3726	4.08	0.049	0.042	0.111	-0.392
NGC 3949	2.69	0.072	0.106	0.056	0.178
NGC 3953	3.96	0.044	0.098	0.113	-0.171
UGC 6917	3.80	0.041	0.057	0.083	0.007
UGC 6983	4.43	0.032	0.022	0.128	-0.213
NGC 4051	2.86	0.082	0.113	0.109	-0.087
NGC 4088	4.13	0.089	0.076	0.092	0.001
Mean		0.057 ± 0.021	0.069 ± 0.034	0.095 ± 0.025	-0.106 ± 0.172

dicates the importance of multiple simultaneous tidal interactions that can occur under the special conditions of a group environment.

3.4 Discussion

1. Distribution of lopsidedness

We have carried out the Fourier harmonic analysis for the HI surface density of the Eridanus and Ursa Major group of galaxies. All the eighteen galaxies studied in Eridanus group show significant average lopsidedness with a mean value of $< A_1 >_K = 0.24$ in the inner regions of < 5 kpc, which is more than twice the average value observed for field galaxies (Zaritsky & Rix 1997, Bournaud et al. 2005). A large fraction $\sim 30\%$ show even higher lopsidedness with a value of $< A_1 >_K \geq 0.3$, whereas only 7% of the field galaxies have such high lopsidedness (Bournaud et al. 2005). In the field

galaxies $\sim 12\%$ of galaxies show $A_1 \geq 0.2$, whereas in the Eridanus sample $\sim 40\%$ of the galaxies show this.

The Ursa Major group of galaxies show a typical lopsidedness of $\sim 14\%$ in the inner regions, which is comparable to the field case, and about half of what is seen in the Eridanus group. We also measured the $< A_1 >$ values in the outer parts between 1-2 R_w, and found this to be $\sim 17\%$. Again this is smaller by a factor of ~ 1.6 compared to the Eridanus case. We have measured the values in the outer disks (> 5 kpc) or outside of 2.5 exponential disk scale lengths as well and found that the average value of mean lopsidedness measured in the outer regions is slightly higher($= 0.27$) for the Eridanus group galaxies. For the Ursa Major group galaxies, the mean lopsidedness measured in the outer regions is comparable to that of the inner regions.

2. Phases of lopsidedness

From Fig. 3.2, we see that the values of the phase angles of 15 galaxies in the Eridanus group remain nearly constant without sudden jumps; the exceptions being NGC 1309, UGCA 077 and NGC 1371. This means that the surface density contours have egg-shaped rather than one-armed profiles, and the potential causing the disk lopsidedness can be taken to have no radial phase dependence. This is similar to the behaviour seen in the inner regions as traced by the near-IR studies in Rix & Zaritsky (1995)- see Jog (1997) for a discussion of this topic. A nearly constant phase implies that these are global m=1 modes. However, in the case of Ursa Major group galaxies, the constant phase is an exception rather than a norm. This might indicate that the argument that the existence of global asymmetry may not be completely valid for galaxies in the Ursa Major group.

3. Origin of disk lopsidedness in group galaxies

We have shown above that the overall average values of A_1 in the Eridanus group galaxies in the inner regions are higher by a factor of two compared to the field galaxies($< A_1 >= 0.11$, (Bournaud et al., 2005)), and $\sim 70\%$ of the sample galaxies show such a high value of lopsidedness. The similar values for lopsidedness measured in both stars and gas in the inner regions show that this indicate true lopsidedness. However we caution that, since the number of galaxies studied in HI and R-band is small and the radial range of overlap for the comparison (see Fig. 3.2, Fig. 3.3) is small, some of the difference in the lopsidedness in the group vs. the field cases could perhaps still be attributed to the different tracers used (HI for the group case and the stars for the field case respectively.)

The overall higher value of A_1 measured implies that a group environment is more effective in generating lopsidedness in disks of galaxies, either via tidal interactions that can distort the halo and then affect the disk (Jog 1997), or via asymmetric gas accretion (Bournaud et al. 2005). While we cannot give a clear preference for either one of these mechanisms based on the present work, tidal interactions appear to be more likely as argued below.

Given the high number density of galaxies in a group, a higher frequency and strength of tidal interactions are expected. Thus a tidal origin can explain the high frequency as well as the higher strength of lopsidedness observed in the Eridanus group of galaxies compared to a sample of field galaxies.

Theoretically one can explain the similarity of the observed values of lopsidedness for stars and HI gas, if the origin of lopsidedness is due to a linear disk response to a distorted halo (Jog, 1997). In this case, the likely origin of the halo distortion or lopsidedness could be due to tidal interactions between galaxies (Weinberg, 1995).

It is interesting to note that the galaxies in the Eridanus group exhibit HI deficiency, which is ascribed to tidal interaction (Omar & Dwarakanath, 2005b). This also might indicate that the higher average values of lopsidedness which we have observed could be due to tidal interaction.

We note that in contrast, a typical field sample showed no correlation in the stellar lopsidedness measured in the inner disk regions with a tidal parameter (Bournaud et al., 2005).

In the field case, the late type galaxies show a higher lopsidedness and are also more likely to be lopsided (see Fig. 7, Bournaud et al., 2005; also see Zaritsky & Rix,1997; Matthews et al., 1998). To check if this could be a spurious reason for the high A_1 measured in our sample, we plotted A_1 vs. the galaxy type for our sample. Interestingly, this shows an opposite trend, namely we get a weak correlation showing a *decrease* in A_1 for later type galaxies (Fig. 3.8). This is in sharp contrast to the strong correlation in A_1 with galaxy type, with A_1 increasing for later type galaxies, that is seen in previous studies which involved field galaxies.

Hence the high values of A_1 measured here cannot be due to the type of galaxies included in the sample.

These two results,*viz.* the higher average value of A_1 measured for the Eridanus group galaxies, and the weak anti-correlation of A_1 vs. galaxy Hubble type, clearly indicate that the main physical mechanism for the origin of the disk lopsidedness in a group environment is different from that for the field galaxies. Perhaps the gas accretion, which plays an important role in causing lopsidedness in the field galaxies (Bournaud et al. 2005), may not be so important in a group, especially since a group probably does not have much cold gas.

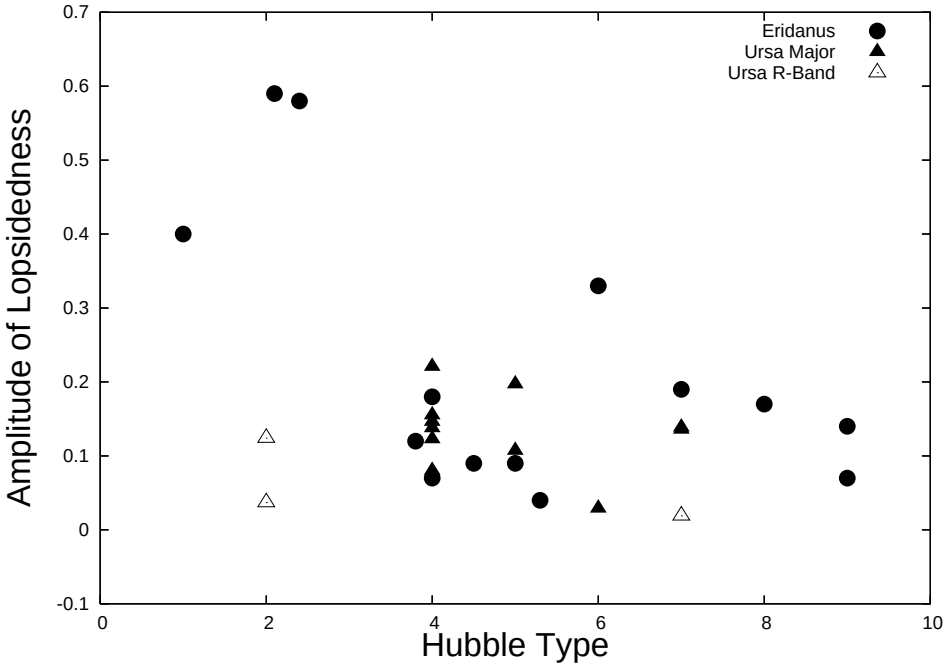

Figure 3.8: $< A_1 >_K$ in the 1.5 -2.5 R_K range Vs. Hubble type.The lopsidedness decreases for late-type galaxies for Eridanus group galaxies. This trend is weaker or flatter for the Ursa Major group of galaxies. The is opposite to the trend seen in the field galaxies (Bournaud et al., 2005). △ correspond to A_1 values estimated from the R-Band analysis of Ursa Major group galaxies.

We note that the earlier work on the measurement of HI asymmetry in Sculptor group galaxies (Schoenmakers, 2000) also showed kinematical lopsidedness in all the five galaxies studied. However, this method gives a value for the perturbation parameter for the potential times a term dependent on the inclination angle only. The average value for this product is ~ 0.06 which is much smaller than the average value of $< \epsilon_1 >= 0.13 \pm 0.13$ obtained for the 18 Eridanus group galaxies.

3.5 Conclusion

We have measured A_1 the amplitude of the first Fourier component over the average value for the surface density of HI in a sample of

18 galaxies in the Eridanus group of galaxies and 11 galaxies of the Ursa Major group, by Fourier analysis of the interferometric 2-D data (Omar & Dwarakanath, 2005a; Verheijen & Sancisi, 2001) of these galaxies. This is the first quantitative measurement of the spatial lopsidedness using HI data. The summary of conclusions from this paper is as follows:

1. All the Eridanus group galaxies studied show significant lopsidedness, with average $A_1 > 0.2$ in the region of 1.5-2.5 disk scale lengths. A large fraction $\sim 30\%$ show even higher average lopsidedness (> 0.3). For a few of the galaxies, the stellar R-band data available in the inner regions were analyzed, and the resulting values of lopsidedness are shown to be similar to the HI lopsidedness. The same amplitudes for stars and gas can be naturally explained if both arise due to a linear response of the disk to a distorted or lopsided halo (Jog, 1997).

2. The lopsidedness is observed to increase with radius, and the outer regions of Eridanus group galaxies have an average A_1 value of ~ 0.27. A few galaxies belonging the Ursa Major group showed such a trend.

3. The present work measures A_1 in disks up to the edge of the optical disks or four exponential disk scale lengths, and in a few cases even beyond that. This is more than twice the distance that is typically studied in the stellar distribution via near-IR photometry. This can help provide constraints on the origin of lopsidedness in disks, especially since lopsidedness is higher at larger radii. From the observed A_1 values, the halo distortion is deduced to be $\sim 10\%$ for Eridanus group galaxies.

4. The overall higher value of lopsidedness A_1 measured in the inner regions in the Eridanus group galaxies compared to the field galaxies

(e.g., Bournaud et al. 2005); and the smaller values of lopsidedness observed for the later Hubble type galaxies - which is opposite to the trend seen in field galaxies, together imply that a different physical mechanism is responsible for the origin of the disk lopsidedness in a group environment.

The present work highlights the need for a future dynamical study of the origin and evolution of disk lopsidedness in galaxies in groups. This can help in understanding the interactions and also the halo properties for galaxies in groups.

In all things of nature there is something of the marvelous.

–Aristotle (384 BC - 322 BC)

4

A Study of HI Content, Radio Continuum and Lopsidedness of Six Hickson Compact Group of Galaxies

4.1 Introduction

Atomic Hydrogen(HI) gas contents of galaxies in the field, groups and clusters reveal many aspects of their evolution (Hunter& Wilcots, 2002). HI studies can also throw light on the interactions of galaxies with their environment (Giovanelli & Haynes, 1985; Dressler, 1986). Characteristics of their past interactions can be seen in the HI gas contents of galaxies in groups (Verheijen & Sancisi, 2001; Omar & Dwarakanath, 2005a; Omar & Dwarakanath, 2005b) and in clusters (Bravo-Alfaro et al., 2000; Chung et al., 2007). In groups where the typical velocity dispersion is $\sim$ 200km s^{-1} the observed HI deficiency is often ascribed to tidal interactions (Omar & Dwarakanath, 2005c). In a cluster environment, close to the cluster centre, it is believed that HI is stripped due to ram pressure while

in the outer regions disturbances indicate tidal effects (Chung et al., 2007). The increased fraction of early Hubble type galaxies in clusters also shows the effect of environment(Dressler, 1980).

The Hickson Compact Groups (HCG) of galaxies is one class of compact groups where the environment of galaxies is dominated by their immediate neighbours. The isolation criterion (Hickson, 1982; Hickson, 1992) which is one of the classification parameters of HCGs ensures nearest neighbour interactions. In addition, it is seen that HCGs have typical projected number densities comparable to the cluster cores (Verdes-Montenegro et al., 2001) and have typical velocity dispersions (σ) $\sim$ 200 km s^{-1}. This implies that the galaxies belonging to HCGs have higher probability of undergoing tidal interactions with each other compared to cluster galaxies where the velocity dispersion is $\sim$ 1000 km s^{-1}. As a result the observed HI deficiency in HCGs is ascribed to tidal interactions (Verdes-Montenegro et al., 2001). Hence, compact groups will be ideal for studying the effect of tidal interactions on HI distribution and also to study the associated HI asymmetry or HI lopsidedness.

Lopsidedness or deviation from circular symmetry in the distribution and motion of matter in the disk of a spiral galaxy was first detected in radio observations (Baldwin et al., 1980). However, a method to quantify the observed asymmetry in the brightness distribution of a spiral galaxy was first developed for the K-band observations of galaxies (Rix&Zaritsky, 1995; Zaritsky& Rix, 1997; Bournaud et al., 2005). This procedure was based on the Fourier analysis of optical images and was later extended to the HI observations (Schoenmakers et al., 1997; Angiras et al., 2006; Angiras et al., 2007). In this analysis, lopsidedness as a function of radius and azimuthal angle in the velocity and surface density

maps of a galaxy is quantified in terms of the normalised Fourier coefficients (see section 4.3.1). Schoenmakers et al.(1997) used the HI velocity field and the associated Fourier coefficients to estimate the ellipticity of dark matter halo potential. Angiras et al. (2006) used the HI surface density maps in conjunction with the HI velocity maps to quantify the observed HI surface density lopsidedness in terms of Fourier coefficients. If lopsidedness is assumed to be the result of the disk response to a distorted halo (Jog, 1997; Jog, 2000), then the surface density Fourier coefficients can be used to estimate the ellipticity of the halo potential (Angiras et al., 2007). Both the surface density and the velocity field Fourier coefficient values gave similar ellipticity values for the dark matter halo potential (Angiras et al., 2007). It is also seen that in a group environment where there is higher probability of tidal interactions, early type spiral galaxies show more lopsidedness (Angiras et al., 2006). In the field galaxies, where lopsidedness may be due to asymmetric HI accretion from the cosmic filaments, the opposite trend is seen (Bournaud et al., 2005). However, a direct relation between lopsidedness and tidal interactions in a group environment is not yet confirmed. This is because the strength of tidal interactions on a galaxy cannot be measured explicitly. An isolated system of galaxies which is gravitationally bound and interacting is required for carrying out such a study. HCG galaxies provide such a system (Ponman et al., 1996).

We have observed galaxies belonging to six HCGs (Hickson, 1982) in the HI 21 cm-line emission using the Giant Meterwave Radio Telescope (GMRT). The groups selected for observation were HCG061, HCG030, HCG068, HCG007, HCG010 and HCG021. These groups were mainly selected on the basis of the group size (size of the smallest circle containing the centres of the member galaxies (Hickson, 1982)) which is related to the

compactness of the group. The galaxies in our sample are arranged according to decreasing compactness i.e., the most compact group is HCG061 and the least compact one HCG021. These galaxy groups have sizes in the range of 57-300kpc. Each of these isolated groups typically has 3-5 galaxies of similar types (Hickson, 1982). The selected groups contain at least one spiral galaxy whose inclination and optical diameter is suitable for the lopsidedness analysis (Angiras et al., 2006). Details of these groups are given in Table 4.1. Since the number and the Hubble types of galaxies in these groups are similar the tidal interactions can be related to the respective group sizes.

This paper is organised as follows. In section 4.2, a brief description of the GMRT and of the observations carried out are given. The basic radio data analysis and harmonic analysis methods are given in section 4.3. Section 4.4 gives the results. Interpretation of the results are given in section 4.5.

4.2 Radio Observations

The Giant Meterwave Radio Telescope (GMRT) is an aperture synthesis array consisting of 30 fully steerable parabolic dishes of 45 m diameter. The detailed description of the GMRT is given elsewhere (Swarup et al., 1991), but a summary is given here. The GMRT array configuration is such that it is capable of imaging small as well as extended structures. This is achieved by adopting a hybrid configuration for the antenna distribution. Fourteen of the thirty dishes are randomly located in the central one square kilometer. The remaining 16 dishes are distributed in the shape of a `Y`. The largest separation between the ends of the `Y` is $\sim$ 25 km and the smallest separation between the antennas is $\sim$ 100 m. This enables the GMRT to image structures in the range $2''$ - $7'$ at 21 cm wavelength. Since the typical angular

Table 4.1: HCG groups selected for observation with the GMRT.

Name	RA (J2000)	Dec(J2000)	V_{sys}	Group Size	Comments	B_{maj}	B_{min}
	h m s	° ′ ″	(km s^{-1})	(kpc)		(′)	(′)
HCG061A	12 12 18.8	+29 10 46	3784	∼57	S0/a Sy2	−−	−−
HCG061B	12 12 21.4	+29 12 25	1127		Sdm	−−	−−
HCG061C	12 12 31.0	+29 10 06	4012		Sbc AGN	1.8	0.4
HCG061D	12 12 26.9	+29 08 57	3980		S0	0.8	0.3
HCG030A	04 36 18.6	-02 49 53	4697	∼81	(R')SB(rs)0+	1.2	0.8
HCG030B	04 36 30.2	-02 51 59	4625		(R')SAB(rs)0+	1.1	0.9
HCG030C	04 36 23.4	-02 48 00	4508		SBbc	0.58	0.42
HCG030D	04 36 36.6	-02 50 35	4666		S0	0.51	0.34
HCG068A	13 53 26.7	+40 16 59	2325	∼86	S0 AGN	2.2	1.1
HCG068B	13 53 26.7	+40 18 10	2579		SA0 sp LINER	1.4	1.3
HCG068C	13 53 21.6	+40 21 50	2321		SB(r)b Sbrst	3.2	2.3
HCG068D	13 53 45.5	+40 20 19	2344		E3	1.12	0.72
HCG068E	13 54 00.4	+40 16 38	2401		S0/a	1.24	0.49
HCG007A	00 39 13.4	+00 51 51	4133	∼94	(R')SB(r)a HII	1.9	0.9
HCG007B	00 39 17.8	+00 54 46	4238		SB0 pec	1.2	0.8
HCG007C	00 39 34.8	+00 51 36	4415		SAB(r)c	1.75	1.15
HCG007D	00 39 18.8	+00 53 31	4121		SB0 pec	0.95	0.76
HCG010A	01 26 21.8	+34 42 11	5189	∼204	SB(r)b AGN	3.0	1.1
HCG010B	01 25 40.4	+34 42 48	4822		E1	2.4	2.1
HCG010C	01 26 18.9	+34 45 14	4660		SB0/a	1.9	0.5
HCG010D	01 26 30.9	+34 40 31	4662		Scd	1.0	0.2
HCG021A	02 45 18.0	-17 42 30	7552	∼315	SB(rs)ab	1.8	0.6
HCG021B	02 45 36.1	-17 41 20	7525		SA(r)a	1.7	0.7
HCG021C	02 44 53.7	-17 39 33	7453		SA(s)0-	1.8	1.3
HCG021D	02 45 29.6	-17 32 32	8835		E2	0.9	0.8
HCG021E	02 45 22.4	-17 31 59	8819		(R')SAB(rs)a pec?	0.9	0.6

Notes :B_{maj} and B_{min} are the major and minor optical diameters

sizes of the selected HCG galaxies are in the range $\sim 1'$ - $4'$, it is possible to image these galaxies with the GMRT. The group sizes of the selected HCGs lie in the range $\sim 4' - 11'$. These sizes are well within the primary beams of the GMRT antennas ($\sim 24'$ at 1420 MHz). Hence each of these groups could be imaged in a single pointing.

The observations of four groups were carried out on four consecutive days in August 2006 while the fifth group was observed in September 2006. Each of these groups was observed for ~ 6.5 hours in the High Resolution Mode (256 channels). Observations of these groups were carried out with 4MHz($\sim$ 800 km s^{-1} at 1420 MHz) bandwidth. This gave a channel resolution of ~ 15.6 kHz (~ 3.3 km s^{-1}).

HCG010 group was observed in March 2008 for about 6.5 hours. This group was observed with 8MHz (~ 1700 km s^{-1} at 1420 MHz) bandwidth to include all the galaxies. The baseband bandwidth was divided into 128 channels giving a channel resolution of ~ 62 kHz (~ 13 km s^{-1}).

4.3 Data Analysis

Major part of the data reduction was carried out using the Astronomical Image Processing System(AIPS). After carrying out gain and bandpass calibrations, the target source visibilities were extracted. The channels from the flat portion of the spectrum and free from HI line emission were used to estimate continuum visibilities. Spectral line visibilities in each of the spectral channels were obtained by subtracting the estimated continuum contribution to the visibilities (task UVLIN in AIPS). After continuum subtraction the resulting visibility data set was imaged and CLEANed (AIPS task IMAGR). During this process pure natural weighting scheme was used for obtaining the highest signal to noise ratio (SNR). In addition, 4 channel

averaging (except for HCG010) was carried out which improved the SNR by a factor of two. Since we are interested in the extended structure with high SNR, we further introduced a taper of ~ 40 kλ while imaging. The CLEANing was carried out till the residual image was left with values less than 3σ. The resulting cubes were convolved to a resolution of $35'' \times 35''$. These image cubes had a velocity resolution of $\sim$ 13km s^{-1} and a typical rms of $\sim$ 0.7mJy beam^{-1} channel^{-1}. They were used for generating the channel maps and the moment maps.

In the case of HCG010, while generating the CLEANed cube we introduced a uvtaper of 10 kλ. The resulting cube had a resolution of $29'' \times 23''$ (Position Angle (PA) $= -14^{\circ}$) and an rms of ~ 0.7 mJy beam^{-1}.

From the resulting CLEANed cubes, we obtained the HI surface density (mom 0) and HI velocity (mom 1) maps. For this purpose, we visually identified those channels with HI signal corresponding to the positions of various galaxies. From these channels, flux densities above 3σ level were added together to generate the moment maps (AIPS task MOMNT).

As a result of these analyses we detected HI emission signals from three of the groups, *viz.*, HCG007, HCG010 and HCG068. In the other three groups (HCG061, HCG030 and HCG021) we did not detect any HI. The moment 0 images of HCG007,HCG010 and HCG068 are given in figures 4.1, 4.2 and 4.3 respectively. The velocity field images of the members belonging to these groups are given in figures 4.4, 4.5 and 4.6 respectively.

The line free channels from the target source visibility data were used to make continuum maps. These channels were imaged with natural weighting and averaged together. For this imaging we used the full spatial frequency domain without introducing any taper. As a result of this analysis, we obtained continuum maps of all these HCGs with rms $\sim$ 0.4mJy/beam and

a synthesized beam of $\sim 25'' \times 15''$. However, continuum was detected corresponding to HCG group members only in the case of HCG007 and HCG068.

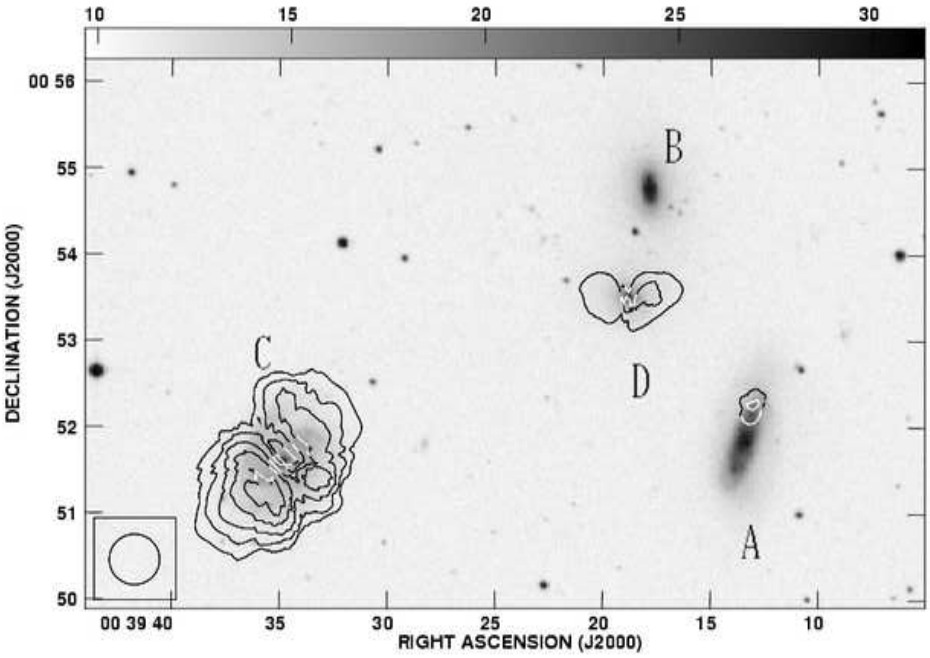

Figure 4.1: HCG007: HI surface density map superposed on DSS optical image. The HI column density contours are in units of 10^{20} cm^{-2} starting at 10^{20} cm^{-2}. Details of the galaxies marked A,B,C and D are given in Table 4.1.The synthesised beam (shown at the bottom left corner) is $35'' \times 35''$

4.3.1 Harmonic Analysis

The departure from azimuthal symmetry in the velocity or matter distribution is termed lopsidedness. From earlier work (Angiras et al., 2006; Angiras et al., 2007) it is seen that the lopsidedness can be quantified by carrying out the Fourier series analysis or the Harmonic analysis on the deprojected HI surface density maps. The global asymmetry is reflected in the

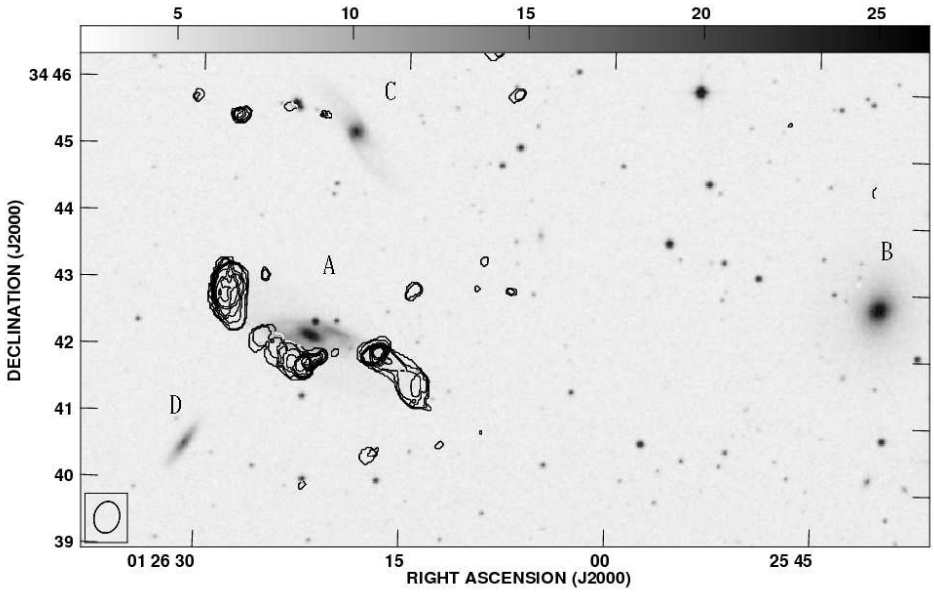

Figure 4.2: HCG010: HI surface density map superposed on DSS optical image. The HI column density contours are in units of 10^{20} cm^{-2} starting at 0.5×10^{20} cm^{-2}. Details of the galaxies marked A,B,C and D are given in Table 4.1.The synthesised beam (shown at the bottom left corner) is $29'' \times 23''$. The PA is $-14°$.

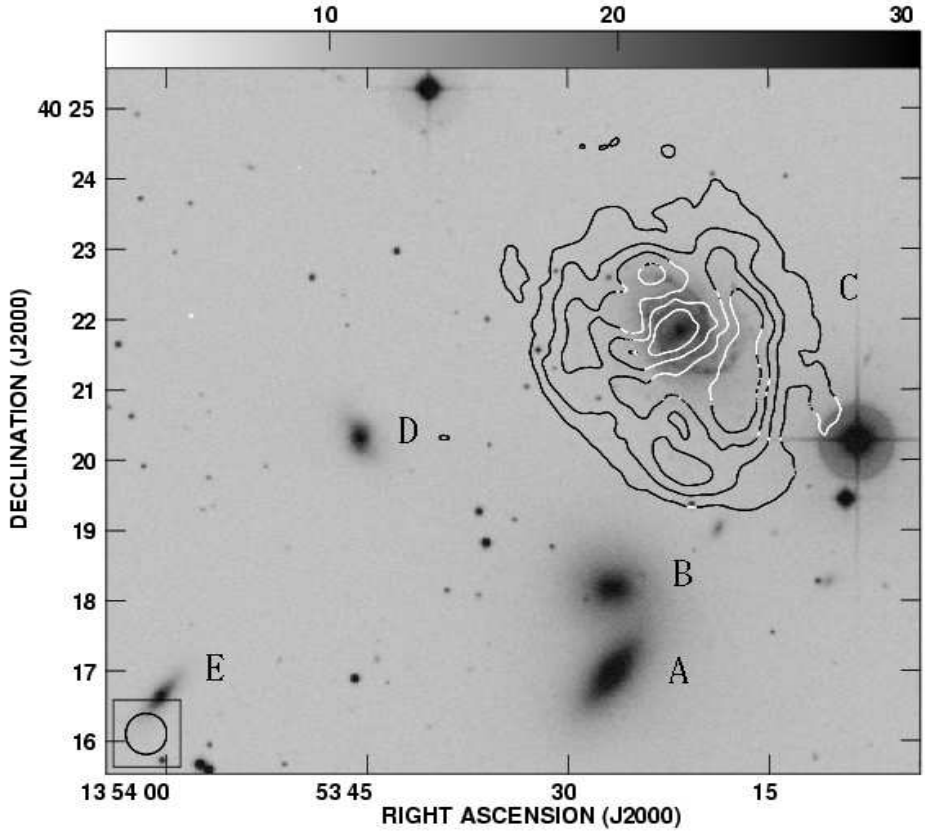

Figure 4.3: HCG068: HI surface density map superposed on DSS optical image. The HI column density contours are in units of 10^{20} cm^{-2} starting at 10^{20} cm^{-2}. Details of the galaxies marked A,B,C,D and E are given in Table 4.1.The synthesised beam (shown at the bottom left corner) is $35'' \times 35''$

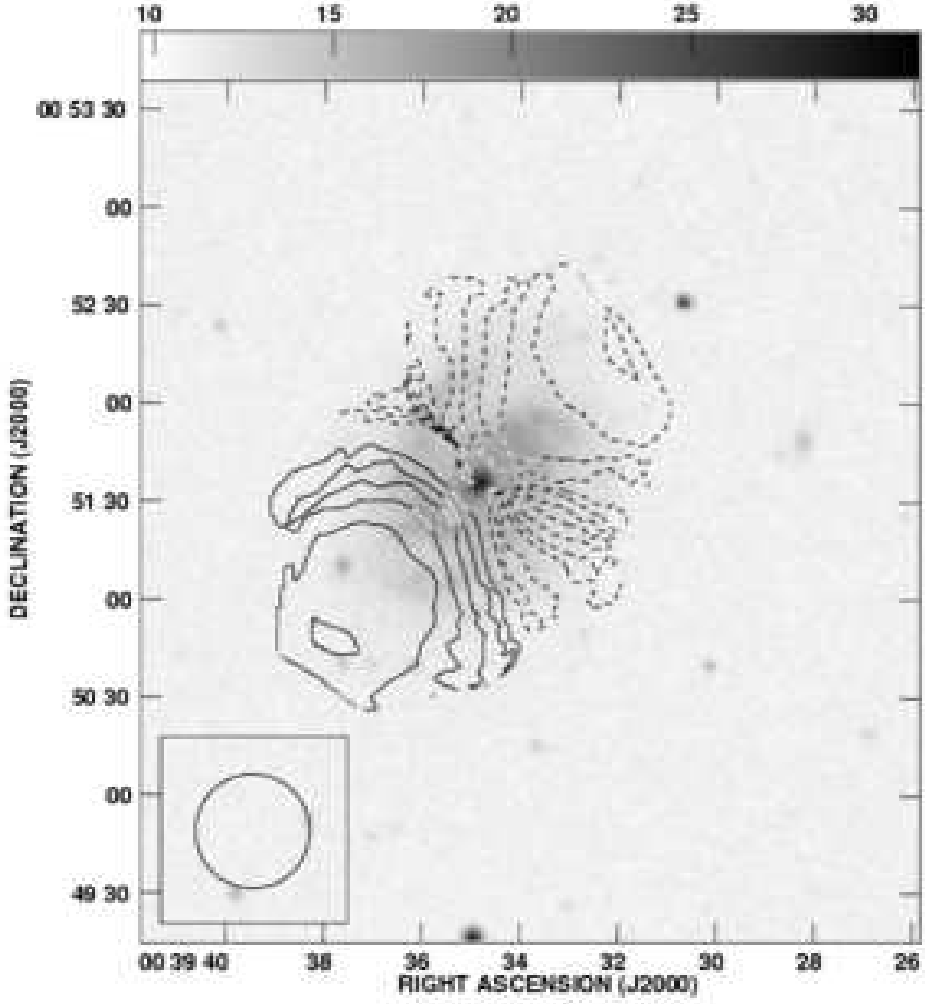

Figure 4.4: Velocity map of HCG007C. The contours are separated by 10 km s^{-1} and the systemic velocity is 4415 km s^{-1}. The solid contours are on the receding side. The broken contours are in the approaching side. The synthesised beam (shown at the bottom left corner) is $35'' \times 35''$

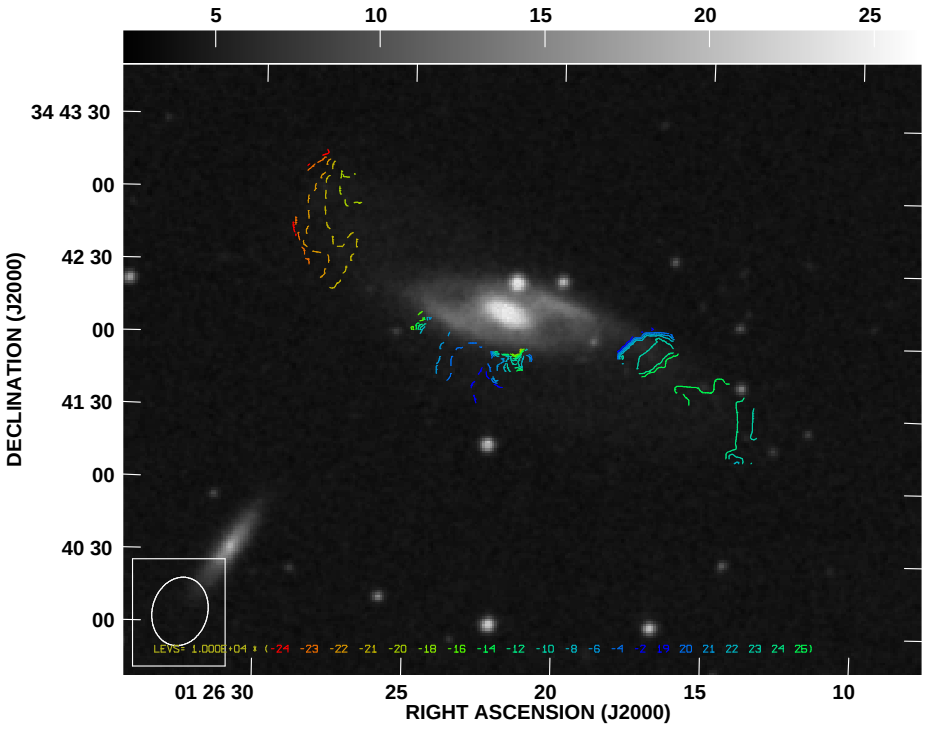

Figure 4.5: Velocity map of HCG010A. The contour levels are shown in colour at the bottom of the figure. The contours are separated by 10 km s^{-1} and the systemic velocity is 5189 km s^{-1}.The broken contours are in the approaching side.The synthesised beam (shown at the bottom left corner) is $29'' \times 23''$. The PA is $-14°$

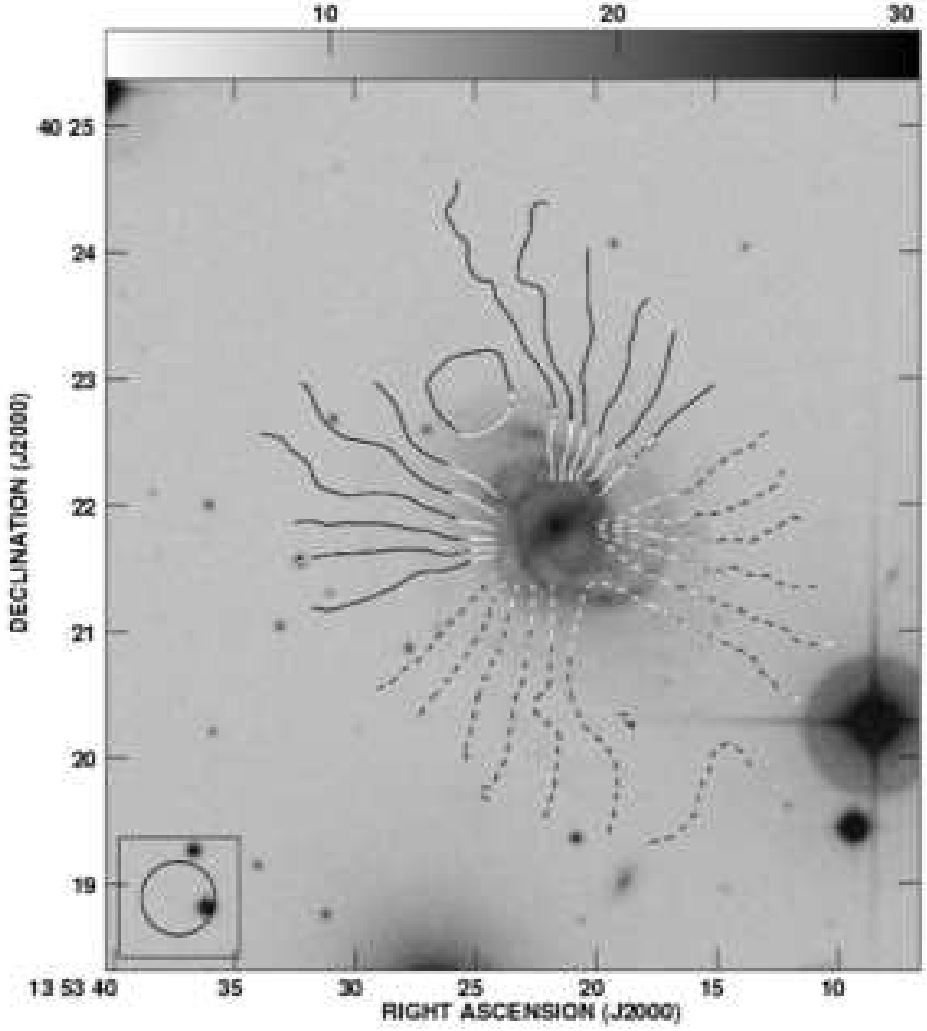

Figure 4.6: Velocity map of HCG068C. The contours are separated by 10 km s^{-1} and the systemic velocity is 2321 km s^{-1}. The solid contours indicate the receding side while the broken contours show the approaching side. The synthesised beam (shown at the bottom left corner) is $35'' \times 35''$

first order Fourier coefficient. Although the details of the analysis are given in earlier work(Angiras et al., 2006; Angiras et al., 2007) a brief summary is given here. Velocity maps are used in estimating the dynamical centre, the systemic velocity, the inclination and the position angle of the given galaxy. Using these values, the surface density maps are de-projected. From the de-projected surface density maps, the surface density ($\sigma(R,\theta)$) values are extracted along concentric circles as a function of the radius (R) and the azimuthal angle (θ). A Fourier series expansion given by

$$\sigma(R,\theta) = \sigma_0(R) + \sum_{m=1}^{10} a_m(R)\cos[m\theta - \phi_m(R)] \qquad (4.1)$$

is carried out on the surface density values. Here $\sigma_0(R)$ is the mean surface density at a given radius R. $\phi_m(R)$ is the phase of the m^{th} Fourier coefficient.

From these parameters, the global asymmetry parameter which is related to the normalised Fourier coefficient, A_1 ($= a_m/\sigma_0(R)$), is estimated. For this analysis to be successful, one requires the velocity maps and surface density maps to be smooth without abrupt changes. Hence such an analysis is possible only for HCG068C and not for any other galaxies in the HCGs selected for the current observations. The A_1 and ϕ_1 values as a function of normalised radius are shown in Figure 7.

For the purpose of comparing with earlier work (Rix&Zaritsky, 1995; Zaritsky& Rix, 1997; Bournaud et al., 2005; Angiras et al., 2006; Angiras et al., 2007) the mean value of A_1 in the 1.5 to 2.5 R-band disk scale length (R_R) was obtained ($A_1 =\sim 0.3$) for HCG068C. This value is three times larger than that for the field galaxies ($A_1 \sim 0.11$) (Rix&Zaritsky, 1995; Zaritsky& Rix, 1997; Bournaud et al., 2005) and is twice the value for the galaxies in a loose group like the Ursa Major group.

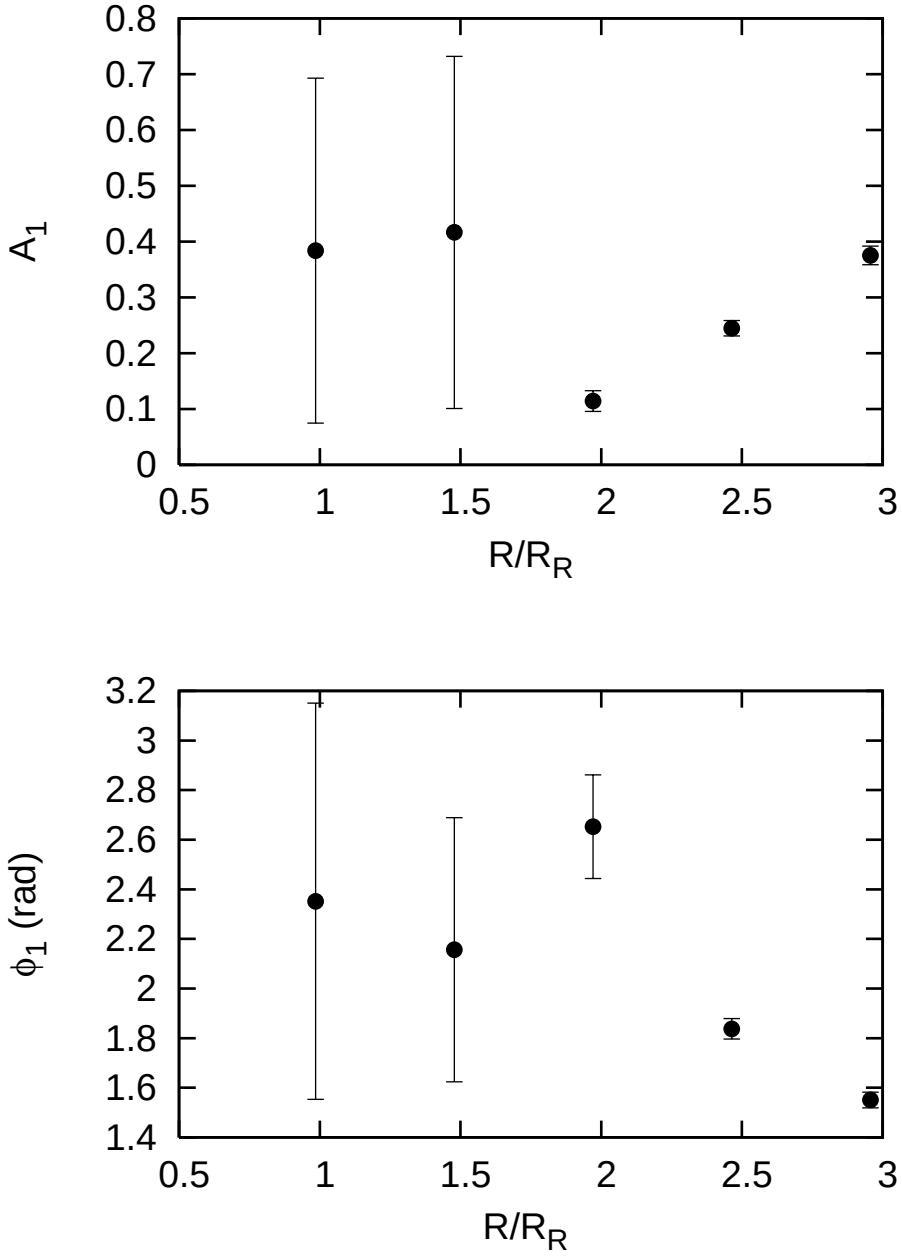

Figure 4.7: The normalized A_1 and ϕ_1 values of HCG068C.

Table 4.2: Results of HI observations of selected HCGs.

Name	V_{sys} (km s^{-1})	Dist. (Mpc)	Group Vel. disp (σ)(km s^{-1})	Group Size (kpc)	M_{HI} ($M_\odot \times 10^9$)	Opt.Dia (kpc)	HI Deficiency
HCG068C	2321	31.0	172	86	2.7	13.4	0.4
HCG007C	4415	58.9	103	94	2.7	22.8	0.3
HCG007D	4121	54.9	103	94	0.3	16.9	0.5
HCG010A	5189	69.2	241	204	2.7	27.3	1.0

Notes :H_0= 75 km $s^{-1}$$Mpc^{-1}$. The velocity dispersions (σ) and group sizes are taken from Hickson catalogue(Hickson, 1982)

In the Ursa Major Group of galaxies, the average A_1 in the 1.5-2.5 R_K was 0.14 ± 0.05 (Angiras et al., 2007) where R_K is the K-band scale length. However, the A_1 value of HCG068C is comparable to those estimated in the Eridanus group of galaxies (average A_1 in the 1.5-2.5 $R_K = 0.22 \pm 0.14$ (Angiras et al., 2006)).

4.4 Results

HI was detected from galaxies in 3 out of the 6 groups observed. The groups from which HI was detected were HCG007, HCG010 and HCG068 (Figures 1,2 and 3). At least one of the spiral galaxies was detected in HI from each of these groups. The velocity maps of these galaxies were also obtained (Figures 4.4, 4.5 and4.6). HI was not detected from HCG061 and HCG030 which are the most compact groups in our sample. In addition, HCG021 which is the farthest (100Mpc) and the most extended group in our sample also showed lack of HI.

The HI masses and the HI deficiencies of these galaxies have been estimated in accordance with earlier works (Haynes et al., 1998; Omar & Dwarakanath, 2005b; Sengupta et al., 2007) and are tabulated in

Table 4.3: Radio continuum & FIR flux densities

Name	$S_{1.4}$ mJy/beam	FIR ($\log(L_\odot)$)	$\log(L_{1.4})$ WHz^{-1}	q
HCG007A	12.3	10.23	21.65	2.59
HCG007B	< 0.43	$--$	$--$	$--$
HCG007C	< 0.43	$--$	$--$	$--$
HCG007D	< 0.43	$--$	$--$	$--$
HCG068A	30.9	8.93	21.55	1.38
HCG068B	6.51	9.10	20.97	2.14
HCG068C	3.16	8.74	20.56	3.19
HCG068D	< 0.27	$--$	$--$	$--$
HCG068E	< 0.27	$--$	$--$	$--$

Table 5.2. Here the HI deficiency (Def_{HI}) is defined as

$$Def_{HI} = \log\left[\frac{M(HI)}{{D_l}^2}\right]_{field} - \log\left[\frac{M(HI)}{{D_l}^2}\right]_{obs} \quad (4.2)$$

where $\log[M(HI)/{D_l}^2]_{field}$ values are taken from Haynes & Giovanelli (1984). The D_l is the corrected optical diameter in the B-Band in kpc (Paturel et al., 1991) at 25 mag arcsec^{-2}. M(HI) is the HI mass in $M_\odot$. The group velocity dispersions and group sizes are also shown in Table 5.2.

Radio continuum was detected in four galaxies belonging to 2 groups (HCG007 and HCG068) and are tabulated in Table 4.3. Using the existing IRAS $60\mu m$ ($S_{60\mu m}$)and $100\mu m$ ($S_{100\mu m}$)flux density values, we have estimated the Far Infra-Red flux (FIR) (Condon, 1992; Yun et al., 2001) which is given by the relation

$$FIR = 1.26 \times 10^{-14}(2.58S_{60\mu m} + S_{100\mu m}) \quad (4.3)$$

The FIR (in $L_\odot$) and the 1420 MHz continuum luminosities (WHz^{-1}) are

given in Table 4.3. Using the FIR values, we have also estimated the q (Yun et al., 2001) parameter which is defined by the equation

$$q = \log\left[\frac{FIR}{3.75 \times 10^{12} W m^{-2}}\right] - \log\left[\frac{S_{1.4GHz}}{W m^{-2} Hz^{-1}}\right] \quad (4.4)$$

These values are given in column 5 (Table 4.3).

4.5 Discussion

The Harmonic analysis was carried out on the HI surface density map of HCG068C. For this galaxy, we have obtained the A_1 coefficient which denotes the global asymmetry parameter. As in the group galaxies, *viz.* Eridanus (Angiras et al., 2006) and Ursa Major (Angiras et al., 2007), the A_1 coefficient as a function of radius shows an increasing trend beyond 2 R_R. The peak value of A_1 is ~ 0.4 (Figure 7) which is more than thrice the value seen in the field galaxies (Bournaud et al., 2005) and about 1.3 times of the value found in the group galaxies of similar Hubble types (Angiras et al., 2006; Angiras et al., 2007). Such an increasing trend in the value of the A_1 coefficient is consistent with tidal interactions being responsible for the observed lopsidedness of galaxies in groups. The value of the A_1 coefficient can be expected to be larger for the galaxies in the HCGs compared to those in loose groups, since HCGs are more compact, thus enhancing the chance and intensity of tidal encounters. The effects of tidal encounters can be erased after a time which is several rotation periods of the galaxy. However, the crossing time in this group is $\sim 4 \times 10^8$ years, which is comparable to the rotation periods of galaxies. Hence the memory of the past interactions is retained by galaxies in such a group. Tidal interactions are also expected to trigger star bursts in the interacting systems.

Interestingly, HCG068C is classified as a star burst galaxy.

The HI deficiencies of four galaxies belonging to three HCGs have been estimated. As can be seen from Table 4.2, all the 4 galaxies are HI deficient. Given the scatter in the HI deficiencies of field galaxies (rms ~ 0.2), the galaxies HCG068C and HCG007C are perhaps part of the scatter. However, HCG007D and HCG010A are significantly deficient, by factors of 2 and 10 respectively. The HI morphologies of these two galaxies are consistent with them being HI deficient. The mean HI deficiencies of galaxies in other HCGs studied in the past is ~ 0.6 (Verdes-Montenegro et al., 2001). The HCGs in this paper are not too different in this respect.

One of the interesting galaxies in the current study is HCG010A. This galaxy is warped as can be seen in deep R-band images. The HI distribution is highly fragmented and shows tidal debris. Earlier CO observations indicated that the star formation efficiency ($\log(L_{FIR}/M_{H_2})$) of this galaxy is low (~ -0.63) (Leon et al., 1998). The reduced HI column density and the reduced HI mass of this galaxy are consistent with the reduced star formation efficiency proposed earlier. In addition, the projected separations of HCG010A from HCG010D and HCG010C are < 50 kpc. Furthermore, the systemic velocities of these galaxies are comparable. Hence it is possible that the fragmented nature of the HI distribution in HCG010A is the result of tidal interactions between these systems. The velocity field of HCG010A (Fig. 4.5) indicates a systematic velocity gradient to the SW as would be expected when a tidal debris is pulled away from this galaxy.

We have estimated the q values (Condon, 1992; Yun et al., 2001) for four galaxies belonging to two HCG groups. The average value of q for field spirals is $\sim 2.34 \pm 0.01$ (Yun et al., 2001), with an rms ~ 0.12. In the case of field spirals, it is assumed that both the far-infrared and radio emission

from these spirals are due to star formation in the disk of the galaxy. In this scenario, the radio emission is extended over the entire disk of the galaxy from which the far-infrared emission is also detected. In the case of the HCG galaxies from which the radio continuum was detected (Table 4.3), all the radio sources were unresolved at the observed resolution of $\sim 20''$, although the optical extents of these galaxies are in the range ~ 1 to $3'$. Furthermore, the expected radio continuum luminosities from these galaxies, based on the FIR-radio correlation in the field galaxies, is an order of magnitude lower than that observed. Based on these two facts, it is clear that the detected radio emission from all these four HCG galaxies (Table 4.3) must have a more localised origin in the respective galaxies like an active galactic nucleus, or, a nuclear star burst. The data from the RC3 catalogue on these galaxies (Table 4.1) classifies them as HII, AGN, LINER and Star burst respectively, consistent with the current conclusions based on their radio emission properties.

Radio properties of spiral galaxies in the HCGs have been studied in the past (Menon 1995). In most of the 56 HCG spirals that were detected, the radio emission is confined to the central regions of the galaxies, similar to what is observed in the current sample. It is further noted that 3 out of the 4 galaxies detected in radio belong to HCG068, the closest Hickson group in the current sample. The faintest detection in this group corresponds to a 1.4 GHz luminosity of 20.56 (Table 4.3). This is close to the detection limit of the current observations. The other 5 HCGs in this sample are at least twice as far compared to HCG068 (Table 4.1). This increased distance implies that only galaxies with 4 (or, more) times higher luminosities will be detected in these other 5 HCGs. Based on the known radio luminosity function of spirals in the HCGs (Menon 1995), less than 20% of the galaxies

in the HCGs are at these, or, higher radio luminosities. The rather poor detection rate in the current observations is consistent with such a radio luminosity functions of spirals in HCGs.

When you know a thing, to hold that you know it, and when you do not know a thing, to allow that you do not know it - this is knowledge.

–Confucius (551 BC - 479 BC)

5

Conclusions and Future Plans

In this thesis, we have estimated the kinematical and spatial lopsidedness of galaxies belonging to groups of different compactness. The selected galaxies belong to a loose group like the Ursa Major(Angiras et al., 2007), a more compact group like the Eridanus (Angiras et al., 2006) and an extremely compact group like the Hickson Compact Group (Angiras & Dwarakanath 2008). In these groups, tidal interactions between the galaxies are the dominant mechanism causing lopsidedness.

The kinematical and spatial lopsidedness in the atomic hydrogen were quantified using the Fourier series decomposition of the velocity and the surface density maps respectively. These maps were obtained as a result of aperture synthesis observations carried out using the Giant Meterwave Radio Telescope (GMRT) and Westerbork Synthesis Radio Telescope (WSRT). The Fourier series decomposition carried out on these maps resulted in normalized Fourier coefficients as a function of galacto-centric radius.

One of the primary aims of our study was to check whether the spatial asymmetry as obtained from an analysis of the stellar disk matter distribu-

tion is comparable to that seen in the HI distribution. This was a contentious issue because HI is subjected to shocks generated by local events like super novae. Although earlier theoretical work hinted that asymmetries seen in both stellar and HI distributions should be comparable, in this thesis we experimentally verified it for the first time.

If the asymmetry seen in the velocity and spatial domains are the reflection of the asymmetry of dark matter halo potential, then it is possible to estimate the ellipticity of the dark matter halo potential under certain assumptions. As demonstrated in Appendix A.1 and in Schoenmakers et al. (1997) , if the dark matter potential is initially assumed to be axisymmetric and later develop a perturbation due to tidal interactions, then it is possible to obtain the ellipticity of the potential directly from the harmonic coefficients obtained from the velocity maps. In a similar manner, the ellipticity of the potential can be obtained from the surface density harmonic coefficients under the assumption of the validity of Poisson's equation, equation of continuity and the form of HI mass distribution (Jog, 1997; Jog, 2000). In this thesis, we have compared the ellipticity of the dark matter halo potential obtained using both these methods. It is seen that the ellipticities so obtained are consistent with each other.

As a result of our study, we have arrived at three major conclusions. The first and foremost among them is that in group environments, the major cause for asymmetries in the matter distribution of galaxies is tidal interactions. This conclusion was arrived at by studying three different groups, *viz.* Eridanus, Ursa Major and Hickson Compact Group of galaxies. Galaxies in the Ursa Major group, which is a very loose group, are almost akin to the field galaxies, have very low values for the asymmetry parameter(Angiras et al., 2007). For galax-

ies belonging to the Eridanus group, a group having group properties intermediate (Omar & Dwarakanath, 2005a; Angiras et al., 2007) between that of the Ursa Major group and a compact group like the Hickson Compact Group (Hickson, 1982; Hickson, 1992), the asymmetry parameter values were higher than those of Ursa Major group galaxies (Angiras & Dwarakanath 2008). The highest asymmetry parameter is obtained for the only HCG galaxy for which we could estimate the lopsidedness by harmonic analysis.

The second was the observed relation between asymmetry parameter and the galaxy morphology. In the Eridanus group of galaxies, the early type spiral galaxies tended to be more lopsided compared to the late type spirals. In the Ursa Major group no such clear trend is seen. The earlier work using near infra-red images of field galaxies indicated an opposite trend, *viz.*, late type spirals are more lopsided compared to early type spirals. The reverse trend seen in field galaxies is believed to be due to asymmetric in-fall of HI gas from large scale filaments and associated star formation (Bournaud et al., 2005).

The third outcome of our study is the observation that the asymmetry in the velocity fields of galaxies is of similar strength to that of surface density asymmetry. This may indicate a common origin for the kinematical and spatial lopsidedness (Jog, 2000).

5.1 Future Plans

As of now, we have only studied three types of groups classified on the basis of their compactness. The first step in establishing the effect of tidal interactions on lopsidedness, whether it is in the kinematical or spatial domain, is to ascertain the strength of tidal interactions. We have tried to estimate the

strength of tidal interactions in an *ad hoc* manner by studying the HCGs. This study, however could not give a statistically significant result. A more robust way of doing the same would be by studying a group which has been observed in X-rays. X-ray observation will help in finding the position of the centre of the group. By studying a group with a known centre, it will be possible to estimate the degree of lopsidedness as a function of group-centric distance for each of the spiral galaxies. In a cluster, early type galaxies are seen towards the core of the cluster. Hence, such an observation will also give partial explanation to the observed trend of early type spiral galaxies showing more lopsidedness than the late type spirals as seen in Eridanus group. For this purpose, we would like to study a spiral dominated group, with a known centre and we are right now in the process of identifying few of such groups.

Another problem which we faced in our study of lopsidedness is the estimation of lopsidedness due to random, inherent processes within a galaxy such as the effect of shocks and turbulence developed in the HI gas and the stellar distribution due to the enhanced star formation rates and super nova activity. Although low resolution numerical simulations of galactic disk carried out by us and earlier workers (Bournaud et al., 2005) indicate an asymmetry parameter of 0.05 for random process, this has no observational validity. Observing an isolated, face-on galaxy which does not show any signs of interaction and carrying out the lopsidedness analysis on it will go a long way in mitigating this uncertainty. Studying low surface brightness galaxies or ultra-thin galaxies will be of great importance in studying the effect of random processes on galaxy lopsidedness. Such a study is already on the anvil.

The numerical simulation of galaxies and their lopsidedness estimates

can lead us in another direction also. In many of the N-body simulations of galaxies, the initial galactic disk is generated by introducing particles into an external potential. As a result of such simulations, it is possible to study the effect of different potentials on the lopsidedness. In addition, if one assumes that the galaxy is undergoing a secular evolution in the presence of such a potential, then an estimate of the lopsidedness as a function of time can be generated. This will help us in understanding the development of lopsidedness, if any, in an isolated system. Such a study is important in the context of galaxy evolution and the periodic development and decay of galactic bars postulated by earlier workers (Bournaud & Combes, 2002). We have started a programme to numerically simulate spiral galaxies using N-body simulations (Barnes & Hut, 1986; Teuben, 1995). Our preliminary results are shown in Fig. 5.1 and Fig. 5.2.

In the other extreme limit, it will be interesting to study the lopsidedness in the stellar and HI disks of highly lopsided galaxies like M101, NGC 1637. These studies can reveal the upper limit of the lopsidedness of galaxies. This is one such work we hope to carry out in the future.

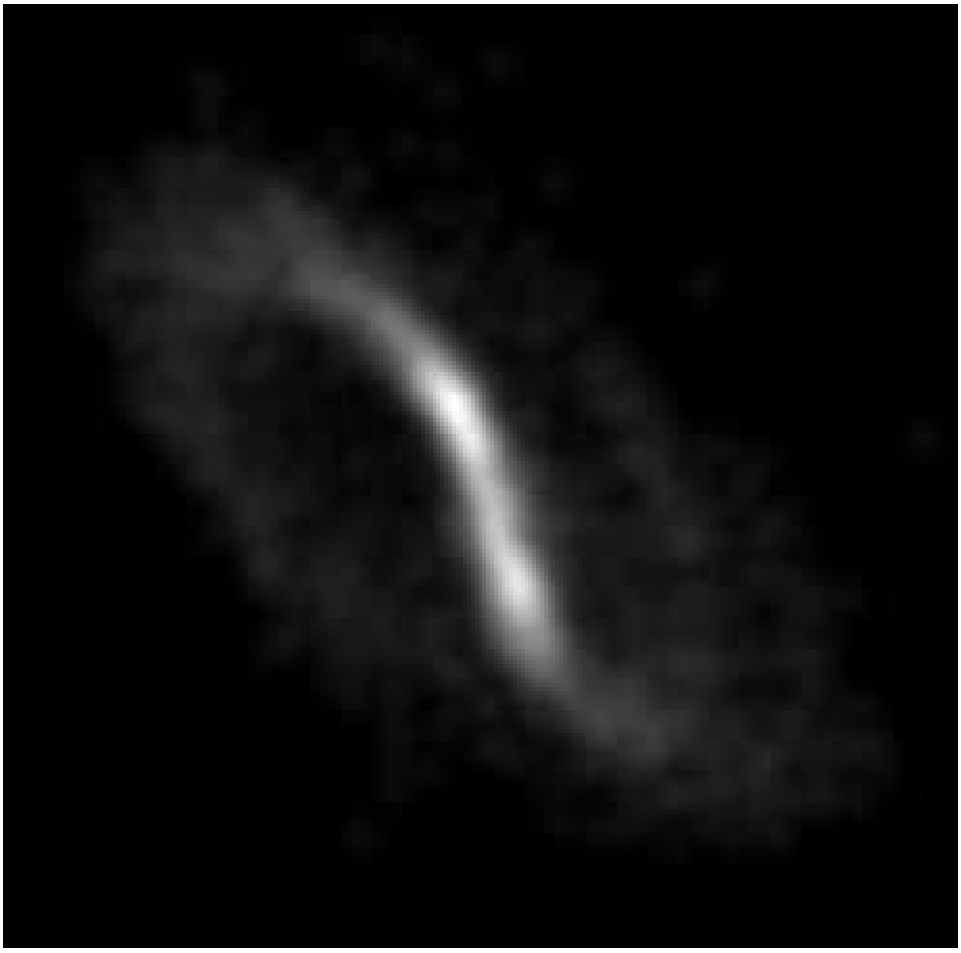

Figure 5.1: N-Body simulation of a barred galaxy. Tree-code is used to evolve 10000 particles within an initial logarithmic potential

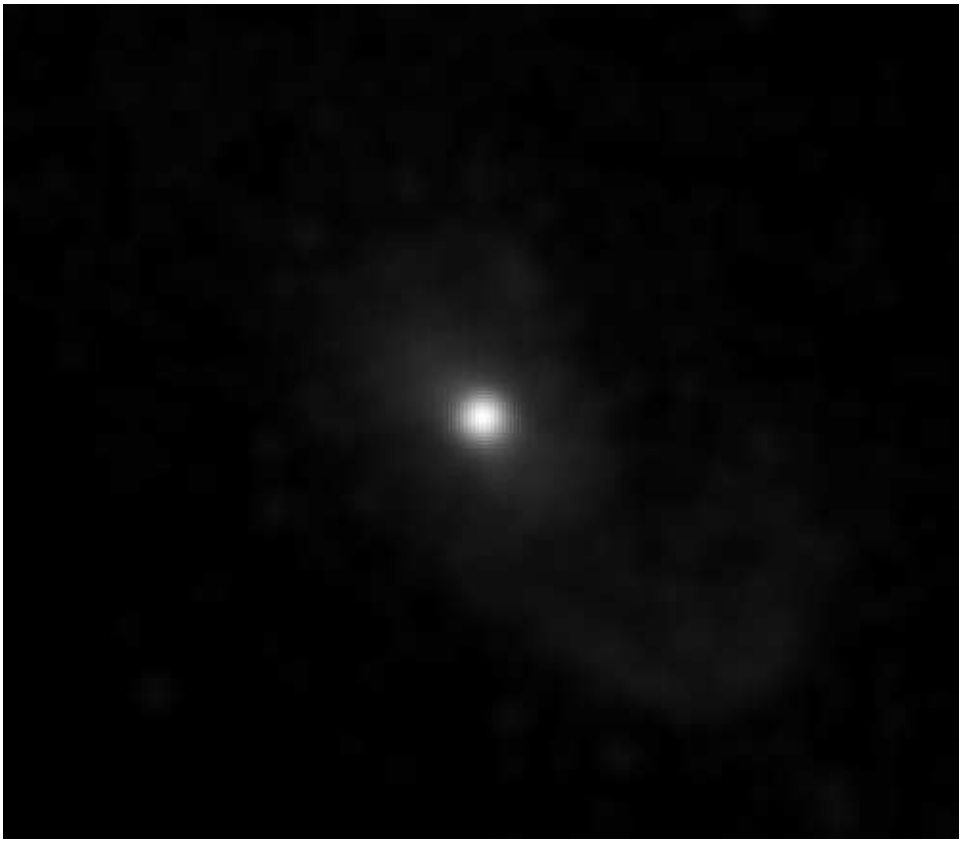

Figure 5.2: N-Body simulation of an asymmetric galaxy. Here the core is assumed to be made of 1000 particles in a Plummer potential. The disk is made of 10000 particles in an initial logarithmic potential. Disk particles are given an initial angular velocity.

Bibliography

[Angiras et al., 2006] Angiras,R.A.; Jog,C.J.; Omar,A.; Dwarakanath,K.S.; 2006, MNRAS, 369, 1849

[Angiras et al., 2007] Angiras,R.A.; Jog,C.J.; Dwarakanath,K.S.; Verheijen, M. A. W; 2007, MNRAS, 378, 276

[Angiras & Dwarakanath 2008] Angiras,R.A.; Dwarakanath,K.S.; 2008, MNRAS, submitted

[Athanassoula et al. 1997] Athanssoula,E.; Makino,J.; Bosma,A.; 1997, MNRAS, 286, 825

[Athanassoula, 2005] Athanassoula, E.; 2005, MNRAS, 358, 1477

[Bagchi et al. 2002] Bagchi,J.; Enlin,.A; Miniati,.O; Stalin,C. S.; Singh,M.; Raychaudhury,.S; Humeshkar,N.B.; 2002, NewA., 7, 249

[Baldwin et al., 1980] Baldwin,J. E.; Lynden-Bell,D.; Sancisi,R.; 1980,MNRAS,193,313

[Barnes & Hut, 1986] Barnes, J. ; Hut, P. ; 1986, Nature, 324, 446

[Baugh, Cole, & Frenk, 1996] Baugh,C. M.; Cole,S.; Frenk,C. S.; 1996, MNRAS, 283, 1361

[Begeman, 1989] Begeman,K. G.;1989,A&A,223,47

[Binney & Tremaine, 1987] Binney,J.; Tremaine,S.; 1987, Galactic Dynamics, Princeton Univ. Press, New Jersey

[Block et al., 1994] Block,D. L.; Bertin,G.; Stockton,A.; Grosbol,P.; Moorwood,A. F. M.; Peletier,R. F.;1994,A&A,288,365

[Block et al. 2002] Block, D. L.; Bournaud, F.; Combes, F.; Puerari, I.; Buta, R.; A&A, 2002, 394, L35

[Bosma, 1981] Bosma, A.; 1981, AJ, 86, 1825

[Bournaud & Combes, 2002] Bournaud,F.; Combes,F.; 2002,A&A,392,83

[Bournaud et al., 2005] Bournaud,F.; Combes,F.; Jog,C. J.; Puerari,I.; 2005,A&A,438,507

[Bravo-Alfaro et al., 2000] Bravo-Alfaro,H.; Cayatte,V.; van Gorkom,J. H.; Balkowski,C; 2000, AJ, 119, 580

[Burstein & Rubin, V.C. 1985] Burstein, D.; Rubin, V. C.; 1985, ApJ, 297, 423

[Buta et al., 1998] Buta,R.; Alpert,A. J.; Cobb,M. L.; Crocker,D. A.; Purcell,G. B.; 1998,AJ,116,1142

[Buta et al. 2003] Buta,R.; Block,D.L.; Knapen,J.H.; 2003, AJ, 126, 1148

[Butcher & Oemler, 1978] Butcher,H.; Oemler,A.; 1978, ApJ, 219, 18

[Chung et al., 2007] Chung,A.; van Gorkom,J.H.; Kenney,J.D.P.; Vollmer,B.; 2007, AJ, 659, L115

[Condon, 1992] Condon,J.J.; 1992, ARA&A, 30, 575

[Crowl et al., 2006] Crowl,H. H.; Kenney,J. D.; vanGorkom,J. H.; Chung,A.; Rose,J. A.; 2006, AAS, 38, 1192

[da Costa et al., 1988] da Costa, L. N.; Pellegrini, P. S.; Sargent, W.L. et al.; 1988, ApJ, 327, 544

[Dressler, 1980] Dressler,A.; 1980, ApJ, 236, 351

[Dressler, 1986] Dressler,A.; 1986, AJ, 301, 35

[Dressler et al., 1997] Dressler,A.; et al., 1997, ApJ, 490, 577

[Franx et al. 1994] Franx,M.; van Gorkom,J.M.; de Zeeuw,P.T.; 1994, ApJ, 436, 642

[Franx & de Zeeuw, 1992] Franx, M.; de Zeeuw, P.T.; 1992, ApJ, 392, L47

[Giovanelli & Haynes, 1985] Giovanelli,R.; Haynes,M.P.; 1985, ApJ, 292, 404

[Gunn & Gott, 1972] Gunn, J. E.; & Gott, J. R.; 1972, ApJ, 176, 1

[Haynes & Giovanelli, 1984] Haynes,M.P.; Giovanelli,R.; 1984, AJ, 89, 758

[Haynes et al., 1984] Haynes, M. P.; Giovanelli, R.; Chincarini, G. L.; 1984, ARA&A, 22, 445

[Haynes et al., 1998] Haynes,M.P., Hogg,D.E., Maddalena,R.J., Roberts,M.S., van Zee,L., 1998, AJ, 115, 62

[Haynes et al., 1998] Haynes, M. P.; van Zee, L.; Hogg, D. E.; Roberts, M. S.; Maddalena, R. J.; 1998, AJ, 115, 62

[Hernández-Toledo et al., 2006] Hernández-Toledo, H. M., Avila-Reese, V., Salazar-Contreras, J. R., Conselice, C. J., 2006, AJ, 132, 71

[Hickson, 1982] Hickson,P.; 1982, ApJ, 255, 382

[Hickson, 1992] Hickson,P.; Mendes de Oliveira,C.; Huchra,J. P.; Palumbo,G.; 1992, ApJ, 399, 353

[Hubble, 1936] Hubble, E. P.; 1936, The Realm of the Nebulae, New Haven: Yale Univ. Press

[Hunter& Wilcots, 2002] Hunter,D.A.; Wilcots,E.M.; 2002, AJ, 123, 2449

[Jog, 1997] Jog, C. J.; 1997,ApJ,488,642

[Jog, 2000] Jog, C. J.; 2000,ApJ,542,216

[Jog, 2002] Jog, C. J.; 2002,A&A,391,471

[Jog & Maybhate, 2006] Jog, C.J.; Maybhate A.;2006, MNRAS, 370, 891

[Kamphuis, Sancisi, & van der Hulst, 1991] Kamphuis, J.; Sancisi, R.; van der Hulst, T.; 1991, A&A, 244, L29

[Leon et al., 1998] Leon,S.; Combes,F.; Menon,T.K.; 1998, A&A, 330, 37

[Matthews et al., 1998] Matthews, L. D.; van Driel, W.; Gallagher,J. S.; 1998,AJ,116,1169

[Menon, 1995] Menon, T. K., 1995, MNRAS, 274, 845

[Milgrom, 1983] Milgrom, M.; 1983, ApJ, 270, 365

[Moore et al., 1999] Moore, B.; Lake, G.; Quinn, T.; Stadel, J.; 1999, MNRAS, 304, 465

[Navarro et al., 1997] Navarro, J. F.; Frenk, C. S.; White, S. D. M; 1997, ApJ, 490, 493

[Noordermeer et al., 2001] Noordermeer, E.;Sparke, L. S.; Levine, S. E; 2001,MNRAS,328,1064

[Omar & Dwarakanath, 2005a] Omar, A.; Dwarakanath, K. S.; 2005a,JAA,26,1

[Omar & Dwarakanath, 2005b] Omar, A.; Dwarakanath, K. S.; 2005b,JAA,26,71

[Omar & Dwarakanath, 2005c] Omar,A.; Dwarakanath,K.S.; 2005c, JAA, 26, 89

[Omar & Dwarakanath, 2006] Omar, A.; Dwarakanath, K. S.; 2006, JAA, 27, 7

[Paturel et al., 1991] Paturel,G.; Fougue,P.; Buta,R.; Garcia,A.M.; 1991, A&A, 243, 319

[Pellegrini et al., 1989] Pellegrini, P. S.; da Costa, L. N. et al., 1989, AJ, 99, 751

[Ponman et al., 1996] Ponman,T.J.; Bourner,P.D.J.; Ebeling,H.; Bohringer,H.; 1996, MNRAS, 283, 690

[Raimond & Genee, 1996] Raimond and Genee (eds.), 1996. "The Westerbork Observatory, Continuing Adventure in Radio Astronomy," Kluwer Academic Publ.

[Rasmussen et al. 2006] Rasmussen, J.; Ponman, T.J.; Mulchaey, J.S.; Miles, T.A.; Raychaudhury, S.;2006, MNRAS, 373, 653

[Rubin et al., 1980] Rubin, V. C.; Thonnard, N.; Ford, W. K., Jr.; 1980, ApJ, 238, 471

[Richter & Sancisi, 1994] Richter, O.-G.; Sancisi, R.; 1994, A&A, 290, L9

[Rix&Zaritsky, 1995] Rix, H.-W.; Zaritsky, D.; 1995,ApJ,447,82

[Roberts & Haynes, 1994] Roberts, M. S.; Haynes, M. P.; 1994, ARA&A, 32, 115

[Schoenmakers et al., 1997] Schoenmakers, R. H. M.; Franx, M.; de Zeeuw, P. T.; 1997,MNRAS,292,349

[Schoenmakers, 2000] Schoenmakers, R. H. M.;2000,in "Small Galaxy Groups",ASP conference series,vol. 209,eds. M. Valtonen & C. Flynn, 54.

[Sengupta & Balasubramanyam, 2006] Sengupta, C.; Balasubramanyam, R.; 2006, MNRAS, 369, 360

[Sengupta et al., 2007] Sengupta, C.; Balasubramanyam, R.; Dwarakanath, K. S.; 2007, MNRAS, 378, 137

[Shannon, 1949] Shannon, C. E.; 1949, Proc. Institute of Radio Engineers, 37, 10

[Solanes et al., 2001] Solanes, J. M.; Manrique, A.; García-Gómez, C.; González-Casado, G.;Giovanelli, R.; Haynes, M. P.; 2001, ApJ, 548, 97

[Spitzer, 1978] Spitzer, L.; 1978, *Physical Processes in the Interstellar Medium*, A Wiley-Interscience Publication

[Swaters et al., 1999] Swaters, R. A.; Schoenmakers, R. H. M.; Sancisi,R.; van Albada, T. S.; 1999,MNRAS,304,330

[Swarup et al., 1991] Swarup, G.; Ananthakrishanan, S.; Kapahi, V. K. et al.;1991, Curr. Sci., 60, 95

[Tran et al., 2005] Tran, Kim-Vy H.; van Dokkum, P.; Illingworth, G. D. et al.; 2005, ApJ, 619, 134

[Tully & Fisher, 1977] Tully, R. B.; Fisher, J. R.; 1977, A&A, 54, 661

[Tully et al. 1996] Tully,R.B.; Verheijen,M.A.W.; Pierce,M.J.; Huang,J.S.; Wainscoat,R.J.;1996, AJ, 112, 2471

[Valluri & Jog, 1990] Valluri, M.; Jog, C. J.; 1990, ApJ, 357, 367

[van Gorkom, 2004] van Gorkom, J. H.; 2004, cgpc.symp, 305

[Verdes-Montenegro et al., 2001] Verdes-Montenegro,L.; Yun,M. S.; Williams,B. A.; Huchtmeier,W. K.; Del Olmo,A.; Perea, J.; 2001, A&A, 377, 812

[Verheijen & Sancisi, 2001] Verheijen, M. A. W.; Sancisi, R.; 2001, A&A, 370, 765

[Teuben, 1995] Teuben, P. J.; Astronomical Data Analysis Software and Systems IV, ed. Shaw, R., Payne, H. E., Hayes, J. J. E., PASP Conf. Series, 77, 398

[Tully & Fisher, 1977] Tully, R. B.; Fisher, J. R.; 1977, A&A, 54, 661

[van der Hulst et al. 1992] van der Hulst, J. M.; Terlouw, J. P.; Begeman, K. G.; Zwitser, W.; Roelfsema, P. R., 1992, ASPC, 25, 131

[Warmels, 1988] Warmels, R. H.; 1988,A&AS,72,427

[Weinberg, 1995] Weinberg, M. D.;1995,ApJ,455,L31

[Willmer et al., 1989] Willmer, C. N. A.; Focardi, P. et al., 1989, AJ, 98, 1531

[Wong et al. 2003] Wong, T.; Blitz, L.; Bosma, A.; 2003, ApJ, 605, 183

[Yun et al., 2001] Yun,Min S.; Reddy,N. A.; Condon,J. J.; 2001, AJ, 554, 803

[Zaritsky& Rix, 1997] Zaritsky, D.;Rix, H.-W.; 1997,ApJ,447,118

[Zhang & Buta, 2007] Zhang, X.; Buta, R. J.; 2007b, AJ, 133, 2584

A

Equations Used for Velocity Harmonic Analysis

These equations were used to obtain the ellipticity of potential from velocity maps by earlier workers (Franx et al. 1994; Schoenmakers et al., 1997). However, for completeness sake the derivation of these equations are given here.

A.1 Closed Orbits in an Asymmetric Potential

Following the foot steps of Binney & Tremain (Binney & Tremaine, 1987)

$$\ddot{R} - R\dot{\phi}^2 = -\frac{\partial \Phi}{\partial R} + 2R\dot{\phi}\Omega_{p,m} + \Omega_{p,m}^2 R \qquad \text{A.1}$$

$$R\ddot{\phi} + 2\dot{R}\dot{\phi} = -\frac{1}{R}\frac{\partial \Phi}{\partial \phi} - 2\dot{R}\Omega_{p,m} \qquad \text{A.2}$$

where $\phi = (\theta - \Omega_{p,m}t)$

$$\Phi(R,\phi) \quad = \quad \Phi_0(R) + \Phi_1(R,\phi) \tag{A.3}$$

In our case, let us assume that the potential $\Phi(R,\phi)$ is given by:

$$\Phi(R,\phi) \quad = \quad \Phi_0(R) + \Phi_m(R)\cos(m[\phi - \phi_m(R)]) \tag{A.4}$$

with the condition that the perturbing potential is very small. This implies $|\Phi_m(R)/\Phi_0(R)| \ll 1$.

Substituting eq. A.4 in eq. A.1 and eq. A.2 we get

$$\begin{aligned} \ddot{R} - R\dot{\phi}^2 \quad &= \quad -\frac{\partial\Phi_0}{\partial R} - \frac{\partial\Phi_m}{\partial R}\cos(m[\phi - \phi_m(R)]) \\ &\quad -m\Phi_m \sin(m[\phi - \phi_m(R)])\frac{\partial\phi_m}{\partial R} + 2R\dot{\phi}\Omega_{p,m} + \Omega_{p,m}^2 R \end{aligned} \tag{A.5}$$

and

$$R\ddot{\phi} + 2\dot{R}\dot{\phi} \quad = \quad \frac{m\Phi_m \sin(m[\phi - \phi_m(R)])}{R} - 2\dot{R}\Omega_{p,m} \tag{A.6}$$

Now assume that the particle is undergoing epicyclic motion. This implies that the R and ϕ are given by

$$R \quad = \quad R_0 + \delta R \tag{A.7}$$

$$\phi = \phi_0 + \delta\phi \tag{A.8}$$

where R_0 and ϕ_0 correspond to the position of the guiding centre. Substituting eq. A.7 and eq. A.8 in eq. A.5 and eq. A.6 we get

$$\begin{aligned}(R_0 \ddot{+} \delta R) - (R_0 + \delta R)(\phi_0 \dot{+} \delta\phi)^2 = & -|\frac{\partial\Phi_0}{\partial R}|_{R_0} \\ & -|\frac{\partial\Phi_m}{\partial R}|_{R_0}\cos(m[\phi - \phi_m(R)]) \\ & -m\Phi_m\sin(m[\phi - \phi_m(R)])|\frac{\partial\phi_m}{\partial R}|_{R_0} \\ & +2(R_0 + \delta R)(\phi_0 \dot{+} \delta\phi)\Omega_{p,m} \\ & +\Omega_{p,m}^2(R_0 + \delta R)\end{aligned} \tag{A.9}$$

$$\begin{aligned}(R_0 + \delta R)(\phi_0 \ddot{+} \delta\phi) + 2(R_0 \dot{+} \delta R)(\phi_0 \dot{+} \delta\phi) = & \frac{m\Phi_m\sin(m[\phi - \phi_m(R)])}{(R_0 + \delta R)} \\ & -2(R_0 \dot{+} \delta R)\Omega_{p,m}\end{aligned} \tag{A.10}$$

The zeroth order equations become

$$R_0\dot{\phi_0}^2 + 2\Omega_{p,m}R_0\dot{\phi_0} + R_0\Omega_{p,m}^2 = |\frac{\partial\Phi_0}{\partial R}|_{R_0} \tag{A.11}$$

$$R_0\ddot{\phi_0} = 0 \tag{A.12}$$

From the definition of angular velocity, in zeroth order potential, the

angular velocity is given by the equation

$$\Omega_0{}^2 = |\frac{1}{R}\frac{\partial \Phi_0}{\partial R}|_{R_0} \quad \text{A.13}$$

We also notice that from eq. A.12

$$\ddot{\phi_0} = 0 \quad \text{A.14}$$

Comparing eq. A.13 with eq. A.11 we see that

$$\dot{\phi_0} = \Omega_0 - \Omega_{p,m} \quad \text{A.15}$$

which is the angular velocity of the guiding centre.

Choosing the coordinates such that at $t = 0$, $\phi = 0$, we get

$$\phi_0 = (\Omega_0 - \Omega_{p,m})t \quad \text{A.16}$$

The guiding centre is undergoing circular motion. Hence $\dot{R_0} = 0$

$$\begin{aligned} \ddot{\delta R} = & -|\frac{\partial \Phi_m}{\partial R}|_{R_0} \cos(m[\phi - \phi_m(R)]) - m\Phi_m|\frac{\partial \phi_m}{\partial R}|_{R_0} \sin(m[\phi - \phi_m(R)]) \\ & +(\dot{\phi_0}{}^2 + 2\dot{\phi_0}\Omega_{p,m} \\ & +\Omega_{p,m}^2 - \frac{\partial^2 \Phi_0}{\partial R^2})\delta R + 2(R_0\Omega_{p,m} + 2R_0\dot{\phi_0})\dot{\delta\phi} \end{aligned} \quad \text{A.17}$$

$$R_0\ddot{\delta\phi} + \ddot{\phi_0}\delta R + 2(\dot{\phi_0} + \Omega_{p,m})\dot{\delta R} = m\frac{\Phi_m}{R_0}\sin(m[\phi - \phi_m(R)]) \quad \text{A.18}$$

Substituting zeroth order solutions for $\dot{\phi_0}$ and $\ddot{\phi_0}$ in the above equations we

get

$$\begin{aligned}\ddot{\delta R} &= -|\frac{\partial \Phi_m}{\partial R}|_{R_0}\cos(m[\phi-\phi_m(R)]) - m\Phi_m|\frac{\partial \phi_m}{\partial R}|_{R_0}\sin(m[\phi-\phi_m(R)]) \\ &+(\Omega_0{}^2 - \frac{\partial^2\Phi_0}{\partial R^2})\delta R \\ &+2R_0\Omega_0\dot{\delta\phi} \end{aligned} \quad \text{A.19}$$

$$R_0\ddot{\delta\phi} = m\frac{\Phi_m}{R_0}\sin(m[\phi-\phi_m(R)]) - 2\Omega_0\dot{\delta R} \quad \text{A.20}$$

Integrating eq. A.20 with respect to t we get

$$\Omega_0 R_0\dot{\delta\phi} + 2\Omega_0{}^2\delta R = \frac{-m\Phi_m\Omega_0\cos(m[\phi-\phi_m(R)])}{R_0[m(\Omega_0-\Omega_{p,m}) - m\dot{\phi_m}(R)]} + const. \quad \text{A.21}$$

Assuming that the phase of the potential does not change with time, we get

$$\dot{\delta\phi} = \frac{-2\Omega_0\delta R}{R_0} - \frac{\Phi_m\cos(m[\phi-\phi_m(R)])}{R_0{}^2(\Omega_0-\Omega_{p,m})} + const. \quad \text{A.22}$$

Following Binney, (Binney & Tremaine, 1987) on substituting eq. A.22 in eq. A.21 and solving the resultant differential equation, we get for closed loop orbits:

$$\begin{aligned}\delta R &= \frac{-1}{\kappa_0{}^2 - m^2(\Omega_0-\Omega_{p,m})^2}[(\frac{2\Omega_0\Phi_m}{R_0(\Omega_0-\Omega_{p,m})} + |\frac{\partial\Phi_m}{\partial R}|_{R_0})\cos(m[\phi-\phi_m(R)]) \\ &+m\Phi_m\frac{\partial\phi_m}{\partial R}\sin(m[\phi-\phi_m(R)])] \end{aligned} \quad \text{A.23}$$

Here $\kappa_0 = 3{\Omega_0}^2 + \frac{\partial^2 \Phi_0}{\partial R^2}$ (Binney & Tremaine, 1987).

Substituting eq. A.23 in eq. A.22 and integrating with respect to t we get

$$\delta\phi = \frac{[\frac{\Phi_m[4{\Omega_0}^2 - {\kappa_0}^2 + m^2(\Omega_0 - \Omega_{p,m})^2]}{R_0(\Omega_0 - \Omega_{p,m})} + 2\Omega_0 |\frac{\partial \Phi_m}{\partial R}|_{R_0}]\sin(m[\phi - \phi_m(R)]) - 2\Omega_0 m \Phi_m |\frac{\partial \phi_m}{\partial R}|_{R_0} \cos(m[\phi - \phi_m(R)])]}{m(\Omega_0 - \Omega_{p,m}) R_0[{\kappa_0}^2 - m^2(\Omega_0 - \Omega_{p,m})^2]} \quad \text{A.24}$$

Substituting eq. A.23 and eq. A.24 in eq. A.7 and eq. A.8 we get the equation A3 in Schoenmakers et al. (Schoenmakers et al., 1997). Namely

$$R = R_0 + \delta R = R_0(1 - \frac{a_{1m}}{2}\cos(m[\phi - \phi_m(R)]) - a_{2m}\sin(m[\phi - \phi_m(R)]))$$
$$\phi = \phi_0 + \delta\phi = \phi_0 + \frac{(a_{1m} + a_{3m})}{2m}\sin(m[\phi - \phi_m(R)]) - a_{4m}\cos(m[\phi - \phi_m(R)]) \quad \text{A.25}$$

Here

$$a_{1m} = \frac{2}{\Delta_0}(\frac{2\Omega_0 \Phi_m}{R_0(\Omega_0 - \Omega_{p,m})} + |\frac{\partial \Phi_m}{\partial R}|_{R_0})$$
$$a_{2m} = \frac{m\Phi_m \frac{\partial \phi_m}{\partial R}}{\Delta_0}$$
$$a_{3m} = \frac{2}{\Delta_0}[\frac{\Phi_m[(2+m^2){\Omega_0}^2 + 2(1-m^2)\Omega_0\Omega_{p,m} + m^2{\Omega_{p,m}}^2 - {\kappa_0}^2]}{R_0(\Omega_0 - \Omega_{p,m})^2} + \frac{(\Omega_0 + \Omega_{p,m})}{(\Omega_0 - \Omega_{p,m})}|\frac{\partial \Phi_m}{\partial R}|_{R_0}$$
$$a_{4m} = \frac{2\Omega_0 \Phi_m \frac{\partial \phi_m}{\partial R}}{\Delta_0(\Omega_0 - \Omega_{p,m})} \quad \text{A.26}$$

where $\Delta_0 = R_0[{\kappa_0}^2 - m^2(\Omega_0 - \Omega_{p,m})^2]$

These equations will be valid only within the Lindblad resonance pos-

tions.

A.2 Velocity in Asymmetric Potential

If one moves into a frame which is at rest with respect to the galaxy under consideration,

$v_R = \dot{R}$ and $v_\phi = R(\dot{\phi} + \Omega_{p,m})$.

From eq. A.7 we get on simplification

$$v_R = mv_c(1-\omega_m)(\frac{1}{2}a_{1m}\sin(m[\phi-\phi_m(R)]) - a_{2m}\cos(m[\phi-\phi_m(R)]) \quad \text{A.27}$$

$$v_\phi = v_c(1+\frac{1}{2}[(1-\omega_m)a_{3m} - \omega_m a_{1m}]\cos(m[\phi-\phi_m(R)]) + [m(1-\omega_m)a_{4m} - a_{2m}]\sin(m[\phi-\phi_m(R)]$$

Here $\omega_m = \dfrac{\Omega_{p,m}}{\Omega_0}$ and $v_c = R_0\Omega_0$

A.3 Projection of Line of Sight Velocity Field

Let v_{los} be the line of sight velocity.

$$v_{los} = [v_R \sin\psi + v_\phi \cos\psi]\sin i \quad \text{A.29}$$

Here $\psi = \phi - \phi_{obs} + \dfrac{\pi}{2}$ is called the azimuthal angle and is zero along the line of nodes.

substituting for v_R and v_ϕ from eq. A.26 and eq. A.27 and simplifying we finally get

$$v_{los} = c_1 \cos\psi + s_{m-1}\sin(m-1)\psi + c_{m-1}cos(m-1)\psi + \quad \text{A.30}$$

$$s_{m+1}\sin(m+1)\psi + c_{m+1}\cos(m+1)\psi \quad \text{A.31}$$

which is the eq. 5 in Schoenmakers et. al. [1997] . In eq. A.31

$$\begin{aligned}
c_1 &= v_c \sin i \\
s_{m-1} &= c_1(-\frac{1}{4}[[(m-(m+1))\omega_m + \alpha]a_{1m} + (1-\omega_m)a_{3m}]\sin m\varphi_m \\
&\quad + \frac{1}{2}\{m(1-\omega_m)a_{4m} + [m(1-\omega_m) - 1 + \alpha]a_{2m}\}\cos m\varphi_m) \\
c_{m-1} &= c_1(-\frac{1}{4}[[(m-(m+1))\omega_m + \alpha]a_{1m} + (1-\omega_m)a_{3m}]\cos m\varphi_m \\
&\quad + \frac{1}{2}\{m(1-\omega_m)a_{4m} + [m(1-\omega_m) - 1 + \alpha]a_{2m}\}\sin m\varphi_m) \\
s_{m+1} &= c_1(-\frac{1}{4}[[(m-(m+1))\omega_m - \alpha]a_{1m} - (1-\omega_m)a_{3m}]\sin m\varphi_m \\
&\quad + \frac{1}{2}\{m(1-\omega_m)a_{4m} - [m(1-\omega_m) + 1 - \alpha]a_{2m}\}\cos m\varphi_m) \\
c_{m+1} &= c_1(-\frac{1}{4}[[(m-(m-1))\omega_m - \alpha]a_{1m} - (1-\omega_m)a_{3m}]\cos m\varphi_m \\
&\quad + \frac{1}{2}\{m(1-\omega_m)a_{4m} - [m(1-\omega_m) + 1 - \alpha]a_{2m}\}\sin m\varphi_m)
\end{aligned} \quad \text{A.32}$$

Here, $\varphi = \phi_{obs} - \frac{\pi}{2} - \phi_m(R)$. The value of α is related to the circular velocity (v_c) and the radial distance (R) through the relation $v_c \propto R^{\alpha}$. The value of $\alpha = 0$ for flat rotation curves.